7-2-2011

Late Quaternary semiarid eolian system dynamics : distribution, timing, and soil geomorphic controls, Black Mesa, northeastern Arizona, USA

Amy Ellwein

Amy Ellwein
Candidate

Earth and Planetary Sciences
Department

This dissertation is approved, and it is acceptable in quality and form for publication:

Approved by the Dissertation Committee:

Lin D. McFadden, Chairperson

Lora A Snider, Chairperson

Grant A. Meyer

Joe McAuliffe

LATE QUATERNARY SEMIARID EOLIAN SYSTEM DYNAMICS: DISTRIBUTION, TIMING, AND SOIL GEOMORPHIC CONTROLS, BLACK MESA, NORTHEASTERN ARIZONA, USA

BY

AMY ELLWEIN

B.S., Geology and Geophysics, The University of Minnesota, 1993
M.S., Earth and Planetary Sciences, The University of New Mexico, 1997

DISSERTATION

Submitted in Partial Fulfillment of the
Requirements for the Degree of

Doctor of Philosophy
Earth and Planetary Sciences

The University of New Mexico
Albuquerque, New Mexico

May, 2011

Dedication

For my grandmother and my parents. Early mornings bird watching with my grandma fed my curiosity about the natural world; my mother showed me the importance of being true to yourself; my father taught me to answer my own damned questions.

Acknowledgements

First, I would like to thank my entire dissertation committee for their time, valuable insights, and careful consideration of my ideas. A special thanks to my co-advisor Dr. Louis Scuderi and the Center for Rapid Environmental Assessment and Terrain Evaluation (CREATE) for funding the first three years of this project. Shannon Mahan at the USGS Luminescence Lab is an honorary committee member; Shannon lent her unflagging support, insight, and good humor to the great benefit of my research. I am grateful to both Dr. Les McFadden and Dr. Joe McAuliffe for suggesting this project, spending quality time with me in the field, and playing formative roles at all stages of my research. Dr. Grant Meyer has challenged and sharpened my thinking about surficial processes in a variety of important ways. I have been the beneficiary of the wisdom of my committee, but the errors in this dissertation are mine.

Heartfelt thanks are extended to the Navajo Nation and the Hopi Tribe. Terry Morgart at the Hopi Cultural Preservation Office and Brad Nesemeier at the Navajo Nation Minerals Department were both very helpful in navigating the permitting process for this work. I am grateful for the conversations, assistance, stories, and laughs I shared with many people I met while working in the field.

A very special thanks are extended to all who helped me in the field and laboratory: Patrick Ellwein, Jennifer New-Parker, Leah Roberts, Benjamin Swanson, and Tim Wawrzyniec. While it is possible to do field work alone, it is much more efficient and far more enjoyable to conduct field research with such good friends.

And finally, to Tim, who actually comes first. Without his support, encouragement, companionship, humor, love, and of course his shovel, none of this would have gotten done.

LATE QUATERNARY SEMIARID EOLIAN SYSTEM DYNAMICS: DISTRIBUTION, TIMING, AND SOIL GEOMORPHIC CONTROLS, BLACK MESA, NORTHEASTERN ARIZONA, USA

BY

AMY ELLWEIN

ABSTRACT OF DISSERTATION

Submitted in Partial Fulfillment of the
Requirements for the Degree of

Doctor of Philosophy
Earth and Planetary Sciences

The University of New Mexico
Albuquerque, New Mexico

May, 2011

LATE QUATERNARY SEMIARID EOLIAN SYSTEM DYNAMICS: DISTRIBUTION, TIMING, AND SOIL GEOMORPHIC CONTROLS, BLACK MESA, NORTHEASTERN ARIZONA, USA

BY

AMY ELLWEIN

B.S., Geology and Geophysics, The University of Minnesota, 1993
M.S., Earth and Planetary Sciences, The University of New Mexico, 1997
Ph. D., Earth and Planetary Sciences, The University of New Mexico, 2011

ABSTRACT

According to the University of New Mexico's Office of Graduate Studies, this dissertation follows a hybrid format; the chapters were written as manuscripts to be submitted to peer-reviewed journals. Chapter 1 was published in the journal Quaternary Research (May, 2011) and chapters 2 and 3 will be submitted to appropriate journals soon after this dissertation is published.

Chapter 1 announces new age determinations for previously unstudied topographically-controlled eolian deposits and older ages for sand sheets than were reported by previous investigators. Chapter 2 focuses on the distribution, age, and geomorphic implications of topographically-controlled eolian deposits on Black Mesa. Chapter 3 describes the role of advanced soil profile development on the stability of eolian systems; a factor generally overlooked by researchers interested in quantifying the relative activity of

sand dunes. Appendix A contains the results of tests that determine the efficacy of samples used in optically stimulated luminescence dating in all three manuscripts.

TABLE OF CONTENTS

LIST OF FIGURES

Chapter 1

Chapter 2

Chapter 3

LIST OF TABLES

Chapter 1

Chapter 2

Chapter 3

CHAPTER 1

New optically stimulated luminescence ages provide evidence of MIS 3 and MIS 2 eolian activity on Black Mesa, northeastern Arizona, USA

Abstract

Eolian deposition on the semiarid southern Colorado Plateau has been attributed to episodic aridity during the Quaternary. However, OSL ages from three topographically-controlled (e.g. falling) dunes on Black Mesa in northeastern Arizona indicate that eolian sediments were deposited in deep tributary valleys as early as 35-30 ka, with most sand deposited before 20 ka. In contrast, the oldest OSL ages for sand sheets fall within the Pleistocene-Holocene climatic transition (~12-8 ka). Thus most eolian sediment accumulated on Black Mesa under climatic conditions that were in general cooler, moister, and more variable than today, not more arid, pointing to a considerable increase in sediment supply.

Introduction

The Black Mesa region of northeastern Arizona, USA (Fig. 1) has been a focus of many geomorphic investigations party due to the excellent archaeological record of human occupation. Several studies have examined the timing and scope of landscape change in the alluvial record (e.g. Karlstrom and Karlstrom, 1986; McFadden and McAuliffe, 1997; Karlstrom, 2005), but it was John Hack (1941) who first noted the geomorphic significance of the widespread eolian deposits and developed a still widely used model that links dune form to sediment supply, wind speed, and vegetation cover. Through alluvial and eolian stratigraphic characterization, Hack (1942) estimated that relict dunes in the most arid, low elevation areas were deposited during the middle Holocene, but lacking precise age control, the climatic significance of the dunes was not well established. Later estimates of the maximum age of eolian deposits on the nearby Moenkopi Plateau range from 100 ka (Breed and Breed, 1979) to as much as 2.4 Ma (Billingsley, 1987). Only a few numerical ages have been obtained from linear dune crests, dates that Stokes and Breed (1993) conclude demonstrate significant remobilization during the Holocene on the Moenkopi Plateau.

This study provides the first optically stimulated luminescence (OSL) ages for morphodynamically stable eolian deposits (falling dunes) in the Black Mesa region, which is located in one of the largest yet relatively unstudied North American dune fields. The ages reported in this study establish an eolian chronology very different from the eolian chronology reported above, in part because we have dated eolian deposits that were not reactivated due to their landscape position. The volume and age of these immobile deposits suggests that glacial-age paleoenvironmental conditions controlling eolian sediment supply and availability (e.g., Kocurek and Lancaster, 1999) were much different from present. Our

work supports a growing body of research suggesting that a large proportion of eolian deposits may initially accumulate under cool and moist (e.g. Rendell and Sheffer, 1996; Clarke and Rendell, 1998; Reheis et al., 2005), but highly variable climatic conditions (e.g. Broecker, 2000; Overpeck and Cole, 2006) that characterize glacial-age climate in the southwestern US (e.g. Anderson et al., 2000; Pigati et al., 2009; Wagner et al., 2010).

Study Area and Methods

Black Mesa is a topographically inverted Cretaceous structural basin ringed by relatively flat lying sedimentary rocks of the Triassic Chinle Supergroup and Jurassic Glen Canyon and San Rafael Groups, capped by resistant Cretaceous Mesa Verde Group sandstones, which form cliffs up to 300 m high along the Hopi Mesas and valley walls of the major drainages (Fig. 1). Highest elevations in this region (up to 2500 m) are cool and moist with an estimated mean annual precipitation (MAP) of 300-350 mm (WRCC, 2009) and dominant forest cover of *Pseudotsuga menziesii* (Douglas-fir) and *Pinus ponderosa* (ponderosa pine). Lowest elevations along the Little Colorado River (roughly 1300 m) are more arid (mean annual temperature is 12.1°C and MAP is 165 mm at Leupp, AZ; WRCC, 2009). Linear dunes that form parallel to the dominant wind direction are the primary eolian landforms southwest of the Hopi Mesas (Fig. 1), whereas climbing and falling dunes dominate downwind of the Hopi Mesas in deep tributary canyons. Falling dunes are most extensive where local relief is greatest near the Hopi Mesas, in some cases eolian deposits fill entire tributary basins. These deposits decrease in volume towards the northeast, where they are expressed as falling dunes. All eolian landforms were mapped by the authors using landsat imagery and 1-m digital orthophoto quadrangles (DOQs) in a GIS and were subsequently field checked. (See online supplement for photos of active and stable linear

dunes along the Adeii Eechii Cliffs on the Moenkopi Plateau and a falling dune to the northeast of Oraibi, AZ on Third Mesa).

Eolian deposits were characterized using conventional soil stratigraphic techniques (e.g. Birkeland, 1999) applied to hand-dug soil-pits and natural exposures. Optically stimulated luminescence (OSL) age estimates on quartz sand were used to measure the last exposure of eolian sediment to sunlight. In this project, OSL ages are determined using the single-aliquot regeneration approach (SAR) for sand grains. The preferred component for SAR dating is the 'fast' component (e.g., Murray and Wintle, 2000; Wintle and Murray, 2006), a signal usually released in the first 0.8 s of typical blue diode stimulation. A dating precision of ~ 10% can be attained routinely with multigrain SAR quartz methods (e.g., Murray and Olley, 2002) when applied to eolian sand. With SAR, each aliquot yields a distinct equivalent dose (De) value and age estimate. Quartz-rich fractions were prepared by first destroying any carbonates and organic material by use of 4N hydrochloric acid and 35% hydrogen peroxide, respectively. Heavy liquid was employed to concentrate quartz-feldpar mixtures before treatment with 48% hydrofluoric acid for dissolution of remaining feldspars (e.g. Mahan and Brown, 2006). Representative multigrain portions of each sample were then tested for the possible presence of residual feldspar by running an IRSL "wash". No samples showed any sign of feldspar contamination. (See Appendix A for additional details regarding OSL methods.)

Results and Discussion

South of the Moenkopi Plateau, dunes are largely active, but on the Moenkopi Plateau and other mesa top sites they are dominantly stable. Sites WP145 and WP40 (Fig. 1 and Fig. 2) provide good examples of the stratigraphy and soil profile development in eolian deposits

of exposed and windy (high transport-capacity) mesa top landscape positions. Linear dune or sand sheet sediments are typically 1-3 m thick and deposited directly on bedrock. Soils associated with stable eolian landforms exhibit Btk soil horizons and stage II carbonate morphology (Fig. 2), which for this location imply late Pleistocene to early Holocene stabilization (e.g. Machette, 1985; Wells et al., 1990). OSL ages from eolian parent material (Fig. 2 and Table 1) indicate that the oldest eolian deposits on this surface date to the Pleistocene-Holocene climatic transition (ca. 12-8 ka; E-7 and E-19).

The southernmost sand ramp, consisting primarily of eolian sediments interbedded with thin colluvial and alluvial deposits (Lancaster and Tchakerian, 1996), was partially exposed in a meander bend in an arroyo and cleared by hand to a depth of roughly 8m from the surface. Only one weakly developed soil profile (Bw) was observed in this section (Fig. 2). An OSL age from the middle of the exposure (17 ± 1 ka; E-3) yields a late glacial depositional age. Sand ramp deposits were not sampled to their base because of the thick accumulation of colluvium (~2-3 m) shed from the exposure, which covers the underlying deposits.

At Echo Canyon (WP169), falling dune stratigraphy shows that the deposits are largely of eolian origin and the entire section contains four buried soils (Fig. 2). The uppermost weak Bw horizon formed in eolian parent material that contains rare thin gravel lenses, and this profile is capped with ~20 cm of colluvium. Weak soil profile development in the upper meter suggests late Holocene deposition. Below this unit, OSL ages show that the largest volume of sand in this falling dune was deposited ca. 32-20 ka (E-23, E-24, E-25, E-26, Table 1; Fig. 2).

The northernmost observed falling dune on Black Mesa, near Piñon, AZ (WP109), is dissected by an arroyo to its contact with bedrock. A well-developed soil (Btk horizon, stage II carbonate morphology) has formed in the upper meter of the deposit, which yielded an OSL age of 9 ± 0.7 ka (E-11). An erosional unconformity at 3.5 m separates the uppermost eolian unit from an underlying, slightly finer-grained eolian deposit with an estimated age of 29 ± 2 ka (E-12; Fig. 2 and Table 1).

Given the strong relationship between linear dune trends and transport direction (Fryberger and Dean, 1979), the observed northeast-trend of the linear dunes is consistent with deposition of falling dunes on north and northeast facing slopes of tributary canyon walls. Wind speed drops significantly in tributary basins promoting sediment trapping and protecting deposits from subsequent deflation. Our OSL ages from these topographically controlled dunes are evidence that eolian sediments were available, transported to, and deposited in topographic traps from 35-9 ka. When filled with high infiltration-capacity sands, tributary basins have been unable to generate sufficient discharge to remove dune sediments, even under full-glacial conditions. Therefore falling dunes are stable landforms that provide a long record of late Pleistocene to early Holocene eolian sediment transport and deposition on Black Mesa.

In contrast, the 12-8 ka OSL ages for mesa top deposits record the stabilization of migrating eolian deposits (e.g. Chase, 2009), not the initial emplacement of sand. We infer that the majority of sand comprising sand sheets on mesa top positions was delivered to these locations while sand was being emplaced as falling dunes, but were stabilized due to increased dust flux and consequently rapid soil formation (Reheis et al., 2005) at the Pleistocene-Holocene transition. Because of their exposed landscape position, linear dunes

and sand sheets are prone to eolian reactivation; however, these stabilized landforms exhibit only local reactivation during the Holocene.

The observed distribution and ages of eolian deposits strongly imply that eolian sediment transport capacity, availability, and supply were high in the Black Mesa region during glacial climatic conditions significantly windier (e.g. COHMAP, 1988; Kutzbach et al., 1993) and cooler and wetter than Holocene or modern conditions (e.g. Weng and Jackson, 1999; Anderson et al., 2000; Pigati et al., 2009). We infer that the extreme, abrupt climatic variability that characterizes glacial climate (e.g. Broecker, 2000; Overpeck and Cole, 2006) may have been responsible for increased variability of stream flow, resulting in formation of wide braided floodplains and increased sediment supply for the eolian system (e.g. Muhs and Holliday, 1995) from the Little Colorado River as well as the major southwest-trending washes. Therefore, we suggest that the dominant control on topographically-controlled dune deposition during the last glacial period is increased sediment supply, not aridity.

References

Anderson, R.S., Betancourt, J.L., Mead, J.I., Hevly, R.H., and Adam, D.P., 2000, Middle- and late-Wisconsin paleobotanic and paleoclimate records from the southern Colorado Plateau, USA, Palaeogeography, Palaeoclimatology, Palaeoecology, v. 155, p. 31-57.

Billingsley G.H., 1987, Geology and geomorphology of the southwestern Moenkopi Plateau and southern Ward Terrace, Arizona, U.S. Geological Survey Bulletin 1672, 18 p.

Birkeland, P.W., 1999, Soils and Geomorphology, 3rd Ed., Oxford Press, 430 p.

Breed, C.S. and Breed, W.J., 1979, Dunes and other windforms of Central Australia, and a comparison with linear dunes on the Moenkopi Plateau, Arizona, *in* El-Baz, F. and Warner, D.M., eds, Apollo-Souyez Test Project Summary Science Report, v. 2, Earth Observations and Photography: National Aeronautics and Space Administration Special Publication 412, p. 319-358.

Broecker, W.S., 2000, Abrupt climate change: causal constraints provided by the paleoclimate record, Earth Science Reviews, v. 51, p. 137-154.

Chase, B., 2009, Evaluating the use of dune sediments as a proxy for palaeo-aridity: a southern African case study, Earth Science Reviews, v. 93, p. 31-45.

Clarke, M.L and Rendell, H.M, 1998, Climate change impacts on sand supply and the formation of desert sand dunes in the south-west U.S.A., Journal of Arid Environments, v. 39, p. 517-531.

COHMAP members, 1988, Climatic changes of the last 18,000 years: Observations and model simulations, Science, v. 241, p. 1043-1052.

Fryberger S.G. and Dean, G., 1979, Dune Forms and Wind Regimes, *in* McKee, E.D., ed., A Study of Global Sand Seas, US Geological Survey Professional Paper 1052, p. 137-169.

Hack, J.T., 1941, Dunes of the western Navajo Country: Geographical Review, v. 31, p.240-263.

Hack, J.T., 1942, The Changing Physical Environment of the Hopi Indians of Arizona, Papers of the Peabody Museum, v. 35, no. 1, Harvard University, Cambridge.

Karlstrom, E.T., 2005, Late Quaternary landscape history and geoarchaeology of two drainages on Black Mesa, northeastern Arizona, USA, Geoarchaeology, v. 20, no. 1, p. 1-28.

Karlstrom, E.T. and Karlstrom, T.N.V., 1986, Late Quaternary alluvial stratigraphy and soils of the Black Mesa – Little Colorado River Areas, northern Arizona, *in* Nations, J.D., Conway, C.M., and Swann, G.A., eds., Geology of Central and Northern Arizona, Geological Society of America, Rocky Mountain Section Guidebook, p. 71-92.

Kocurek, G. and Lancaster, N., 1999, Aeolian system sediment state: theory and Mojave Desert Kelso dune field example, Sedimentology, v. 46, p. 505-515.

Kutzbach, J.E., 1987, Model simulations of the climatic patterns during the deglaciation of North America, *in* Ruddiman, W.F. and Wright, H.E., Jr. eds., North America and adjacent oceans during the last deglaciation: Boulder, Colorado, Geological Society of America, The Geology of North America, v. K-3, p. 425-446.

Lancaster, N. and Tchakerian, V.P., 1996, Geomorphology and sediments of sand ramps in the Mojave Desert, Geomorphology, v. 17, p. 151-165.

Machette, M.N., 1985, Calcic soils of the southwestern United States, *in* Weide, D.L., ed., Soils and Quaternary Geology of the Southwestern United States, Geological Society of America Special Paper 203, p. 1-21.

Mahan, S. A., and Brown, D. J., 2006. An optical age chronology of late Quaternary extreme flood events recorded in Ugandan dambo soils. Quaternary Geochronology **2**, p. 174-180.

McFadden, L.D., and McAuliffe, J.R., 1997, Lithologically influenced geomorphic responses to Holocene climatic changes in the southern Colorado Plateau, Arizona: A soil-geomorphic and ecologic perspective, Geomorphology, v. 19, p. 303-332.

Murray, A.S. and Olley, J.M., 2002, Precision and accuracy in the optically stimulated luminescence dating of sedimentary quartz: a status review, Geochronometria, v. 21, p. 1-16.

Murray, A.S. and Wintle, A.G., 2000, Luminescence dating of quartz using an improved single-aliquot regenerative-dose protocol, Radiation Measurements 32, p. 57-73.

Overpeck, J.T. and Cole, J.E., 2006, Abrupt change in Earth's climate system, Annual Review of Environment and Resources, v. 31, p. 1-32.

Pigati, J.S., Bright, J.E., Shanahan, T.M., and Mahan, S.A., 2009, Late Pleistocene paleohydrology near the boundary of the Sonoran and Chihuahuan Deserts, southeastern Arizona, USA, Quaternary Science Reviews, v. 28, p. 286-300.

Reheis, M.C., Reynolds, R.L., Goldstein, H., Roberts, H.M., Yount, J.C., Axford, Y., Cummings, L.S., and Shearin, N., 2005, Late Quaternary eolian and alluvial response to paleoclimate, Canyonlands, southeastern Utah, Geological Society of America Bulletin, v. 117, n. 7/8, p. 1051-1069.

Rendell, H.M. and Sheffer, N.L., 1996, Luminescence dating of sand ramps in the Eastern Mojave Desert, Geomorphology, v. 17, p. 187-197.

Stokes, S. and Breed, C.S., 1993, A chronostratigraphic re-evaluation of the Tusayan Dunes, Moenkopi Plateau and southern Ward Terrace, northeastern Arizona, *in* Pye, K., ed., The dynamics and environmental context of aeolian sedimentary systems, Geological Society Special Publication No. 72, p. 75-90.

Wagner, J.D.M, Cole, J.E., Beck, J.W., Patchett, P.J., Henderson, G.M., and Barnett, H.R., 2010, Moisture variability in the southwestern United States linked to abrupt glacial climate change, Nature Geoscience, v. 3, p. 110-113.

Wells, S.G., McFadden, L.D., and Schultz, J.D., 1990, Eolian landscape evolution and soil formation in the Chaco dune field, southern Colorado Plateau, New Mexico, Geomorphology, v. 3, p. 517-546.

Weng, C. and Jackson, S.T., 1999, Late glacial and Holocene vegetation history and paleoclimate of the Kaibab Plateau, Arizona, Palaeogeography, Palaeoclimatology, Palaeoecology, v. 153, p. 179-201.

Western Regional Climate Center (WRCC), Western U.S. Historical Summaries for individual stations, accessed September 22, 2009. Available on-line at [http://www.wrcc.dri.edu/CLIMATEDATA.html] from the Desert Research Institute, Reno Nevada, USA.

Wintle, A.G. and Murray, A.S., 2006, A review of quartz optically stimulated luminescence characteristics and their relevance in single-aliquot regeneration dating protocols, Radiation Measurements, v. 41, p. 369-391.

Figures

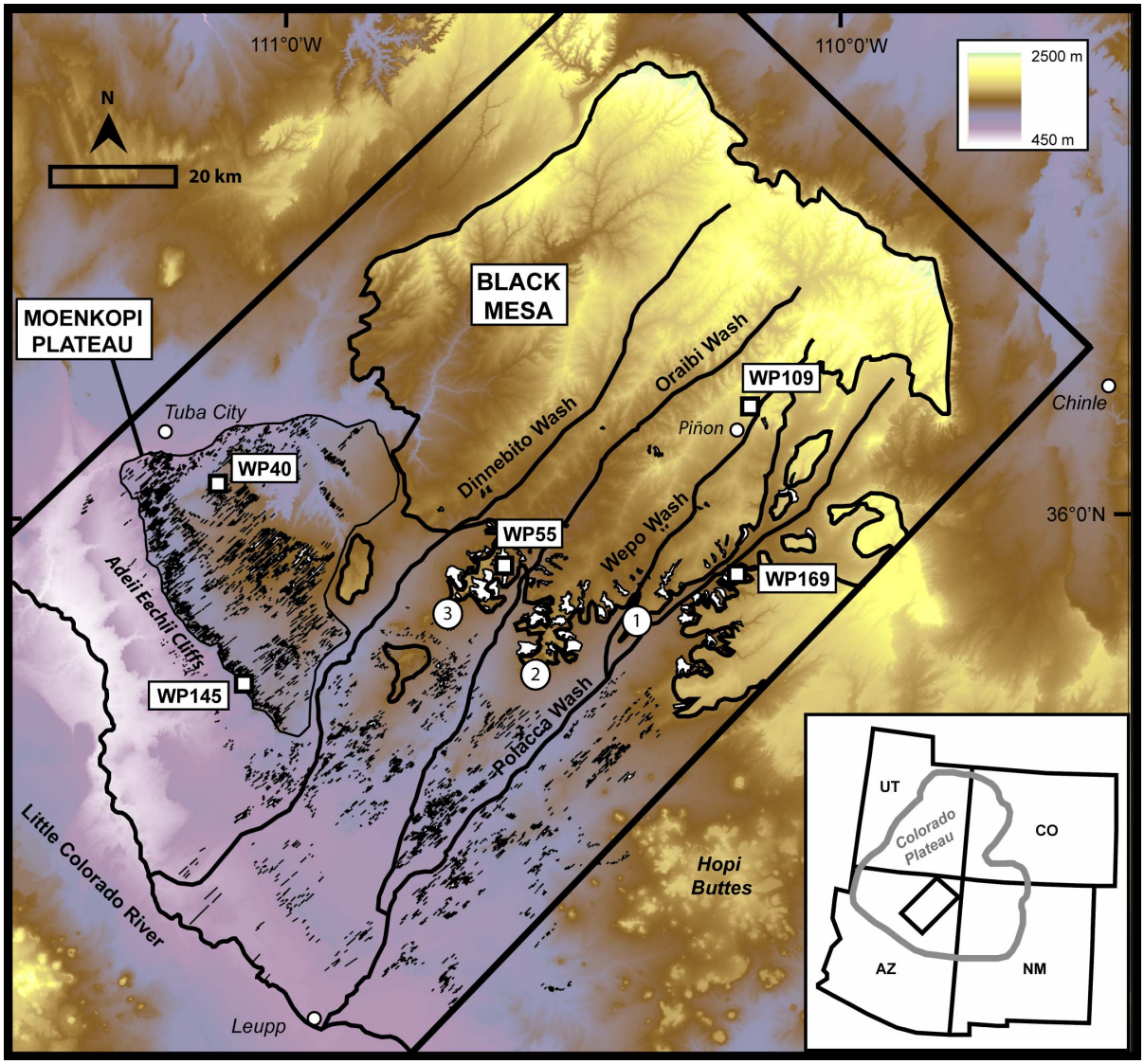

Figure 1: The study area is located in northeastern AZ, in the Four Corners region of the southwestern US. Linear dunes are shown as thin black lines that trend to the northeast. Falling dunes, shown as white polygons, are associated with canyons in the Cretaceous Mesa Verde Group sandstones, these rocks are outlined using a thick black line. The Hopi Mesas (First Mesa, Second Mesa, and Third Mesa) are numbered.

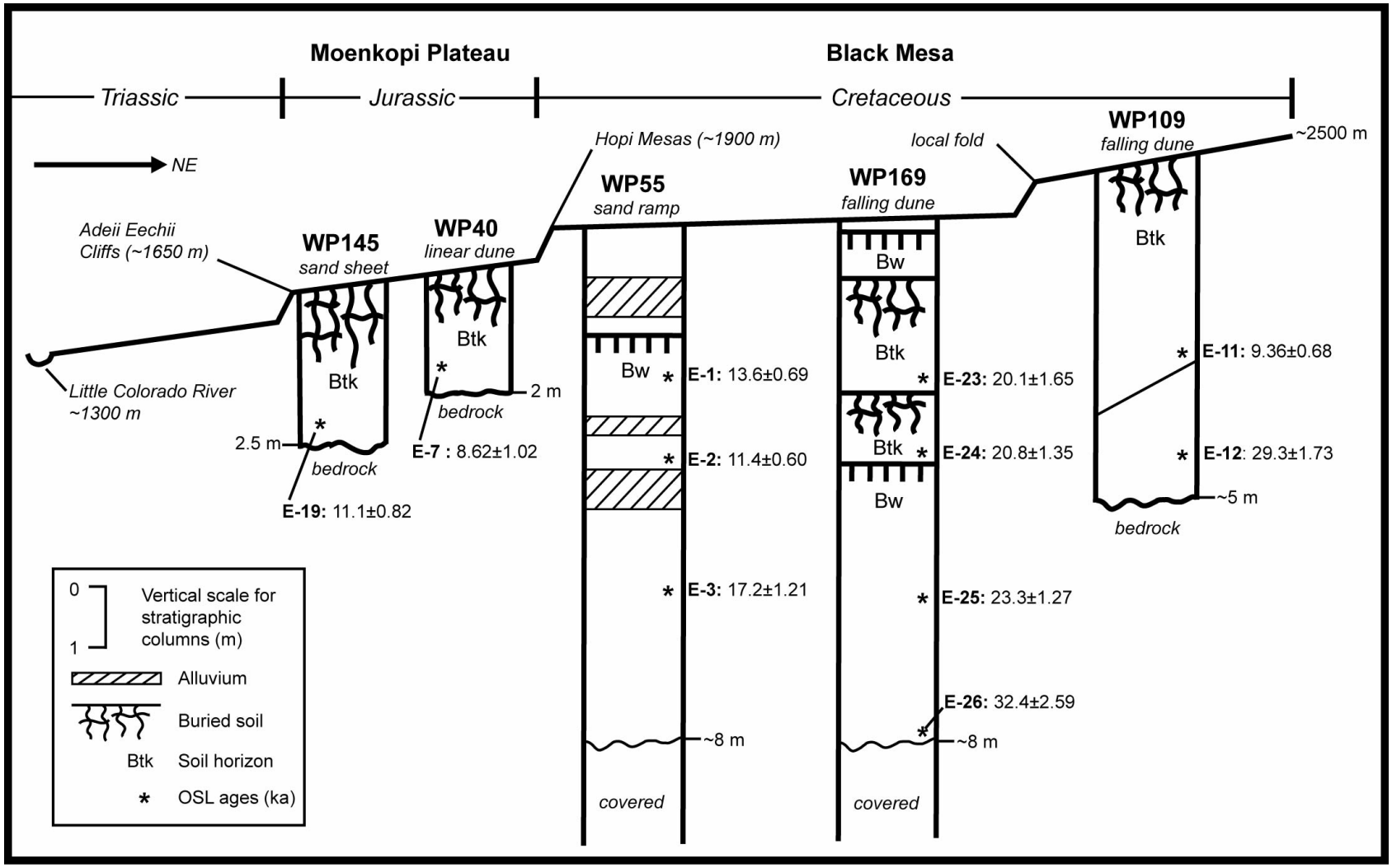

Figure 2: This schematic cross-section shows the distribution of lithology, topography, eolian and soil stratigraphy, and OSL ages of eolian units as well as geographic features mentioned in the text. The two stratigraphic columns on the left were described in one

linear dune and one sand sheet on the Moenkopi Plateau, the three columns to the right depict stratigraphy in one sand ramp and two falling dunes on Black Mesa. Alluvium is indicated by the hatched pattern; all other units in columns are eolian. Colluvium described in the upper 20 cm of WP169 is shown above the weak buried soil profile (Bw). The simplified topographic profile has ~ 20x vertical exaggeration. Scale for stratigraphic columns located in legend. See figure 1 for site locations. The OSL age inversion in WP55 is likely caused by greater water-holding capacity of the fine-grained eolian unit sampled by E-2; increased moisture dampens OSL signal accumulation.

Tables

Table 1: Moenkopi Plateau and Black Mesa area dunes: sample locations, dosimetry, dose rates, equivalent doses, and age estimates. The main SAR parameters included use of the 40-s blue-diode wash step of Murray and Wintle (2000) at the same temperature as the preheat temperature. Signals in the multigrain SAR experiments were recorded with automated Riso Model DA15 OSL-reader systems, also using an EMI 9235Q PMT, and blue light-emitting-diode (LED) stimulation. An aliquot consists of 200-300 grains on a single metal disk. Several quality-control criteria were employed to reject OSL signals and resultant SAR De values. Data rejection criteria were similar to those in common practice (e.g., Wintle and Murray, 2006). We accepted data having 'recycle' ratios within 20% of 1.0, 'recuperation' ratios (e.g., Aitken, 1998) within 2% of zero when recuperation was >20% of the normalized 'natural' signal (Lx/Tx ratio), and test-dose-signal errors were <15%. We forced dose-response curves through the origin.

Sample number	Depth (m)	Water content (%)[a]	K (%)[b]	Th (ppm)[b]	U (ppm)[b]	Cosmic dose additions (Gy/ka)[c]	Total dose rate (Gy/ka)	Equivalent dose (Gy)	n[d]	Age (ka)[e]
WP145: sand sheet near Gold Springs, Adeii Eechii Cliffs, Moenkopi Plateau										
E-19	1.7	3 (37)	1.61 ± 0.11	3.21 ± 0.23	1.43 ± 0.23	0.23 ± 0.02	2.35 ± 0.11	26.0 ± 1.53	15 (24)	11.1 ± 0.82
WP40: linear dune crest north of the Hollow Place, Moenkopi Plateau										
E-7	1.4	2 (20)	0.61 ± 0.01	1.56 ± 0.06	0.58 ± 0.06	0.25 ± 0.02	1.10 ± 0.03	9.50 ± 1.04	34 (40)	8.62 ± 1.02
WP55: sand ramp northeast of Oraibi, Black Mesa										
E-1	2.3	1 (22)	1.33 ± 0.01	2.19 ± 0.12	0.64 ± 0.06	0.21 ± 0.01	1.85 ± 0.05	25.2 ± 1.10	17 (30)	13.6 ± 0.69
E-2	4.1	8 (31)	1.97 ± 0.02	6.71 ± 0.23	1.88 ± 0.13	0.18 ± 0.01	2.97 ± 0.07	33.7 ± 1.68	23 (35)	11.4 ± 0.60
E-3	6.1	2 (21)	1.42 ± 0.01	2.46 ± 0.10	0.67 ± 0.04	0.14 ± 0.01	1.88 ± 0.04	32.4 ± 2.10	22 (38)	17.2 ± 1.21

Table 1 Continued

Sample number	Depth (m)	Water content (%)[a]	K (%)[b]	Th (ppm)[b]	U (ppm)[b]	Cosmic dose additions (Gy/ka)[c]	Total dose rate (Gy/ka)	Equivalent dose (Gy)	n[d]	Age (ka)[e]
WP169: falling dune in Echo Canyon, Black Mesa										
E-23	2.4	2 (27)	1.88 ± 0.04	4.16 ± 0.27	1.15 ± 0.11	0.22 ± 0.02	2.62 ± 0.09	52.7 ± 3.95	20 (20)	20.1 ± 1.65
E-24	3.2	2 (31)	1.98 ± 0.06	3.94 ± 0.21	1.19 ± 0.09	0.20 ± 0.01	2.70 ± 0.07	56.0 ± 3.29	25 (27)	20.8 ± 1.35
E-25	4.5	2 (29)	1.90 ± 0.02	3.60 ± 0.26	1.10 ± 0.09	0.17 ± 0.01	2.54 ± 0.08	59.2 ± 2.60	10 (10)	23.3 ± 1.27
E-26	8.0	5 (30)	1.88 ± 0.05	4.09 ± 0.23	1.21 ± 0.09	0.11 ± 0.01	2.23 ± 0.06	72.2 ± 5.42	28 (30)	32.4 ± 2.59
WP109: falling dune in Wepo Wash Canyon, Black Mesa										
E-11	3.2	2 (26)	1.88 ± 0.07	4.14 ± 0.18	1.09 ± 0.07	0.20 ± 0.01	2.60 ± 0.07	24.3 ± 1.62	41 (50)	9.36 ± 0.68
E-12	4.0	3 (44)	2.37 ± 0.06	5.66 ± 0.22	1.40 ± 0.08	0.18 ± 0.01	3.20 ± 0.07	93.8 ± 4.68	13 (20)	29.3 ± 1.73

[a] Field moisture, with figures in parentheses indicating the complete sample saturation (%). Ages calculated using 10% of saturation values: soils are aridisols and PE is usually greater than P throughout the year, except E-26, which was below water table.
[b] Analyses obtained using laboratory Gamma Spectrometry (high resolution Ge detector).
[c] Cosmic doses and attenuation with depth were calculated using the methods of Prescott and Hutton (1994). See text for details.
[d] Number of replicated equivalent dose (De) estimates used to calculate the mean. Figures in parentheses indicate total number of measurements made including failed runs.
[e] Dose rate and age for fine-grained (125-180 μm) quartz sand. Linear + exponential fit used to estimate equivalent dose data, errors to one sigma.

CHAPTER 2

Black Mesa revisited: Climate change impacts on sand supply and availability and the formation and stability of late Quaternary sand sheets and falling dunes, southern Colorado Plateau, USA

Abstract

Widely used predictive models of eolian system dynamics, typically based entirely on climatic variables, and not accounting for landscape complexity and geomorphic history, fail to give accurate predictions of the dynamics of many dune fields. A growing body of work also suggests that eolian deposits in windy semiarid climates may be more strongly related to increases in sediment supply than to increases in aridity. Topographically controlled falling dunes and sand ramps on Black Mesa are preserved because of their geomorphic position and provide evidence of the paleoenvironmental state of the fluvial and eolian systems before, during, and immediately after the last glacial maximum on the southern Colorado Plateau. In this study, detailed geomorphic mapping and analysis of soil-stratigraphy, in conjunction with optically stimulated luminescence dates from eolian sand dunes of the Black Mesa region of northeastern AZ, reveal a major period of eolian deposition from 17-35 ka, a period of widespread dune stabilization from 8-12 ka, and either localized reactivation of previously stabilized dune forms or local changes in sediment supply during the late Holocene. Cooler, wetter, and more variable climatic conditions during MIS 3 and 2 led to increased sediment supply from stream channels and floodplains allowing eolian sediments to be transported more than 60 km from their source with deposition of this material reducing topographic roughness by filling tributary canyons.

Introduction

Landmark research by Hack (1941) on Black Mesa and surrounding landscapes led to the development of a conceptual model in which sand supply, wind strength, and "aggressiveness of vegetation cover" are combined (Fig. 1) to determine which major dune type will form (Hack, 1941). Because of its utility and simplicity, this conceptual model is still widely used to describe and constrain dominant geomorphic processes in eolian landscapes and estimate paleoenvironmental conditions during eolian transport and deposition. Other more quantitative predictive models using readily available climatic data have been developed to help interpret the current or future state of eolian systems in remote areas with few meteorologic or geomorphic records (e.g. Fryberger and Dean, 1979; Lancaster, 1988, Muhs and Holliday, 1995). We will show that these models, while working well in low-relief landscapes, have limited usefulness in more complicated landscapes with significant spatial variability in relief such as the landscapes studied by Hack.

Topographically controlled eolian landforms, including climbing and falling dunes, are common in dune fields and sand seas where there is sufficient relief, but have not been widely investigated as paleoenvironmental archives. Most paleoenvironmental studies of topographically controlled dunes have been conducted in the Mojave Desert of the southwestern United States (e.g. Lancaster and Tchakerian, 1996; Rendell and Sheffer, 1996; Clarke and Rendell, 1998; Tchakerian and Lancaster, 2002; Pease and Tchakerian, 2003). These studies show that topographically controlled dunes have accumulated over and persisted, in some cases, for at least the last 40,000 years.

Kocurek and Lancaster (1999) developed a conceptual process-response model to describe the state of any eolian system by determining three system factors: the transport

capacity of the wind (a function of speed and turbulence) also referred to as mobility, sediment supply, and sediment availability. This alternative model differs from earlier quantitative models based entirely on climatic information in that it requires an understanding of sediment availability, which is a function of sediment characteristics (e.g. grain size and shape), internal cohesion of sediments and surface roughness. Sediment availability is diminished with increased sediment cohesion (surface crusts, soil moisture, roots, etc.) or above ground vegetation that decreases turbulence and therefore decreases transport capacity. Thus sediment availability is thought to decrease with increasing effective moisture, which encourages growth of vegetative cover, leading to sediment storage (e.g. Kocurek and Lancaster, 1999).

Sediment supply for eolian systems can be derived from channels and floodplains, exposed lake beds, reworking of existing eolian deposits, or directly from the impact of saltating grains on rocks, especially weakly lithified sandstones. The rate or volume of sediment supply can change with weathering rates (e.g. McAuliffe et al., 2006; Scuderi et al., 2008), a change in climatic state, such as during the Pleistocene-Holocene transition (e.g. Bull, 1991) or during transitions from drier to wetter conditions under a dominantly semiarid climate (e.g. McAuliffe et al., 2006; Scuderi et al., 2008), a change in the type or density of vegetation cover (e.g. Schumm and Lichty, 1965; Schlesinger et al., 1990; Okin et al., 2001), or a change in the behavior of the fluvial system supplying sediment to the eolian system (e.g. Muhs and Holliday, 1995; Forman et al., 2008). Sediment supply has also been shown to increase from cannibalization of previously stabilized sand dunes, through increased wind speed (e.g. Bagnold, 1954; Lancaster, 1988) or decreased vegetative cover resulting from land use practices (e.g. Schlesinger et al., 1990) or decreased effective moisture (e.g.

Lancaster, 1988; Muhs and Holliday, 1995; Holliday, 2001; Wolfe, et al., 2000; Lancaster 2003; Forman et al., 2008).

In order to organize the description and discussion of the state of the eolian system in the topographically complex landscapes of Black Mesa, we apply Kocurek and Lancaster's (1999) process-response model of eolian sediment system state to infer how geomorphic processes have changed with changing system drivers. This study uses field observations, aerial and satellite imagery, soil-stratigraphic techniques, and optically stimulated luminescence (OSL) age determinations to quantify and analyze the spatial and temporal distribution of eolian deposits of the Black Mesa region.

Eolian deposits in the study area represent complex interactions between climatically controlled geomorphic processes (e.g. wind regime, effects of stream morphology, variations in bedload, and soil development) and lithologically-controlled relief, which both affect and are influenced by transport capacity, sediment supply and sediment availability. In this paper, we focus on three major questions relative to topographically-controlled dunes in the Black Mesa region: 1) Can these dunes provide a potential source of paleoenvironmental information on Black Mesa, a region with few records of environmental change? 2) Is the timing of the deposition of the largest volumes of eolian sediment in this landscape associated with increases in sediment supply during the late Pleistocene? and 3) Can application of a model that includes the geomorphic history of a landscape, more accurately describe or predict eolian system behavior in complex landscapes?

Previous Work

Eolian landforms on and around Black Mesa were first described in detail by Hack (1941). In this work, largely focused on geomorphic studies on eolian landforms of the

broad, flat portions of the landscape below the Hopi Mesas, documented that eolian deposits were widespread throughout Navajo country and consisted of active dunes at lower elevations with stable forested dunes at higher elevations (Fig. 2). Hack described both climbing and falling dunes within the mapped area, but considered them to be a minor dune type. With little age control besides that provided by Pleistocene fossils or in the archaeological context of cultural materials such as potsherds, Hack assumed that eolian deposition represented periods of increased aridity. Among his important findings, Hack (1941, 1942) demonstrated that 1) eolian sediments are derived from many sources including stabilized dunes, local sedimentary rocks, and floodplains of ephemeral streams, 2) migrating eolian deposits affect the fluvial system by changing the slopes of streams and filling arroyos as they intersect ephemeral channels, 3) sediment recirculates in this landscape (eolian sediment is transported northeast from floodplains and returns to the southwest via the fluvial system), and 4) that because of its high infiltration capacity the "abundant dune sand provides a better groundwater supply and inhibits arroyo cutting" in the region.

Subsequent studies of eolian landscapes of the southern Colorado Plateau documented the timing of multiple periods of eolian activity and stability using numerical age determinations from radiocarbon dating of buried organic material, or thermo- or optically-stimulated luminescence techniques (e.g. Breed and Breed, 1979; Billingsley, 1987; Wells et al., 1990; Stokes and Breed, 1993; Smith and McFaul, 1997; Reheis et al., 2005; Ellwein et al., in press). In the Chaco dunes of northwestern New Mexico, Wells et al. (1990) identified three major ages of eolian deposits at ~16-12 ka, 6.5-2.8 ka and < 1.9 ka. Wells et al. (1990) also showed that sand sheets were the primary eolian landforms on this relatively flat landscape and that extensive sand sheets and associated soil development promote

landscape stability. On the Moenkopi Plateau to the west of our study area, Breed and Breed (1979) speculated that eolian deposits could have been deposited as early as 100 ka, and Stokes and Breed (1993) postulated three eolian reactivation phases during the mid to late Holocene: 4.7 ka, 3-2 ka, and <0.4 ka. Timing of eolian events identified in the Canyonlands region (Reheis et al., 2005) is in broad conformity with some of these studies (see Reheis et al., 2005 for a detailed review of southern Colorado Plateau eolian history). Two major contributions of Reheis et al. (2005) with implications for this study are 1) identification of the oldest known eolian deposits on the Colorado Plateau (ca. 46 ka) and 2) recognition and documentation of increased dust flux during the Pleistocene-Holocene climatic transition that accelerated the formation of soil profiles with illuvial silt and clay (Bt horizons).

Study Area

Black Mesa is a prominent topographic highland in northeastern Arizona sloping from ~2500 m at the steep escarpment that defines its northern edge to 1300m at its southwest margin near the Little Colorado River. The study area lies in the center of the Black Mesa region and is bounded by the northern escarpment, the Little Colorado River, Dinnebito Wash and the Jeddito Wash drainage divide (Fig. 2). This Cenozoic structural basin is ringed with Triassic and Jurassic sedimentary rocks, including many eolianite units, and is capped with the Cretaceous Mesa Verde Group sandstones (Fig. 3). The study area lies entirely on the Navajo and Hopi Reservations.

At the lowest elevations in the study area (roughly 1300 to 1700 m), eolian deposits southwest of the Hopi Mesas support a subshrub grassland (e.g. *Ephedra* spp., *Artemesia filifolia*, *Yucca spp., Hilaria jamesii, Muhlenbergia pungens, Oryzopsis hymenoides*). Higher elevations (2000 to 2500 m), underlain by Mesa Verde Group sandstones, support a mixed

conifer forest dominated by Douglas-fir and Ponderosa pine (*Pseudotsuga menziesii and Pinus ponderosa)*. Sand sheets at mid-range elevations (1700 to 2000 m) are dominated by open, juniper-sage grasslands (*Juniperus monosperma, Artemesia tridentata, A. filifolia, Ephedra and Yucca spp., Bouteloua gracilis, H. jamesii, O. hymenoides)* with piñon-juniper woodlands (*Pinus edulis, J. monosperma, Juniperus osteosperma, B. gracilis*) dominating rocky substrates.

The climate of Black Mesa is semiarid with mean annual precipitation (MAP) ranging from < 20 cm at the Little Colorado River to ~ 40 cm at the northern escarpment of Black Mesa (1961-90; WRCC, 2010). Mean annual temperature (MAT) is ~11 °C (52 °F) for stations in or near the study area (e.g. Piñon, Oraibi, Tuba City, Winslow; WRCC, 2010). MAP and MAT data are not available for the highest elevations of Black Mesa, but the mixed conifer forest indicates higher precipitation and/or substantially reduced evapotranspiration relative to lower elevations. Average annual wind speed of 3.7 m/s is from the southwest at the Winslow Airport (~30 km SE of Leupp) and the three windiest months (April, May, and June) average 4.7 m/s (1996-2006; WRCC, 2010). Winds recorded at the Winslow airport and on the Moenkopi Plateau (USGS Gold Spring station) are more than sufficient to move sand-sized sediment under modern conditions (Helm and Breed, 1995; Muhs and Been, 1999; Lancaster and Helm, 2000).

Methods

Mapping and Image Analysis

The distribution of eolian deposits was mapped using orthorectified Landsat images at ~28.5m resolution and a mosaic of USGS black and white digital orthophoto quadrangles (DOQs) with 1m resolution. Eolian landforms were mapped by analyzing Landsat spectral

variations, the shape, distribution, and relative brightness of features in the DOQ mosaic, interpretation of vegetation type and density, and spatial scale of geomorphic features recognized during field observations and/or in DOQs. All data was georeferenced and compiled in a GIS project file for further analysis (ArcMap: ESRI, 2010).

Eolian deposits, which largely consist of linear dunes, sand sheets, and topographically-controlled falling and climbing dunes, were described during initial field reconnaissance and mapped at scales between 1:5,000 and 1:20,000 on a field-hardened laptop. Field maps were refined using a combination of Landsat imagery (June, 2000), the 1m DOQ mosaic, and a slope map derived from a 10 m digital elevation model (DEM) mosaic. Image processing of Landsat band combinations allowed optimum visualization of eolian deposits and differentiation from non-eolian materials. The upper contacts of topographically controlled dunes were confirmed using the sharp difference in spectral response of eolian sand and bedrock in Landsat imagery and were checked against the higher resolution DOQ mosaic. The lower contact of topographically controlled dunes was identified using a combination of Landsat and DOQ image analysis combined with evaluation of the slope map. Because of the similarity of spectral response between rocks and eolian deposits, falling dunes and eolian valley fills were mapped conservatively. If these deposits were not clearly observable in imagery and were not visited in the field, they were not mapped even if slope characteristics, and/or a decrease in surface roughness suggested their presence. Sand sheets were mapped at coarser scale than other dune types (~ 1:75,000). For clarity, sand sheets less than 4 km^2 are not depicted.

Eolian Stratigraphy and Soil Characterization

The eolian history of the study area was reconstructed through evaluation of stratigraphy using soil stratigraphic techniques and relative and numerical age control. Stratigraphy and soils were described in hand-dug soil-pits or road cuts and in natural exposures, such as blowouts and arroyos. Field descriptions of soil profiles include depth and thickness of soil horizons, horizon boundaries, soil color, texture, structure, consistence, and morphology of clay films and pedogenic carbonate (e.g. Birkeland, 1999). Topographically-controlled dunes were described where internal stratigraphy was exposed by stream erosion. While substantial incision through falling dunes in the study area is uncommon, three localities with > 8 m sub-vertical exposures were identified and sampled: falling dunes near Piñon (WP109) and Echo Canyon (WP169) and an eolian valley fill/sand ramp near Oraibi (WP55).

Bulk soil samples were collected from each horizon of each profile or unit from stratigraphic sections, air-dried, and split for various analyses. Prior to particle size analysis, carbonate was extracted with a 15% hydrochloric acid solution, and organic matter was extracted with a 30% solution of hydrogen peroxide when necessary. Soil carbonate content was measured using a modified Chittick apparatus following procedures described in Machette (1985). Particle size analysis (PSA) on the < 2mm fraction was performed using sodium pyrophosphate dispersion, sieve separation, and pipet extraction following settling time procedures (Day, 1965) for several samples; others were determined as volume percentage by a laser-light scattering method (McCave and Syvitski, 1991) using a Malvern 2000 Laser Particle Size Analyzer. Particle-size distributions measured using the two

methods have been shown to be similar when analyzing sand-sized, quartz-dominated sediments (Buurman et al., 1997; Hayton et al., 2001).

Optically Stimulated Luminescence (OSL) Age Determinations

Eolian quartz sand was OSL dated directly using samples collected from eolian parent materials in known stratigraphic context under light shielded conditions. OSL is a luminescence phenomenon related to the interaction of natural radiation within the mineral grains. The natural radiation activates and traps electrons at defects within a mineral lattice. The latent signal is acquired over time after burial of the mineral grain and released when the grains are exposed to stimulation energy (heat or light).

OSL provides an estimate of burial age according to the following:

$$\text{OSL age} = \frac{\text{equivalent dose (Gy)}}{\text{natural dose rate (Gy/ka)}} = \frac{D_E}{D_R}$$

where the dose rate (D_R) is the combined effect of the naturally occurring radiation contributions from K, U, Th, Rb, and cosmic ray components, dampened by moisture content of the sediment. High-resolution (Ge detector) gamma spectroscopy was used to generate the elemental concentration analyses. Equivalent dose (D_E) was determined by single aliquot regeneration (SAR) methods while using blue stimulated luminescence (BSL) on quartz grains. Replicated equivalent dose measurements were used to calculate mean D_E; methods described in detail below. OSL ages from this study were used to develop correlated ages for otherwise undated soil profiles and stratigraphic sections.

OSL sampling, equivalent dose preparation and measurement

Our sampling strategy consisted of obtaining OSL samples from nine well-defined stratigraphic contexts. Five of the nine selected sites produced a total of fourteen OSL

samples. Each sample was obtained by driving a sharpened polyvinyl chloride (PVC) tube horizontally into a freshly cleaned face of the soil profile or stratigraphic section, entirely filling the tube with sediment. The ends of the PVC tube were capped and taped and the tube was encased for transport in a photography film bag. An additional 0.6 to 0.8 kg of bulk sediment was also extracted from around the OSL sampling sites for dosimetry determination and measurement of the present day saturation moisture content.

Under subdued orange light, possible light-exposed end material was discarded from each tube (~ 3 cm). Samples were prepared for luminescence dating using standard procedures for hydrochloric acid (4N HCl), hydrogen peroxide (35-50%), wet sieving, heavy liquid separation of feldspar from quartz and hydrofluoric acid (50%) on the remaining quartz grains (Millard and Maat, 1994; Singhvi *et al*., 2001; Mahan and Brown, 2006) in this order, with appropriate modifications.

To remove feldspars and to isolate pure quartz from the selected sand fraction, we centrifuged the sand sequentially in lithium sodium tungstate (LST) heavy liquid solutions with densities of 2.58 and 2.66 g ml^{-1}. The float from the 2.66 g ml^{-1} solution was subjected to a 50% solution of HF acid for 40 minutes while in an ultrasonic bath. After pouring off the HF solution, the sample was placed in 6N HCl for five minutes while in an ultrasonic bath and finally resieved to winnow broken grains.

For blue-light OSL, we affixed sand-size grains to the center of a 1-cm diameter steel disc with a light cover of Silicone spray. The OSL on quartz was obtained from fine sand-sized quartz separates between 90-250 μm, although we employed the strategy of using the dominant grain size unique to each particular sample. Each of the discs or aliquots contained approximately 200 to 250 grains (1 mm mask size).

All quartz grain samples were measured using the single-aliquot regenerated dose (SAR) procedure (Murray and Wintle, 2000, 2003; Murray and Olley, 2002, Wintle and Murray, 2006), with continuous wave (CW-OSL) blue-light stimulation. A few of the samples were preceded by an IRSL "wash" of 100 seconds at 60 °C (Bøtter-Jensen et al., 2003; Duller, 2001), but this was discontinued when there was no observed signal. Luminescence measurements were performed using a Risø TL-DA-15 OSL reader, fitted with an internal 90Sr/90Y beta-source. Quartz was stimulated for 40 seconds at 125 °C with blue diodes with a wavelength of 470 ± 30 nm and an intensity of 22 mW cm-2. The emitted photons were filtered through two Hoya U-340 filters.

The growth of the luminescence with increasing dose was represented well by a single saturating exponential and linear function and illustrates the generally fast OSL component of the quartz samples when utilizing the SAR protocol. Comparisons of the equivalent doses obtained on the quartz fraction indicate that the SAR procedure returned reliable, precise measurements. For each aliquot that was measured, the complete growth curve was constructed based on the measurement of three regenerative doses (2x the natural). The response to a zero dose was also measured to see whether the growth curve passes through the origin. To verify if the sensitivity correction works well, a second measurement of the response to the lowest regenerative dose was also made (a recycling ratio). Recycling ratios were between 0.92 and 1.11, within ~10% of unity. The quartz samples were not affected by recuperation and therefore no elaborate protocols were needed to counteract this situation. The samples were initially tested using preheat plateaus and dose recovery tests (see Appendix A). Equivalent dose aliquots were run at either 220 °C for ten seconds or 200

°C for ten seconds, depending on the initial estimate obtained from the preheat plateau test for a specific site. The averaged equivalent dose values are summarized in Table 3.

Dosimetry preparation and measurement

While many naturally occurring elements have radioactive isotopes, only the potassium and the uranium and thorium decay series have radioisotopes that produce gamma rays of sufficient energy and intensity to be measured by gamma ray spectrometry. Average terrestrial abundances of these elements are in the range 2-2.5% K, 2-3 ppm U and 8-12 ppm Th. Dosimetry measurements of potassium (K), uranium (U), and thorium (Th) were obtained using high-resolution germanium gamma ray counts. Germanium semiconductor detectors use the electronic carriers (electron-ion and electron hole pairs) created by the absorption of gamma ray photons in the germanium detector. The energy resolution of these detectors is very high, but because of their small volume, their sensitivity is low and it may take tens of minutes to record a spectrum. Quantitative analysis is essentially comparative: the radiation from a rock sample is compared with the radiation from known standards. The accuracy and precision of the results depends on many factors: the size and energy resolution of the detector; the mass and geometry of the sample; the shielding of laboratory background; counting time; data processing procedures; and the quality of the radioactive standards.

Bulk samples were dried, homogenized by gentle disaggregation, weighed, sealed in plastic planchets having a diameter of 15.2 cm by 3.8 cm (some modification from Murray *et al*., 1987), and immediately placed in a gamma-ray spectrometer for ~8.5 hours. Samples were stored for a minimum of twenty-one days to allow radon to achieve radioactive equilibrium, and the measurements were repeated. The fraction of radon emanation was estimated from the difference of these two spectrometer measurements. A sealed/unsealed

ratio of <1.10 is not considered to represent significant radon escape or disequilibrium under laboratory conditions. These count rates are accurate for calculating dose rates (Aitken, 1985; Aitken, 1998; Snyder and Duval, 2003); the range of ratio change was 0.94 to 1.09.

Dose rates are given for the quartz component, which is missing the alpha component, as well as about 10% of the beta component, due to the hydrofluoric etch performed on the quartz grains before they were analyzed for OSL. Cosmic-ray dose rate was estimated for each sample as a function of depth, elevation above sea level, and geomagnetic latitude (Prescott and Hutton, 1994) and all contributions to the dose rate were corrected for the effect of moisture. Measured elemental concentrations, associated dose rates, and cosmic ray contributions are shown (Table 3). Alpha and beta contributions to the dose rate were corrected for grain-size attenuation (Aitken, 1985).

Results

Distribution of eolian deposits

In general, dune morphology and stability are strongly linked to the distribution of lithology, relief, and elevation throughout the study area (Fig. 3). Topographically controlled eolian landforms are especially widespread downwind from the prominent, steep cliffs of the Hopi Mesas that define the southern extent of the Cretaceous Mesa Verde Group sandstones, though preserved climbing dunes are uncommon in the study area. Most falling dunes and sand ramps are deposited downwind of the Hopi Mesas in small canyons cut into the Cretaceous Mesa Verde Group sandstones. The canyons trend roughly perpendicular to the ephemeral Tusayan Washes, especially Oraibi and Polacca Washes. Stabilized sand sheets are the dominant eolian landforms in high elevation, low-relief settings (e.g. drainage divides) on the relatively flat lying Mesa Verde sandstones. Active eolian landforms,

especially linear dunes, dominate the low-relief landscape southwest of the Hopi Mesas known as the Painted Desert.

Topographically controlled dunes have the greatest volume (Fig. 4) and are largest in aerial extent where tributary basins are widest and relief is greatest near the Hopi Mesas. In these locations, eolian sand fills tributary basins with interfingering falling and climbing dunes (Fig. 5). Eolian landforms progress from eolian valley fills in the southwest, to distinct falling and climbing dune pairs, to unpaired falling dunes at the furthest northeast extent of Black Mesa (Fig. 4). Field observations and image analysis suggest that 4° is the minimum toe slope for these landforms. As mapped, topographically controlled eolian deposits cover almost 15 km^2 between the Dinnebito and Polacca drainage basins northeast of the Hopi Mesas.

Sand sheets are the most aerially extensive eolian landforms. In general, sand sheets have poorly defined edges and uneven thickness, and are commonly less than 2 m thick in the study area. Linear dunes are common within the low-relief sand sheets mapped in the Painted Desert southwest of the Hopi Mesas. Where sand sheets occur on divides on Mesa Verde sandstones, such as between Dinnebito and Oraibi or between Wepo and Polacca washes, linear dunes are uncommon. Conservatively mapped, sand sheets cover 30% (2110 km^2) of the study area (Fig. 5).

The trends of linear dune crests, which appear distinctly brighter than interdune areas in the gray-scale DOQs, were mapped as lines that extend along the apparent length of the crest. Linear dunes are oriented parallel to the dominant southwest wind direction and document the direction of sand transport from the southwest to the northeast. In the Painted Desert, linear dunes principally occur downwind of non-incised stream channels and

floodplains and include abundant linear dunes and sand sheets downwind from the distributary system at the Oraibi-Polacca confluence (Fig. 6), local occurrences from Black Mesa washes as they become non-incised downstream from the Hopi Mesas, and the wide meandering channels and largely non-incised floodplains upstream of the Oraibi-Little Colorado River confluence east of Leupp. Widely varying spectral responses of the fluvial and eolian sediments and bedrock in these regions support Hack's observations (1941, 1942) that eolian sediment is contributed from a variety of sources. Because transport directions of the eolian and fluvial system oppose each other, sediment transported to the northeast by wind is likely re-entrained by the fluvial system, further mixing source signals, and returned to the Painted Desert as first suggested by Hack (1941).

Stratigraphy and Soils

Topographically-controlled dunes

The southernmost topographically-controlled dune stratigraphic section , WP55, is located in the Oraibi Wash drainage basin ~7 km north-northeast of Oraibi, AZ. This high relief tributary basin is almost completely filled with sand as falling dunes merge with climbing dunes and eolian sediments are intercalated with hillslope and alluvial deposits (Fig. 4C). The resulting landform is most appropriately termed a sand ramp (Lancaster and Tchakerian, 1996). The ephemeral channel in this unnamed tributary basin excavated a sub-vertical 15 m exposure through the deposit. Six 1-2 m pits were excavated by hand on the exposed face to a total depth of 7.5 m from the surface to observe and describe internal stratigraphy. The entire exposure was not cleared to its base as it was buried by a thick accumulation (~2-3 m) of slumped material.

Approximately 75% of the described section is comprised of subhorizontal laterally continuous units composed of frosted, rounded to well-rounded, well sorted, medium- to fine-grained eolian sand, often featuring foreset beds that dip ~20° to the northeast. Most of these eolian units are brown to yellowish brown (7.5YR or 10YR Munsell colors), with the exception of a yellowish red bed (5YR5/6) from 3.5-4 m composed of well-sorted, very fine sand. Eolian deposits are intercalated with colluvial and alluvial deposits throughout the upper 4 m of the section. Pedogenic modification was weak to nonexistent in these sediments; as a result, this section was not described using soil description nomenclature (Table 2).

Three eolian units at the WP55 site (Table 3) were dated using OSL. Sample E-3 was collected at 6.1m near the middle of the outcrop from moderately sorted, light yellowish brown eolian sand. The OSL age of 17 ± 1ka suggests that the majority of this deposit was emplaced before the last glacial maximum though unexcavated underlying deposits could be appreciably older. OSL age estimates from the top 4 m of this section date are 14 ± 1 ka at 2.3 m in a moderately sorted unit with prominent foresets (sample E-1) and 11 ± 1 ka in a massive very fine yellowish red sand at 4 m (sample E-2). This age inversion is addressed in the discussion section.

Paired falling and climbing dunes such as those at Echo Canyon, 34 km east northeast of WP55 (Fig. 4B) become common ~15 km northeast of the Hopi Mesas. At the Echo Canyon site ~12m of falling dune stratigraphy is exposed where the small tributary stream fed by Echo Spring has eroded the dune toe. Six 1-2 m pits were excavated by hand to a total depth of 8 m from the surface. As with WP55, the entire exposure was not cleared to the base because of ~2-3m thick slumped material covering the footslope.

The stratigraphic section at Echo Canyon (WP169) is comprised of predominantly eolian sediments interbedded with a thin bed of colluvium near the top of the section and rare thin gravel lenses within the upper 2.7 m of the section (Table 4). Black on white slip and corrugated sherds were observed at the lower contact of the uppermost eolian unit (~0.9 m from the surface at the base of horizon 2Cb). Four buried soils were identified: two weakly developed soil profiles characterized by reddening and the accumulation of soil carbonate (horizons 2Bwb, 2Bkb, and 5Bwkb) and two moderately developed soils with faint illuvial clay accumulations (3Btkb and 4Btkb). Eolian sediment in the lowest exposed portions (5-8 m) exhibits prominent, hard, 2-4 cm thick yellowish red bands alternating and anastomosing with 2-4 cm thick bands of reddish yellow pedogenically unaltered quartz sand. This unit was at field saturation when sampled in June 2008, strongly suggesting that the bands represent groundwater staining.

OSL ages from eolian units in the Echo Canyon strata range from 20 ± 2 to 32 ± 3 ka (Table 1). Ceramic sherds observed at the base of the uppermost eolian unit, which shows very weak soil profile development, strongly suggests that this unit was deposited during the latest Holocene (~1200-600 yrs BP; F. Scott Worman, 2010 personal communication). Eolian sediments below 2.5 m, which comprise 90% of the sediments described in this deposit, are estimated to be between 20-35 ka based on OSL ages.

The falling dune in Wepo Wash Canyon near Piñon (WP109) is both the highest elevation falling dune observed on Black Mesa and the furthest downwind from the Hopi Mesas. This falling dune is comprised of two eolian units and is dissected by an arroyo that exposes both the dune and adjacent valley fill alluvium that buries the dune toe. The uppermost unit is well-sorted, brown medium sand with 5-10% lithics and features a well-

developed soil at the surface (Btk horizon with a stage I+ soil carbonate horizon) that has formed in the upper meter of the deposit. The unit was sampled at 3.2 m depth and yields an OSL age of 9 ± 0.7 ka (E-11). Below the uppermost unit is a pedogenically unaltered, well sorted, fine- to very fine-grained, yellowish brown sand with <5% lithics. This unit was sampled at 4 m (E-12) and yielded an OSL age of 29 ± 2 ka. This is the only falling dune deposit that was exposed, described, and sampled to the underlying contact with bedrock.

Sand sheets

Sand sheets located on low relief generally undissected uplands locally contain linear dunes, blowouts, and parabolic dunes, but are predominantly slightly undulating with few distinct eolian landforms. These flat expansive high fetch areas are characterized by sand deposits < 2 m thick with well-developed soil profiles (Btk) that often extend to the underlying contact with bedrock. Soil profiles are often capped with up to 50 cm of pedogenically unmodified, fine to medium, well-sorted sand. Active dunes in the mesa top landscape positions are uncommon except to the west on the Moenkopi Plateau (e.g. Billingsley, 1987) and the southernmost extent of First Mesa (Hack, 1941).

Three representative sand sheet sites occur at roughly similar elevations and distances downwind from the Hopi Mesas. Site WP73 is located between Dinnebito and Oraibi Washes, WP164 between Oraibi and Wepo Washes, and WV10-06 between Wepo and Polacca Washes (Fig. 5). All exhibit similar vegetation, sediment, and soil characteristics (Tables 1, 3, and 4). The uppermost unit at each site is composed of an unweathered thin sand mantle (10-50 cm deep) underlain by a buried soil with an abrupt, smooth to wavy upper boundary, weak to moderate Btk horizon development, and up to stage II carbonate morphology (e.g. Gile, 1961; Birkeland, 1999). The abrupt boundaries that commonly occur

between stacked eolian parent materials are interpreted to reflect periods of erosion probably formed during saltation that occurred during transportation of the overlying unweathered sand mantle. Accumulations of illuvial clay and carbonate in the buried B horizons, however, provide cohesion and therefore confer some resistance to erosion. An OSL sample from the base of the soil profile above the contact with bedrock at site WP164 yielded an age of 11 ± 1 ka. A similar degree of soil development at the other three stable sand sheet sites suggests that all three are roughly time correlative.

A stable sand sheet in the Polacca Wash drainage basin at ~1970 m was described where exposed in a borrow pit near Blue Gap, AZ, 57 km northeast of the Hopi Mesas. The stratigraphic column is an amalgamation of three sub-sections (WP112, WP113, WP114) described where stratigraphy could be traced laterally. The lowermost parent material is composed of poorly sorted, subangular, quartz sand, which we infer is an alluvial deposit. All other parent materials in the compiled section consist of well-sorted, rounded to well-rounded, dominantly quartz sand interpreted to be of eolian origin. Interestingly, this site is unusual in that quartz grains in the eolian units are very weakly frosted, which suggests a local, non-eolian sand source, possibly from the sandstones of the Mesa Verde Group.

The buried soils at the Blue Gap borrow pit provide an exception to the single profile pattern seen in most stable sand sheet sites (Fig. 7). A thin mantle of weakly pedogenically altered sand is present at this site and is underlain by a parent material hosting a weak color B horizon (3Bw). The additional underlying parent material hosts a Btk horizon with an abrupt upper boundary and very similar soil properties to those found in the other stable sand sheet soils. A prominent steeply inclined soil carbonate zone (5Btbk; 9.11% carbonate; Table 4)

occurs at the southern end of the described exposure; this unit was only locally identified and was not traceable throughout the outcrop.

The largest volume of sediments at the Blue Gap borrow pit return OSL ages of 8 ± 0.5 ka from 4C, 8 ± 1 from 5C, and 9 ± 1 ka from 6 C (Table 3). These ages suggest that the largest volume of sediments exposed at the Blue Gap borrow pit have similar ages to the other stable sand sheet sections. The late Holocene OSL age (2 ± 0.2 ka) from the thin, laterally discontinuous third eolian parent material at the Blue Gap borrow pit suggests either local reactivation of eolian deposits or a local increase in sediment supply, perhaps from Polacca Wash, during the Holocene.

Active eolian landforms

Most active eolian landforms occur south of the Hopi Mesas. Linear dunes and sand sheets in the Painted Desert were not formally described in this study or sampled for OSL age estimates. Preliminary field investigation and mapping of these eolian deposits indicates that most dunes in this landscape position either completely lack soils, or show very weak color reddening or few incipient carbonate nodules. Because of these field relationships, we infer that the majority of dunes located between the Little Colorado River and the Hopi Mesas are either currently active or were deposited during the latest Holocene.

Discussion

The Little Colorado River, and the Dinnebito, Oraibi, and Polacca Washes southwest of the Hopi Mesas, are all low gradient streams with broad flood plains that drain basins dominated by sedimentary rocks. These floodplains are inferred to be the primary source of sand for the eolian system in the Black Mesa region throughout the late Quaternary. Sand volumes in the topographic lows of tributary canyons decrease to the northeast with

decreased tributary basin size and relief in part because of diminished accommodation space, but also as supply decreases with distance from these sources.

Sand comprising falling dunes and eolian valley fills on Black Mesa was trapped episodically during the last glacial and interglacial periods, as shown by OSL age estimates that range from 9-35 ka, but the distribution of OSL age estimates and the number of buried soils varies substantially (Fig. 8). The Echo Canyon falling dune (WP169) exhibits multiple buried soils each representing a period of relative stability (nondeposition and soil formation) before the last glacial maximum (LGM). This portion of the eolian record does not exist in Wepo Wash Canyon (WP109), where the unconformity between the two eolian parent materials and an absence of a buried soil profile likely reflects local erosion of contemporaneous eolian deposits between roughly 10 and 30 ka. However, at both falling dune sites, the lowermost sampled sand is of roughly similar age (30-35 ka).

Geomorphic processes interpreted from the Oraibi sand ramp section (WP55) clearly differ from those dominating at the falling dune sites. Interbedded eolian, alluvial, and colluvial sediments show that the sand ramp has a more complex late Pleistocene geomorphic history probably due to a larger contributing basin area, greater relief, and closer proximity to sand supply. The lack of buried soil profiles at the WP55 site suggests either that there were few extended periods of landscape stability during deposition at this location or that soil profiles were eroded before subsequent deposition. The oldest eolian units were probably deposited against bedrock outcrops on the southwestern wall of the canyon as they began to accumulate and build out in the downwind direction. Modern streams have not excavated the vast volume of sand in this tributary, so these deposits are not exposed. As

such, the oldest age from this site (17 ± 1ka; E-3) does not reflect the oldest possible eolian deposits within this basin.

The Grand Falls lava dam emplacement along the Little Colorado River at roughly 20 ka is one well-constrained regional event with implications for the stratigraphy at WP55. The dam impounded water and sediment along the Little Colorado River (Duffield et al., 2006) upstream of the confluence with Dinnebito Wash. Aggradation associated with this local event increased local eolian sediment supply and may be the source for some of the sediments at the Oraibi sand ramp (WP55) directly downwind from the lava dam. OSL ages from WP55 are not included as a distinct period of sand deposition in figure 10 because they are only recorded at one site. Channel damming would explain the somewhat anomalous 12-18 ka OSL dates obtained from these sediments. However, eolian deposits from the late glacial period may not be regionally anomalous as they are identified in other Colorado Plateau eolian systems (Wells et al., 1990; Reheis et al., 2005).

Ages of topographically controlled dunes represent periods when sand was trapped in landscape lows during conditions of high sand supply and availability. In contrast, OSL ages from the stable upland sand sheets do not represent periods when sand was delivered to this landscape position, but rather the timing of landform stabilization (e.g. Lancaster and Tchakerian, 2003; Chase, 2009). Thin sand sheets located on the low-relief mesa top or divide positions north and east (downwind) of the Hopi Mesas exhibit stratigraphically simple, moderately developed soil profiles. These landforms typically display one well-developed buried soil characterized by a Btk horizon, which is usually buried by a thin layer of active eolian sand. Field relationships suggest that eolian sediments within stable sand sheets have been only locally modified since stabilization. OSL ages show that the stable

sand sheets were stabilized between roughly 8-12 ka, during or shortly after the Pleistocene-Holocene climate transition.

Paleoenvironmental context for eolian chronostratigraphy

Full glacial (MIS 2; 27-15 ka) paleoclimatic and paleoenvironmental conditions are fairly well documented for regions surrounding the southern Colorado Plateau. During the last glacial maximum, ca. 18 ka, Grand Canyon vegetation ranges were depressed by 600-1000 m below modern limits (e.g. Cole, 1990; Betancourt, 1990; Thompson et al., 1993). Moraines that record glacial advances near Fish Creek, Utah are documented at 23.1 ka, 20 ka, 16.8 and 15.2 ka using helium exposure ages (Marchetti et al., 2005). Regional lake (Hevly, 1985; Anderson, 1993; Hasbargen, 1994; Anderson et al., 2000; Jimenez et al., 2008; Anderson et al., 2008) and groundwater levels on Black Mesa (Zhu et al., 1998) and in southeastern Arizona (Waters, 1989; Pigati et al., 2009) were high (Fig. 9). During full glacial conditions, with a southerly depressed jet stream and strong pressure gradients, winds are estimated to have been even more powerful than present (e.g. COHMAP, 1988; Kutzbach et al., 1993).

The Pleistocene-Holocene transition in this region was probably also effectively moister than modern conditions. Plant assemblages reconstructed from packrat middens show that by 12 ka temperatures were still 3-5 °C cooler than modern and summers ranged between 35-120% wetter (Betancourt, 1990) depending on location. Weng and Jackson (1999) show that cool moist conditions persisted from 11 ka until approximately 8 ka in lakes on the Kaibab Plateau in north central Arizona ~150km west northwest of the study area.

The oldest eolian sediments currently in storage on Black Mesa were deposited during MIS 3 (the last interstadial during the Wisconsin), but few chronologically

constrained records of paleoclimatic and paleoenvironmental conditions from this period have been developed for the southern Colorado Plateau. The records that do exist are primarily constructed from undated pollen and macrofossil evidence in lake cores (e.g. Wright et al., 1973; Jacobs, 1983; Hevly, 1985; Anderson, 2000), which suggest that the average summer temperature during MIS 3 was 2-4°C lower than modern conditions and tree line was depressed by ~500-600 m (Anderson et al., 2000). Lake levels were lowest at both Walker Lake and Potato Lake near the end of MIS 3, which roughly corresponds to the oldest eolian deposits identified in this study. Low lake levels and the oldest eolian deposits were preceded by significant fluvial aggradation in both the Canyonlands (Reheis et al., 2005) and in the eastern Grand Canyon (Anders et al., 2005). This aggradation, if regional, would have increased sediment supply to the fluvial and eolian systems in the study area.

As this is only the second study from the Colorado Plateau to identify eolian deposits that date to the previous interglacial period, we extend our eolian chronostratigraphic comparisons by examining eolian records from the Mojave Desert and southern California (e.g. Rendell and Sheffer, 1996; Lancaster, 1997; Stokes et al., 1997; Clarke and Rendell, 1998; Kocurek and Lancaster, 1999; Tchakerian and Lancaster, 2002; Lancaster and Tchakerian, 2003). The southern California deserts are a good analog to Black Mesa because eolian deposits are extensive and topography is complex; consequently topographically controlled dunes are common. Because the jet stream and winter storm tracks were depressed to the south during glacial conditions (e.g. Kutzbach, 1987), storms tracked from southern California over northeastern Arizona, suggesting that the two regions may have had broadly similar precipitation histories during full glacial conditions. Deglaciation allowed the summer monsoon to intensify ca. 9-6 ka and the winter storm track to move northward,

resulting in the two regions being less coupled with respect to precipitation patterns (e.g. COHMAP members, 1988).

Rendell and Sheffer (1996) identified two major depositional phases in the eastern Mojave Desert at 20-30 ka, probably correlative with Qe1 at Silver Lake Playa (summarized in Wells et al., 2003) and 15-7 ka. The Kelso dunes appear to have been dominantly active throughout MIS 2 and the early to middle Holocene with a brief hiatus from 15-12 ka (Kocurek and Lancaster, 1999). The complex history of the eolian deposits in the Mojave Desert have been interpreted as representing either 1) periods of increased aridity, which led to increased sediment availability either from exposure of lacustrine sediments with decreasing lake levels (summarized in Lancaster and Tchakerian, 2003) or decreasing vegetative cover (e.g. Kocurek and Lancaster, 1999; Tchakerian and Lancaster, 2002) or 2) increased sediment supply from ephemeral sediment-laden fluvial systems (e.g. Rendell and Sheffer, 1996; Clarke and Rendell, 1998; Laity, 2003). Clarke and Rendell (1998) show that 94% of dated eolian deposits in the Mojave Desert were deposited during pluvial conditions (24-9 ka) and at times when large floods were recorded in Arizona and Utah rivers (Ely, 1997), arguing that topographically controlled dunes form when fluvial discharge is flashy and sediment loads in streams are high. While Lancaster and Tchakerian (2003) acknowledge that "sediment supply is a major control on eolian dynamics in the region", they caution that interactions between fluvial, lacustrine, and eolian systems are complex in the Mojave Desert often resulting in sediment storage in lacustrine systems during times of high lake levels. Unlike the Mojave Desert, there is no evidence of late Quaternary pluvial lakes immediately downwind from Black Mesa.

Qualitative controls on eolian system state with changing climate conditions

The state of the eolian system depends on transport capacity, sediment supply, and sediment availability (after Kocurek and Lancaster, 1999). Because fluvial systems are the likely initial and primary source of eolian sediments (e.g. Muhs and Holliday, 1995; Bullard and McTainsh, 2003) in our study area, we also briefly and qualitatively discuss the state of the fluvial system and have divided the study are into three zones to simplify this discussion (fig. 10).

Late Pleistocene eolian system state of the Black Mesa study area

Environmental conditions of the late Pleistocene were conducive to the transport and deposition of large volumes of eolian sand in the study area. Cooler and moister conditions during the late Pleistocene (MIS 2 and 3) suggest higher stream discharge, especially during spring floods from snowmelt runoff. Accelerated chemical and physical weathering of the predominantly sedimentary rocks of the Little Colorado River drainage basin combined with greater discharge implies higher stream sediment loads. Extreme, abrupt climatic variability that characterizes glacial climate (e.g. Broecker, 2000; Overpeck and Cole, 2006; Wagner et al., 2010) likely increased variability of stream flow, resulting in the formation of wide braided floodplains and concurrent increased sediment supply for the eolian system (e.g. Muhs and Holliday, 1995; Bullard and McTainsh, 2003) from the Little Colorado River as well as the Tusayan Washes. If fluvial system sediment loads are high and dominated by sand-sized sediments, and streams are braided and/or aggrading, sand is most available in the low gradient floodplains in low-relief valleys where eolian transport capacity is maximized, as has been hypothesized for the Great Plains dunes (e.g. Muhs, 1995; Forman et al., 2001). Widespread aggradation during MIS 3 identified in the eastern Grand Canyon (roughly 50-34

ka, Anders et al., 2005) could represent elevated sediment loads in Colorado River tributaries such as the Little Colorado River. Because of the lack of pluvial lakes in the study area, little of that sediment was held in storage during effectively wetter climatic conditions, as it was in the Mojave Desert (e.g. Lancaster and Tchakerian, 2003). Eolian valley fills and falling dunes that were deposited up to 60 km north of the Hopi Mesas (WP109) during the late Pleistocene must represent both an increase in sediment supply and availability to both eolian and fluvial systems.

Many researchers have suggested that increased effective moisture, such as that during full glacial-age conditions in the southwest, leads to increased vegetation resulting in decreased eolian sediment availability (e.g. Hack, 1941; Pye and Tsoar, 1990; Lancaster, 1997; Kocurek and Lancaster, 1999; Tchakerian and Lancaster, 2002). Is it possible to generate, transport, and deposit large volumes of eolian sand under cooler and wetter conditions like those of the late Pleistocene? Iceland provides one potential modern analog (Arnalds, et al., 2001) for the late Pleistocene eolian system in the study area. Iceland is certainly not arid and sediments are supplied to the eolian system from the fluvial system. Channels are braided and aggrading and because of fluctuating discharge, floodplains are not vegetated. As sand derived from the floodplains is mobilized by wind and migrates over the landscape, sand alternately buries and kills vegetation or scours through previously vegetated geomorphic deposits down a meter or more. Advancing sand fronts have been recorded to move over 300 m in a single year. Sediment supply, transport capacity and availability are all high in Iceland, despite the cool, moist climate. In this system, vegetation only decreases sediment availability if either sand supply or sediment transport capacity is low.

The timing of deposition of topographically-controlled dunes implies that increased sediment supply during MIS 3 and 2 was a stronger driving force than any decrease in sediment availability due to increased effective moisture leading to an increase in vegetation density. The few studies that document pre-Holocene eolian deposits in Arizona and New Mexico, also show that the largest volumes of currently stabilized sand were deposited during the late Pleistocene (Wells et al., 1990; Reheis, et al., 2005; Holliday, 2006).

Current eolian system state of the Black Mesa study area

The eolian system in zone 3 is characterized by high sediment supply as well as high sediment availability and transport capacity. The apparent spatial correlation between aggrading streams and active dunes, when coupled with regionally strong persistent winds (high transport capacity), suggests that zone 3 dunes are built downwind from the floodplains of unconfined channels where sediment supply is high and sediments are readily available. Migrating dunes that intersect stream channels increase bedload of streams causing aggradation, feeding linear dunes downwind (Hack, 1941, 1942). The coupled Black Mesa eolian-fluvial system in zone 3, where eolian and fluvial transport directions are roughly opposite, is a system of recirculating and mixing sediments from various sources.

In zone 2, falling dunes have been deposited in landscape positions where transport capacity of the wind drops to near zero. In this portion of the landscape, although sand is abundant, eolian deposits are effectively stored and unavailable to the eolian system (as is the current state). In the Cretaceous outcrops of zone 2, Dinnebito, Oraibi, and Wepo, and Polacca Washes are incised through at least a portion of their length, but streams in small tributary basins containing falling dunes or eolian valley fills are rarely incised and often unconnected to the main channels. Tributary basin size is small and infiltration capacity of

the sand is high; therefore tributary streams have been unable to substantially erode these landforms since deposition. Thus, these falling dunes and eolian valley fills are the most stable and persistent eolian landforms in the Black Mesa region and provide a record of paleoenvironmental conditions during the late Pleistocene to early Holocene. In addition, their presence indicates an irreversible stabilizing influence resisting landscape change throughout the late Quaternary.

Most landscape positions in the study area, except for those in zone 2, are located in zones of high eolian transport capacity as low-relief settings experience the most persistent and powerful winds in the landscape. In spite of high transport capacity, sediment availability and sediment supply are low for the stable sand sheets, vegetated primarily by grasses and shrubs, north of the Hopi Mesas in zone 1. The primary channels (Dinnebito, Oraibi, Wepo, and Polacca Washes) are confined to narrow valleys with subvertical canyon walls, and are commonly incised from 2 m up to 20 m. Where valleys are confined or streams incised, both eolian transport capacity and eolian sediment supply are low, even though the channel bedload is dominantly sand.

Perhaps more important than low sand supply in zone 1 is the continued low sediment availability within the stabilized sand sheets. Stabilization probably resulted from a combination of decreasing transport capacity (diminishing wind speeds with melting of continental ice sheets), decreasing sediment supply as climatic variability diminished in the Holocene, and also decreasing sediment availability. During the late glacial to early Holocence, increased atmospheric dust loading led to rapid soil formation (Reheis et al., 2005; Reynolds et al., 2006) and subsequent increased availability of soil water and nutrients for plants (e.g. McDonald, 1994; Reynolds et al., 2006). Soil development and enhanced

water holding capacity, along with increased summer precipitation and warmer temperatures, encouraged plant growth, promoting stability and further soil formation. While most eolian studies do not explicitly consider soil profile development as a stabilizing factor in eolian systems (e.g. Kocurek and Lancaster, 1999; Gillette and Chen, 2001; Tsoar, 2005), the 8-12 ka deposits that comprise the stable sand sheets in the study area indicate that well-developed soil profiles that formed during the dusty Pleistocene-Holocene climatic transition (Reheis et al., 2005) clearly resist wind erosion and re-entrainment under generally more arid modern and Holocene conditions.

In summary, the stability and age of eolian deposits varies widely between landscape positions, but eolian deposits in similar landscape positions have similar forms, stratigraphic characteristics, soil profile development, and OSL ages. In other words, eolian deposits in similar landscape positions have similar geomorphic histories. The ages of eolian deposits and timing of activity described in this study are in general agreement with other regional eolian chronologies (Fig. 9) with the OSL age estimates for this study suggesting three, and possibly four, periods of eolian deposition or stabilization. The late Holocene deposits (roughly 0-2.5 ka) likely represent local reactivation or local increases in sediment supply, the deposits that date to the Pleistocene Holocene climate transition (8-12 ka) represent stabilization of upland sand sheets, and the falling dunes record deposition of sand in topographic traps during a period of high sediment supply during the last glacial period.

Conclusions

- The large elevation and precipitation gradients and consequent soil and vegetation gradients of Black Mesa produce a topographically and climatically complex landscape and thus a complex eolian geomorphic history.

- In this study, the largest volumes of stable eolian deposits were deposited under cooler and wetter, and more variable, climatic conditions during periods of increased sediment supply from the fluvial system. Falling dunes and eolian valley fills are the most stable and persistent eolian landforms on Black Mesa and provide important information about paleoenvironmental conditions during the late Pleistocene to early Holocene.
- Though the parameters are difficult to quantify, the eolian system state model (Kocurek and Lancaster, 1999) provides a functional qualitative structure for considering the driving and resisting forces in eolian systems. However, sediment availability in this study area depends strongly on factors not explicitly delineated in the eolian system state model, such as degree of soil development in eolian deposits and complex topography. Predictive models that rely solely on climatic data to predict eolian activity fail in this study area because they do not take into account the complexity and history of the geomorphic system (distribution of topography, variation in sediment supply, stabilizing influence of soil properties, etc.).
- The eolian deposits, whether currently active or stabilized for thousands of years, provide negative stabilizing feedback to hillslopes and the fluvial system. The antiquity and persistence of these landforms point to the need for an understanding of the geomorphic history of any landscape when predicting future landscape changes that may occur with future climate change.

References

Al-Enzel, A, Pye, K., Misak, R., and Al-Harjraf, 2008, Morphological characteristics and development of falling dunes, northeastern Kuwait, Journal of Arid Environments, v. 72, p. 423-439.

Aitken, M. J., 1985, Thermoluminescence Dating. Academic Press, London, 359 p.

Aitken, M.J., 1998, An introduction to optical dating: London, Oxford University Press, 267 p.

Anders, M.D., Pederson, J.L., Rittenour, T.M., Sharp, W.D., Gosse, J.C., Karlstrom, K.E., Crossey, L.J., Goble, R.J., Stockli, L., and Yang, G., 2005, Pleistocene geomorphology and geochronology of eastern Grand Canyon: linkages of landscape components during climate changes, Quaternary Science Reviews, v. 24, p. 2428-2448.

Anderson, R.S., 1993, A 35,000 year vegetation and climate history from Potato Lake, Mogollon Rim, Arizona, Quaternary Research, V. 40, p. 351-359.

Anderson, R.S., Betancourt, J.L., Mead, J.I., Hevly, R.H., and Adam, D.P., 2000, Middle- and late-Wisconsin paleobotanic and paleoclimate records from the southern Colorado Plateau, USA, Palaeogeography, Palaeoclimatology, Palaeoecology, v. 155, p. 31-57.

Anderson, R.S., Jass, R.B., Toney, J.L., Allen, C.D., Cisneros-Dozal, L.M., Hess, M., Heikoop, J., and Fessenden, J., 2008, Development of the mixed conifer forest in northern New Mexico and its relationship to Holocene environmental change, Quaternary Research, v. 69, p. 263-275.

Armour, J., Fawcett, P.J., and Geissman, J.W., 2002, 15 k.y. paleoclimatic and glacial record from northern New Mexico, Geology, v. 30, n. 8, p. 723-726.

Arnalds, O., Gisladottir, F.O., and Sigurjonsson, H., 2001, Sandy deserts of Iceland: an overview, Journal of Arid Environments, v. 47, p. 359-371.

Bagnold, R.A., 1941, The Physics of Blown Sand and Desert Dunes, Methuen, London, 265 pp.

Benson L.V., Burdett, J.W., Kashgarian, M., Lund, S.P., Phillips, F.M., and Rye, R.O., 1996, Climatic and hydrologic oscillations in the Owens Lake Basin and adjacent Sierra Nevada, California, Science, v. 274, p. 746-749.

Betancourt, J.L., 1990, Late Quaternary biogeography of the Colorado Plateau, *in* Betancourt, J.L., Van Devender, T.R., and Martin, P.S., eds., Packrat Middens: The Last 40,000 Years of Biotic Change, The University of Arizona Press, Tucson, AZ, 467 p.

Billingsley G.H., 1987, Geology and geomorphology of the southwestern Moenkopi Plateau and southern Ward Terrace, Arizona, U.S. Geological Survey Bulletin 1672, 18 p.

Birkeland, P.W., 1999, Soils and Geomorphology, 3rd Ed., Oxford University Press, 430 p.

Bøtter-Jensen, L., McKeever, S. W. S., and Wintle, A. G., 2003, Optically Stimulated Luminescence Dosimetry. Elsevier Science, Amsterdam, 374 p.

Bullard, J.E. and McTainsh, G. H., 2003, Aeolian-fluvial interactions in dryland environments: examples, concepts, and Australian case study, Progress in Physical Geography, v. 27, n. 4, p. 471 - 501.

Buurman, P., Pape, T., and Muggler, C.C., 1997, Laser grain-size determination in soil genetic studies: 1. Practical problems: Soil Science, v. 162, p. 211–218.

Chase, B., 2009, Evaluating the use of dune sediments as a proxy for palaeo-aridity: a southern African case study, Earth Science Reviews, v. 93, p. 31-45.

Clarke, M.L. and Rendell, H.M, 1998, Climate change impacts on sand supply and the formation of desert sand dunes in the southwest USA, Journal of Arid Environments, v. 39, p. 517-531.

COHMAP members, 1988, Climatic changes of the last 18,000 years: Observations and model simulations, Science, v. 241, p. 1043-1052.

Cole, K.L., 1990, Late Quaternary vegetation gradients through the Grand Canyon, *in* Betancourt, J.L., Van Devender, T.R., and Martin, P.S., eds., Packrat Middens: The Last 40,000 Years of Biotic Change, The University of Arizona Press, Tucson, AZ, 467 p.

Davis, O.K., and Shafer, D.S., 1992, A Holocene climatic record for the Sonoran Desert from pollen analysis of Montezuma Well, Arizona USA, Palaeogeography, Palaeoclimatology, Palaeoecology, v. 92, p. 107-119.

Day, P.R., 1965, Particle fractionation and particle-size analysis, in Black, C.A., and Evans, D.D., White, J.L., Ensminger, L.E., and Clark, F.E., eds., Methods of Soil Analysis, Part I, n. 9, p. 545-567.

Duffield, W., Riggs, N., Kaufman, D., Champion, D., Fenton, C., McIntosh, W., Hereford, R., Plescia, J., and Ort, M., 2006, Multiple constraints on the age of a Pleistocene lava dam across the Little Colorado River at Grand Falls, Arizona, Geological Society of America Bulletin, v. 118, n. 3/4, p. 421-429.

Duller, G. A. T., 1991, Equivalent dose determination using single aliquots, Nuclear Tracks and Radiation Measurements, 18, p. 371–378.

Ellwein, A.L., 1997, Quaternary evolution of eolian landforms, soils, and landscapes of the Petrified Forest National Park, Arizona, New Mexico Geology, v. 19, no. 2.

Ellwein, A.L., Mahan, S.A., and McFadden, L.D., in press, New OSL ages provide evidence of MIS3 and MIS2 eolian activity on Black Mesa, northeastern Arizona, USA, Quaternary Research.

Ely, L.L., 1997, Response of extreme floods in the southwestern United States to climatic variations in the late Holocene, Geomorphology, v. 19, p. 175-201.

Forman, S.L., Oglesby, R., and Webb, R.S., 2001, Temporal and spatial patterns of Holocene dune activity on the Great Plains of North America: megadroughts and climate links, Global and Planetary Change, v. 29, p. 1-29.

Forman, S.L., Marin, L., Gomez, J.,and Pierson, J, 2008, Late Quaternary eolian sand depositional record for southwestern Kansas: landscape sensitivity to droughts, Paleogeography, Paleoclimatology, Paleoecology, v. 265, p. 107-120.

Fryberger S.G. and Dean, G., 1979, Dune Forms and Wind Regimes, *in* McKee, E.D., ed., A Study of Global Sand Seas, US Geological Survey Professional Paper 1052, p. 137-169.

Gile, L.H., 1961, A classification of ca horizons in the soils of a desert region, Doña Ana County, New Mexico, Soil Science Society of America Proceedings, v. 25, n. 1, p. 52-61.

Gillette, D.A. and Chen, W., 2001, Particle production and aeolian transport from a "supply-limited" source area in the Chihuahuan desert, New Mexico, United States, Journal of Geophysical Research, v. 106, n. D6, p. 5267-5278.

Hack, J.T., 1941, Dunes of the western Navajo Country: Geographical Review, v. 31, p.240-263.

Hack, J.T., 1942, The Changing Physical Environment of the Hopi Indians of Arizona, Papers of the Peabody Museum, v. 35, no. 1, Harvard University, Cambridge.

Hasbargen, J., 1994, A Holocene paleoclimatic and environmental record from Stoneman Lake, Arizona, Quaternary Research, v. 42, p. 188-196.

Hayton, S., Nelson, C.S., Ricketts, B.D., Cooke, S., and Wedd, M.W., 2001, Effect of mica on particle-analysis using the laser diffraction technique, Journal of Sedimentary Research, v. 71, p. 507–509.

Helm, P.J., and Breed, C.S., 1999, Instrumented field studies of sediment transport by wind, *in* Breed, C.S., and Reheis, M.C., eds., Desert winds: Monitoring wind-related surface processes in Arizona, New Mexico, and California: U.S. Geological Survey Professional Paper 1598, p. 31–54.

Hevly, R.H., 1985, A 50,000 year record of Quaternary Environments: Walker Lake, Coconino Co., Arizona, AASP Contribution Series 16, p. 141-154.

Holliday, V.T., 2001, Stratigraphy and geochronology of upper Quaternary eolian sand on the Southern High Plains of Texas and New Mexico, United States, Geological Society of America Bulletin, v. 113, p. 88-108.

Jacobs, B.F., 1983, Past Vegetation and Climate of the Mogollon Rim Area, Arizona. Unpubl. Thesis, Univ. Arizona, 166 p.

Karlstrom, E.T., 2005, Late Quaternary landscape history and geoarchaeology of two drainages on Black Mesa, northeastern Arizona, USA, Geoarchaeology, v. 20, no. 1, p. 1-28.

Karlstrom, E.T. and Karlstrom, T.N.V., 1986, Late Quaternary alluvial stratigraphy and soils of the Black Mesa – Little Colorado River Areas, northern Arizona, *in* Nations, J.D., Conway, C.M., and Swann, G.A., eds., Geology of Central and Northern Arizona, Geological Society of America, Rocky Mountain Section Guidebook, p. 71-92.

Kocurek, G. and Lancaster, N., 1999, Aeolian system sediment state: theory and Mojave Desert Kelso dune field example, Sedimentology, v. 46, p. 505-515.

Kutzbach, J.E., 1987, Model simulations of the climatic patterns during the deglaciation of North America, *in* Ruddiman, W.F. and Wright, H.E., Jr. eds., North America and adjacent oceans during the last deglaciation: Boulder, Colorado, Geological Society of America, The Geology of North America, v. K-3, p. 425-446.

Laity, J., 2003, Aeolian destabilization along the Mojave River, Mojave Desert, California: linkages among fluvial, groundwater, and aeolian systems, Physical Geography, v. 24, n. 3, p. 196-221.

Lancaster, N., 1988, Development of linear dunes in the southwestern Kalahari, southern Africa: Journal of Arid Environments, v. 14, p. 233–244.

Lancaster, N., 1997, Response of eolian geomorphic systems to minor climate change: examples from the southern Californian Deserts, Geomorphology, v. 19, p. 333-347.

Lancaster, N., 2008, Desert dune dynamics and development: insights from luminescence dating, Boreas, v. 37, p. 559-573.

Lancaster, N. and Helm, P., 2000, A test of a climatic index of dune mobility using measurements from the southwestern United States, Earth Surface Processes and Landforms, v. 25, p. 197-207.

Lancaster, N. and Tchakerian, V.P., 1996, Geomorphology and sediments of sand ramps in the Mojave Desert, Geomorphology, v. 17, p. 151-165.

Lancaster, N. and Tchakerian, V.P., 2003, Late Quaternary eolian dynamics, Mojave Desert, California, *in* Enzel, Y., Wells, S.G., and Lancaster, N., eds., Paleoenvironments and Paleohydrology of the Mojave and Southern Great Basin Deserts, Geological Society of America Special Paper 368, p. 231-249.

Lane, E.W., 1955, Design of stable channels: American Society of Civil Engineers Transactions, v. 120, p. 1234-1260.

Lin, J.C., Broecker, W.S., Hemming, S.R., Hajadas, I., Anderson, R.F., Smith, G.I., Kelley, M., and Bonani, G., 1998, A reassessment of U-Th and ^{14}C ages for late-glacial high-frequency hydrological events at Searles Lake, California, Quaternary Research, v. 49, p. 11-23.

Machette, M.N., 1985, Calcic soils of the southwestern United States, *in* Weide, D.L. ed., Soils and Quaternary Geology of the Southwestern United States, Geological Society of America Special Paper 203, p. 1-21.

Mahan, S. A., and Brown, D. J., 2006. An optical age chronology of late Quaternary extreme flood events recorded in Ugandan dambo soils. Quaternary Geochronology 2, p. 174-180.

Marchetti, D.W., Cerling, T.E., and Lips, E.W., 2005, A glacial chronology for the Fish Creek drainage of Boulder Mountain, Utah, USA, v. 64, p. 263-271.

McAuliffe, J.R., Scuderi, L.A., and McFadden, L.D., 2006, Tree-ring record of hillslope erosion and valley floor dynamics: landscape responses to climate variation during

the last 400 yr in the Colorado Plateau, northeastern Arizona, Global and Planetary Change, v. 50, p. 184-201.

McCave, I.N. and Syvitski, J.P.M., 1991, Principles and methods of geological particle size analysis, *in* Syvitski, J.P.M., ed., Principles, methods and applications of particle size analysis: New York, Cambridge University Press, p. 3–21.

McDonald, E.V., 1994, The relative influence of climatic change, desert dust, and lithologic control on soil-geomorphic processes and hydrology of calcic soils formed on Quaternary alluvial fan deposits in the Mojave Desert, California. PhD thesis, Univ. of New Mexico, Albuquerque, NM. 383 pp.

McFadden, L.D., and McAuliffe, J.R., 1997, Lithologically influenced geomorphic responses to Holocene climatic changes in the southern Colorado Plateau, Arizona: A soil-geomorphic and ecologic perspective, Geomorphology, v. 19, p. 303-332.

Millard, H. T., and Maat, P. B., 1994, Thermoluminescence Dating Procedures in use at the U.S. Geological Survey, Denver, Colorado, US Geological Survey Open File Report 94-249, 112 p.

Muhs, D.R., and Been, J.M., 1999, Reactivation of stabilized sand dunes on the Colorado Plateau: U.S. Geological Survey, http://geochange.er.usgs.gov/sw/impacts/geology/sand (last accessed 7/24/2010).

Muhs, D.R. and Holliday, V.T., 1995, Evidence of active dune sand on the Great Plains in the 19th century from accounts of early explorers, Quaternary Research, v. 43, p. 198-208.

Murray, A.S., Marten, R., Johnston, A., and Martin, P., 1987, Analysis for naturally occurring radionuclides at environmental concentrations by gamma spectrometry, Journal of Radioanalytical and Nuclear Chemistry, Article 115, p. 263-288.

Murray, A.S. and Olley, J.M., 2002, Precision and accuracy in the optically stimulated luminescence dating of sedimentary quartz: a status review, Geochronometria, v. 21, p. 1-16.

Murray, A.S. and Wintle, A.G., 2000, Luminescence dating of quartz using an improved single-aliquot regenerative-dose protocol, Radiation Measurements 32, p. 57-73.

Murray, A. S., and Wintle, A. G., 2003, The single aliquot regenerative dose protocol: Potential for improvements in reliability, Radiation Measurements 37, p. 377–381.

Okin, G.S., Murray, B., and Schlesinger, W.H., 2001, Degradation of sandy arid shrubland environments: observations, process modeling, and management implications, Journal of Arid Environments, v. 47, p. 123-144.

Pease, P.P and Tchakerian, V.P, 2003, Geochemistry of sediments from Quaternary sand ramps in the southeastern Mojave Desert, California, Quaternary International, v. 104, p. 19-29.

Phillips, F.M., Campbell, A.R., Smith, G.I., and Bischoff, J.L., 1994, Interstadial climatic cycles: a link between western North America and Greenland?, Geology, v. 22, p. 1115-1118.

Prescott, J. R., and Hutton, J. T., 1994, Cosmic-ray contribution to dose-rates for luminescence and ESR dating large depth and long-term time variations, Radiation Measurements, v. 23 (2-3), p. 497-500.

Pye, K., & Tsoar, H., 1990, Aeolian Sand and Sand Dunes. London: Unwin Hyman, 396 p.

Reheis, M.C., Reynolds, R.L., Goldstein, H., Roberts, H.M., Yount, J.C., Axford, Y., Cummings, L.S., and Shearin, N., 2005, Late Quaternary eolian and alluvial response to paleoclimate, Canyonlands, southeastern Utah, GSA Bulletin, v. 117, n. 7/8, p. 1051-1069.

Rendell, H.M. and Sheffer, N.L., 1996, Luminescence dating of sand ramps in the Eastern Mojave Desert, Geomorphology, v. 17, p. 187-197.

Reynolds, R.L., Reheis, M.C., Neff, J.C., Goldstein, H., and Yount, J., 2006, Late Quaternary eolian dust in surficial deposits of a Colorado Plateau grassland: controls on distribution and ecological effects, Catena, v. 66, p. 251-266.

Schumm, S.A. and Lichty, R.W., 1965, Time, space, and causality in geomorphology, American Journal of Science, v. 263, p. 110-119.

Schlesinger W. H., Reynolds, J.F., Cunningham, G. L., Huenneke, L.F., Jarrell, W.M., Virginia, R.A., and Whitford, W.G., 1990, Biological feedbacks in global desertification, Science, v. 247, p. 1043-1048.

Scuderi, L.A., McFadden, L.D., and McAuliffe, J.R., 2008. Dendrogeomorphically derived slope response to decadal and centennial scale climate variability: Black Mesa, Arizona, USA. Natural Hazards and Earth System Science v. 8, p. 869–880.

Singhvi, A.K., Bluszcz, A., Bateman, M.D., and Rao, M.S., 2001, Luminescence dating of loess-palaeosol sequences and coversands: Methodological aspects and palaeoclimatic implications, Earth-Science Reviews, v. 54, p. 193-211.

Snyder, S.L., and Duval, J.S., 2003, Design and construction of a Gamma-ray Spectrometer system for determining natural radioactive concentrations in geological samples at the

U.S. Geological Survey in Reston, Virginia,: *U.S. Geological Survey Open-File Report 03-29 (on-line only)* (http://pubs.usgs.gov/of/2003/of03-029/).

Stokes, S. and Breed, C.S., 1993, A chronostratigraphic re-evaluation of the Tusayan Dunes, Moenkopi Plateau and southern Ward Terrace, northeastern Arizona, *in* Pye, K., ed., The dynamics and environmental context of aeolian sedimentary systems, Geological Society Special Publication No. 72, p. 75-90.

Stokes, S., Kocurek, G., Pye, K., and Winspear, N.R., 1997, New evidence for the timing of Aeolian sand supply to the Algodones dunefield and East Mesa area, southeastern California, USA, Palaeogeography, Palaeoclimatology, Palaeoecology, v. 128, p. 63-75.

Tchakerian, V.P. and Lancaster, N., 2002, Late Quaternary arid/humid cycles in the Mojave Desert and western Great Basin of North America, Quaternary Science Reviews, v. 21, p. 799-810.

Thompson, R.S., Whitlock, C., Bartlein, P.J., Harrison, S.P., and Spaulding, W.G., 1993, Climatic changes in the western United States since 18,000 yr B.P., *in* Wright, H.E., Jr., Kutzbach, J.E., Webb, T. III, Ruddiman, W.F., Street-Perrott, F.A., and Bartlein, P.J., eds., Global Climates since the Last Glacial Maximum, University of Minnesota Press, Minneapolis, MN, 569 p.

Toney, J.L. and Anderson, R.S., 2006, A postglacial palaeoecological record from the San Juan Mountains of Colorado, USA: fire, climate and vegetation history, The Holocene, v. 16, p. 1-15.

Tsoar, H., 2005, Sand dune mobility and stability in relation to climate, Physica A, v. 357, p. 50-56.

Waters, M.R., 1989, Late Quaternary lacustrine history and paleoclimatic significance of Pluvial Lake Cochise, southeastern Arizona, Quaternary Research, v. 32, p. 1-11.

Wells, S.G., McFadden, L.D., and Schultz, J.D., 1990, Eolian landscape evolution and soil formation in the Chaco dune field, southern Colorado Plateau, New Mexico, Geomorphology, v. 3, p. 517-546.

Wells, S.G., Brown, W.J., Enzel, Y., Anderson, R.Y., and McFadden, L.D., 2003, Late Quaternary geology and paleohydrology of pluvial Lake Mojave, southern California, *in* Enzel, Y., Wells, S.G., and Lancaster, N., eds., Paleoenvironments and Paleohydrology of the Mojave and Southern Great Basin Deserts, Geological Society of America Special Paper 368, p. 79-114.

Weng, C. and Jackson, S.T., 1999, Late glacial and Holocene vegetation history and paleoclimate of the Kaibab Plateau, Arizona, Palaeogeography, Palaeoclimatology, Palaeoecology, v. 153, p. 179-201.

Western Regional Climate Center (WRCC), Western U.S. Historical Summaries for individual stations, accessed September 22, 2009. Available on-line at [http://www.wrcc.dri.edu/CLIMATEDATA.html] from the Desert Research Institute, Reno Nevada, USA.

Wintle, A.G. and Murray, A.S., 2006, A review of quartz optically stimulated luminescence characteristics and their relevance in single-aliquot regeneration dating protocols, Radiation Measurements, v. 41, p. 369-391.

Wolfe, S.A., Huntley, D.J., David, P.P., Ollerhead, J., Sauchyn, D.J., and MacDonald, G.M., 2001, Late 18th century drought-induced sand dune activity, Great Sand Hills, Saskatchewan, Canadian Journal of Earth Science, v. 38, p. 105-117.

Wright, H.E., Jr., Bent, A.M., Hansen, B.S., and Maher, L.J., Jr., 1973, Present and past vegetation of the Chuska Mountains, northwestern New Mexico, Geological Society of America Bulletin, v. 84, p. 1155-1180.

Zhu, C., Waddell, R.K., Jr., Star, I., and Ostrander, M., 1998, Responses of groundwater in the Black Mesa basin, northeastern Arizona, to paleoclimatic changes during the late Pleistocene and Holocene, Geology, v. 26, p. 127-130.

Figures

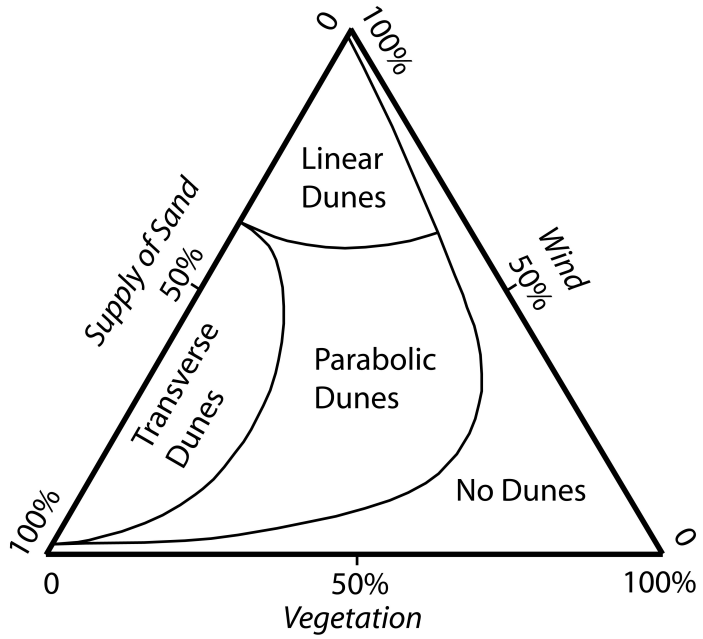

Figure 1: Ternary diagram depicting the relationships between dune form, wind strength, vegetative cover, and sand supply. Constant, unidirectional wind is assumed. (Modified from Hack, 1941.)

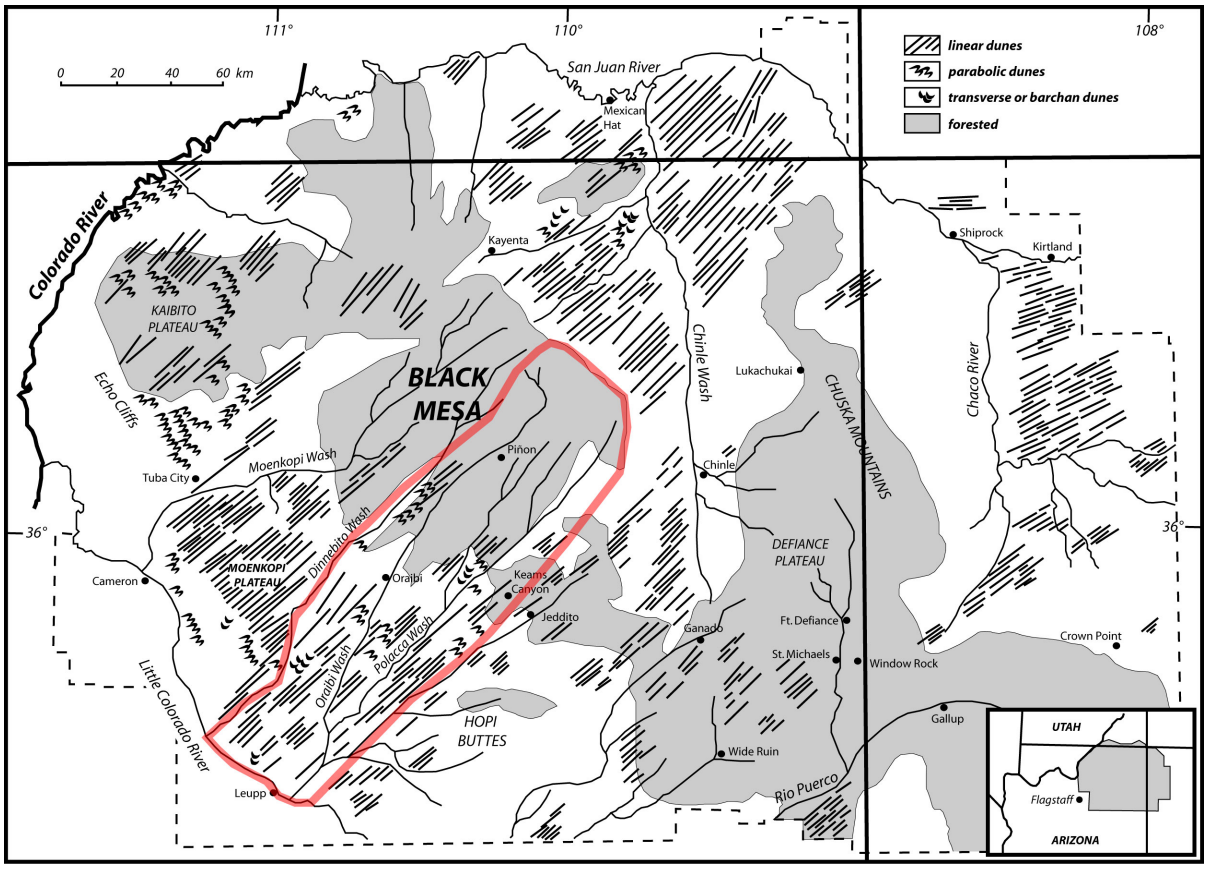

Figure 2: Distribution of eolian landforms and forested areas of the Navajo Nation and Hopi Lands as mapped by J.T. Hack (1941). The study area is outlined in red.

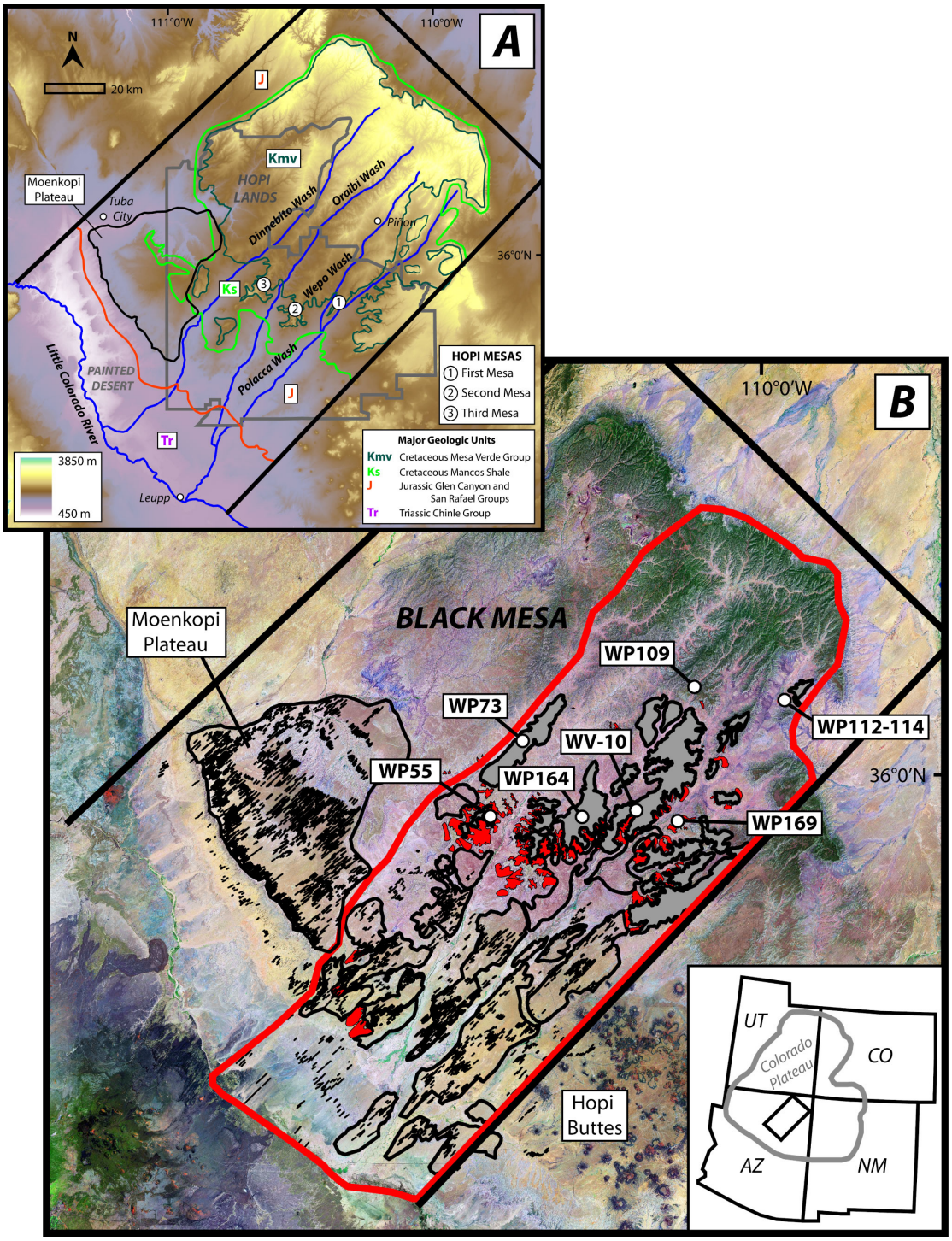

Figure 3A: Geography and distribution of geology and elevation within the Black Mesa region. DEM base imagery. **B:** Distribution of eolian landforms. Open polygons are active sand sheets, gray polygons are stable sand sheets, red polygons are topographically

controlled dunes. The thick red line delineates the study area within the Black Mesa region. Landsat base imagery.

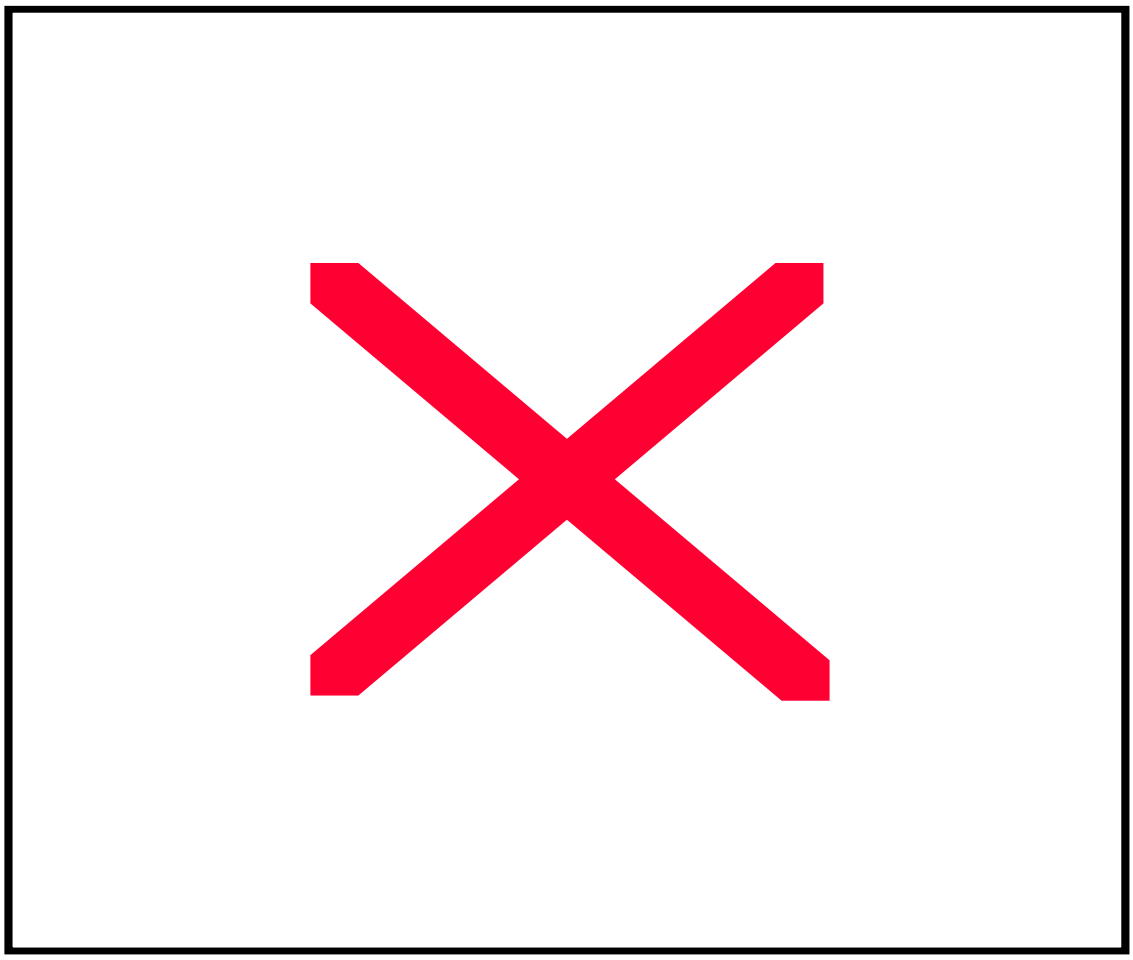

Figure 4: Schematic cross-sections showing common landscape relationships between lithology, tributary width, distance from sand source, alluvial and topographically-controlled eolian deposits. **A)** Falling dune with toe buried by alluvium (analogous to WP109). **B)** Apparent falling dune, climbing dune pair. In this cartoon, a falling dune climbing dune pair (2) is deposited on hillslopes and alluvium (1), another eolian deposition event occurs (3), the toes of the dunes are eroded by fluvial processes, followed by aggradation (4). This is a hypothetical representation of the landscape relationships at Echo Canyon (WP169), however

the subsurface relationships were not exposed and are not known at this site. **C)** Eolian valley fill composed primarily of sand ramps, this hypotherical diagram represents the site near Oraibi (WP55). The alluvial valley floor (1) is buried by eolian deposits that fill the valley (2), which are subsequently modfied by fluvial processes and aggradation (3), followed by more eolian deposition, and fluvial incision (5).

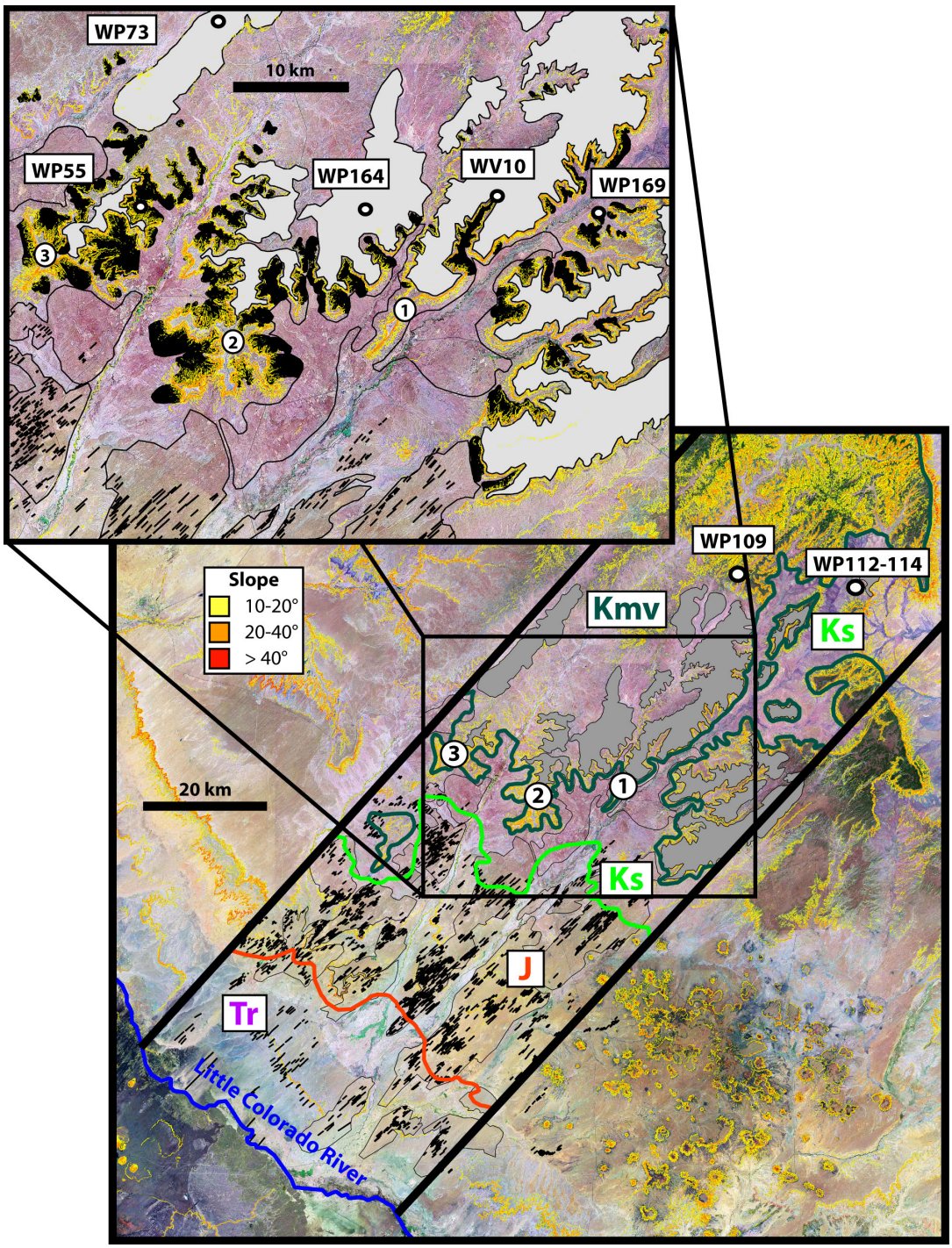

Figure 5: Distribution of lithology, topography, linear dunes, and active and stable sand sheets, and topographically controlled dunes within the study area. The Hopi Mesas (First, Second, and Third, in numbered circles) occur along the prominent cliffs defined by the

Mesa Verde Group (Kmv) which trap the majority of climbing and falling dunes (filled black polygons in inset box). Linear dunes (black lines) and active sand sheets (polygons bounded by thin black outline) commonly overlie Jurassic sandstones (J; Glen Canyon Group Wingate and Navajo sandstones and San Rafael Group units). The lower contact of the Triassic units (Tr) roughly corresponds with the position of the Little Colorado River. Geologic contacts simplified from USGS digital map of geology, slope was calculated from a 30-m digital elevation model. The base image is a true color landsat mosaic (June, 2000).

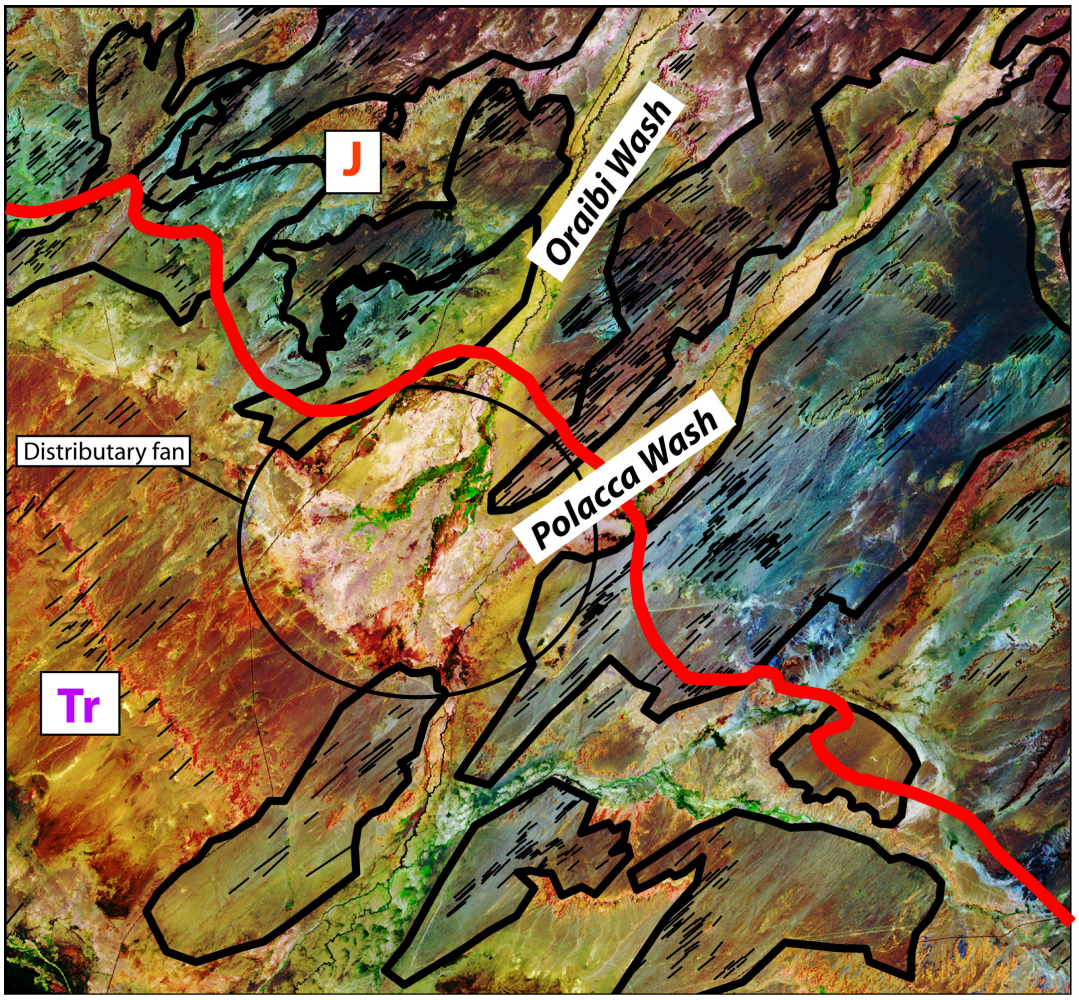

Figure 6: Active sand sheets and linear dunes mapped on top of a landsat image (bands 2, 4, 7 in RGB; June, 2000) with an overlay of geology from the USGS digital map of geology of

AZ. North is at the top of the map. Thick black line polygons are active sand sheets, thin black lines are mapped linear dunes. Triassic units appear reddish orange in this band combination, while Jurassic Glen Canyon Group rocks appear blue or pink, alluvium appears yellowish in many parts of this image and vegetation is bright green. These spectral difference show that eolian sand is coming from both bedrock and alluvium. This image also shows that linear dunes are particularly common downwind from alluvial sources, such as the distributary fan that forms at the confluence of Oraibi and Polacca Washes. Note the abundant linear to the northeast of the fan. This image was captured at 1:250,000 scale.

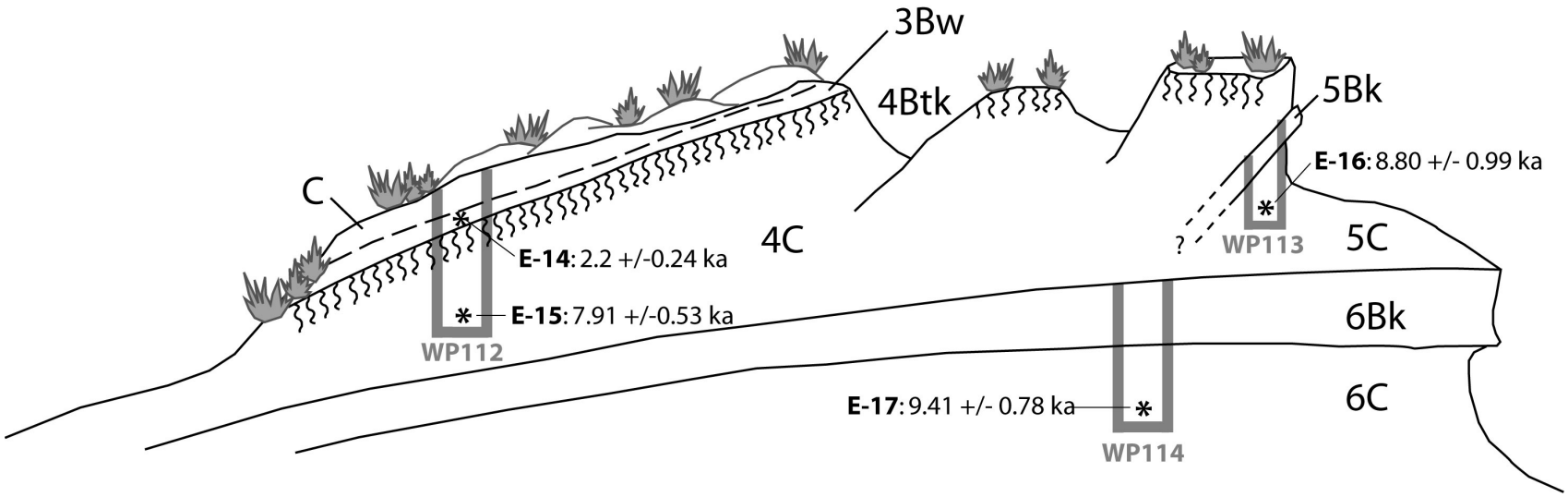

Figure 7: Stratigraphic relationships and age estimates between units at the dune complex near Blue Gap, AZ (WP112-114). Gray boxes at WP112, WP113, and WP 114 show the locations of described sections. All units are interpreted to be of eolian origin except parent material 6, which is interpreted to be alluvium. See Table 3 for OSL age estimates and Table 4 for stratigraphic details.

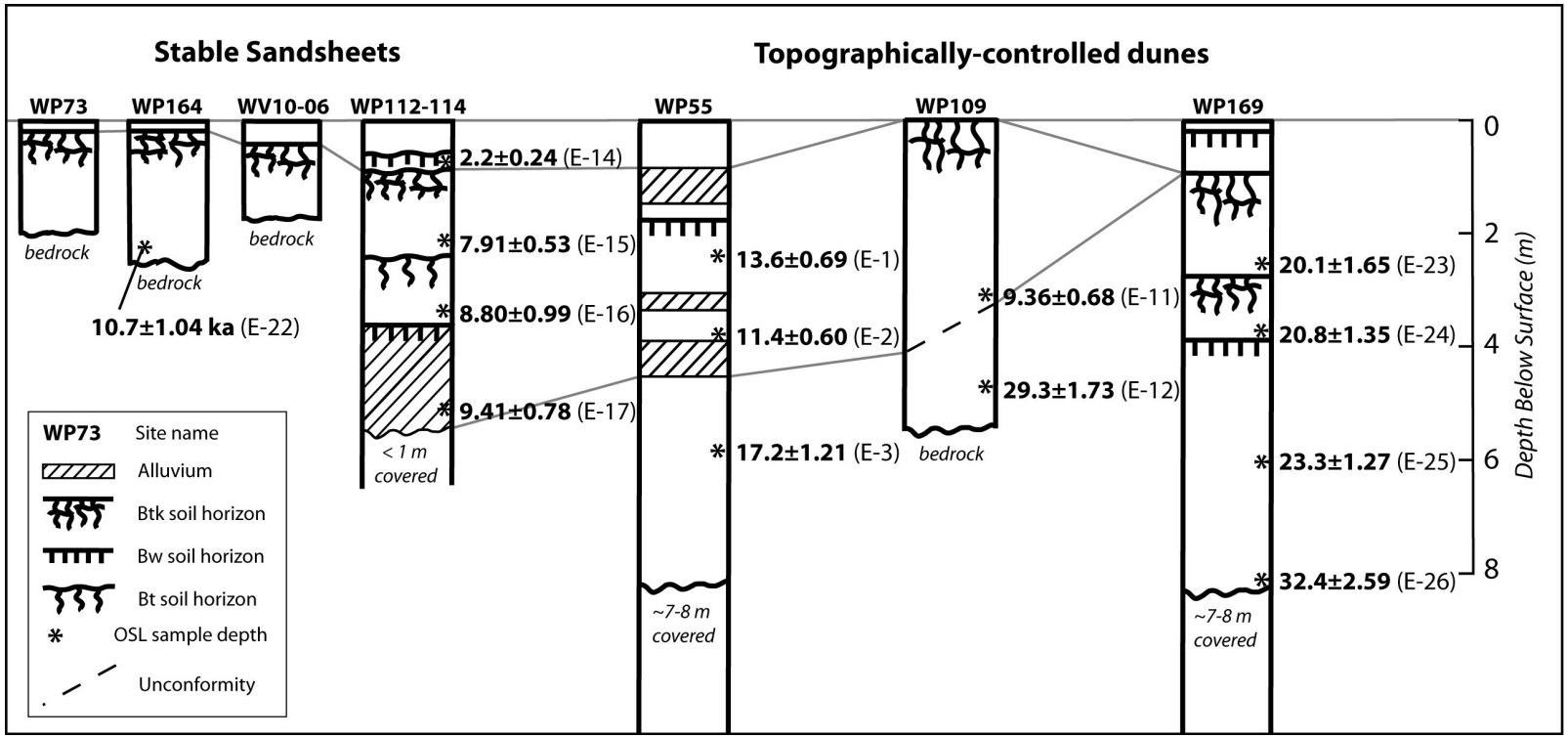

Figure 8: Simplified soil stratigraphy, OSL age estimates (in ka), and correlations of eolian units. The four columns on the left represent stratigraphy within sand sheets; the three columns on the right represent the falling dune or sand ramp sites.

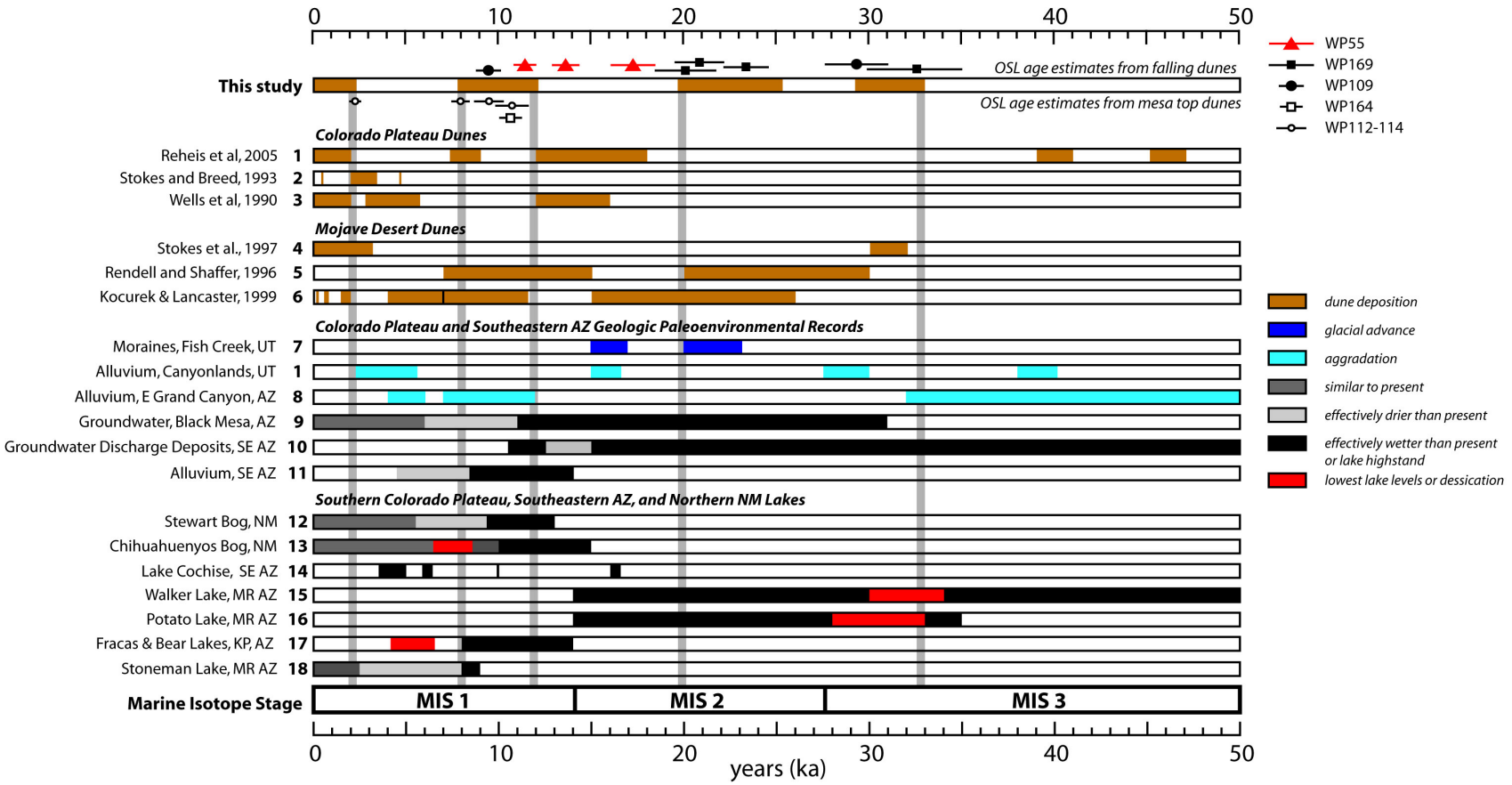

Figure 9: Correlation of OSL age estimates from falling dunes and mesa top sandsheets and dune complexes from Black Mesa (this study) with paleoenvironmental records from the southwestern United States.

Regional glacial, alluvial, and groundwater records: 7) Marchetti et al., 2005; 8) Anders et al., 2005; 9) Zhu et al., 1998; 10) Pigati et al., 2009; 11) Waters and Haynes, 2001.
Regional lacustrine records: 12) Jiménez-Moreno, et al., 2008; 13) Anderson et al., 2008; 14) Waters, 1989; 15) Hevly, 1985; 16) Anderson, 1993; 17) Weng and Jackson, 1999; 18) Hasbargen, 1994.

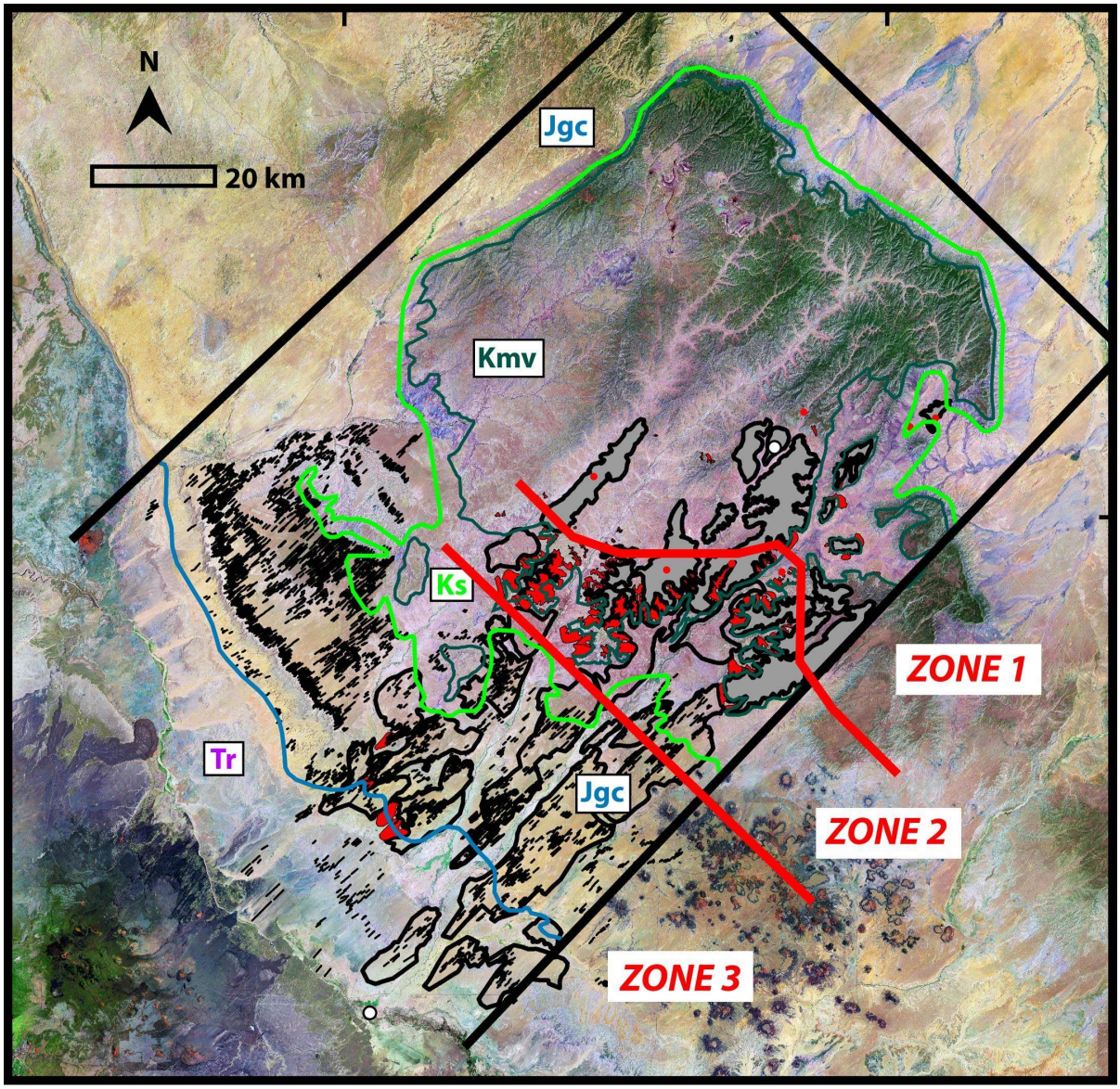

Figure 10: Eolian zones of the study area.

Tables

Table 1: Site locations, coordinates, and dominant vegetation. Latitude, longitude, and elevation acquired at field sites using a Garmin GPSmap 60 handheld unit. Datum: WGS 1984. WP112-114 are one site with three subsections.

Site Name	Site Location	Latitude (°N)	Longitude (°W)	Elevation (m)	Dominant vegetation
WP55	Northeast of Oraibi	35.94	110.61	1796	*Juniperus monosperma, Artemesia filifolia, Atriplex canescens, Ephedra spp.,Yucca spp., Gutierrezia sarothrae, Muhlenbergia pungens, Bouteloua gracilis, Oryzopsis hymenoides, Bromus tectorum*
WP169	Echo Canyon	35.93	110.20	1829	*J. monosperma, A. filifolia, A. canescens, G. sarothrae, M. pungens, B. gracilis, O. hymenoides, B. tectorum*
WP109	Wepo Wash Canyon	36.17	110.15	2016	*J. osteosperma, Artemesia tridentata, A. canescens, G. sarothrae, B. gracilis, B. tectorum*
WP164	Northwest of Wepo Village	35.94	110.41	1834	*J. monosperma, J. osteosperma, Ephedra spp., G. sarothrae, B. gracilis, O. hymenoides, Hilaria jamesii, M. pungens*
WP112	Blue Gap borrow pit section 1	36.15	109.96	1972	*Juniperus osteosperma, A. canescens, G. sarothrae, M. pungens, B. gracilis, O. hymenoides, B. tectorum*
WP113	Blue Gap borrow pit section 2	36.15	109.96	1975	same as WP112
WP114	Blue Gap borrow pit section 3	36.15	109.96	1972	same as WP112
WP73	West of Hard Rocks	36.08	110.54	1859	*J. monosperma, G. sarothrae, B. gracilis*
WV10	Head of One Cottonwood Canyon	35.95	110.17	1878	*J. monosperma, A. filifolia, A. tridentata, Ephedra spp., B. gracilis*

Table 2: Field description of the stratigraphic section WP55 at the Oraibi sand ramp exposure. Particle size analyses using pipet extraction at the University of New Mexico Quaternary Soils and Sediment Laboratory, % soil carbonate performed at USGS Soils Laboratory.

Depth (cm)	Dry Color[a]	Moist Color[a]	Description[b]	Interpretation	OSL sample number	Sand (%)	Silt (%)	Clay (%)	$CaCO_3$ (%)
0-26		7.5YR5/4	Rounded, frosted, well sorted fine sand (fU-fL), no primary structures, bioturbated	Eolian		88.61	6.62	4.77	1.28
26-76		7.5YR5/4	Rounded, frosted, poorly sorted sand (cL-vfU), 0.5-1 cm horizontal beds	Colluvial		ND	ND	ND	ND
76-92		7.5YR5/4	Rounded, frosted, well-sorted fine sand (fU-fL), no primary structures, bioturbated	Eolian		93.48	3.22	3.30	0.60
92-180	7.5YR5/6		Subrounded to well rounded, poorly sorted sand (cU-vfU), < 10% gravel, common climbing ripples from 1.4-1.5m, ~20% oblate non-armored 5-10 cm diameter mudballs from 1.5-1.8 m depth	Fluvial		96.60	0.76	2.64	1.04
180-235	7.5YR5/6		Rounded to well rounded, frosted, moderated sorted sand (cL-mU), well sorted within 2-3 mm beds that compose foresets, foresets dip ~20° to northeast	Eolian	**E-1**	96.97	0.29	2.74	0.48
235-240		10YR4/3	Finely laminated silt and very fine sand (vfL), prominent horizontal bed traceable across outcrop	Fluvial		ND	ND	ND	ND
240-310	7.5YR5/6		Subrounded to well rounded, frosted, well sorted medium sand (mU-mL), 1-2 cm beds that compose foresets dipping ~20° to north	Eolian		95.15	0.76	4.09	0.54
310-350	7.5YR5/4		Subrounded to well rounded, poorly sorted sand (vcL-vfU), ripples common, fining upward	Fluvial		95.49	1.08	3.43	0.60
350-420		5YR5/6	Well rounded, frosted, well sorted, fine sand (fU-fL), massive, top of unit defined by discrete 1-4 mm thick bed of 7.5YR5/6 (dry) well rounded, very fine (vfU) sand	Eolian	**E-2**	84.66	6.77	8.57	1.29
420-750	10YR6/4		Rounded to well rounded, frosted, moderately sorted sand (mU-fL), 1-2% lithics, weak foresets, abundant krotovina, bioturbated	Eolian	**E-3**	96.63	1.78	1.59	0.95

[a]Color codes from Munsell soil color chart, sediments were described under field moisture conditions.
[b]Grain size codes after modified Wentworth Scale.
ND – no data, these units were not analyzed.

Table 3: Optical ages for eolian sand sedimentary deposits from sites on Black Mesa, northeastern Arizona. Equivalent dose and OSL age determined using single aliquot regeneration (SAR) protocols under blue light excitation (514 nm; Murray and Wintle, 2003).

Sample number	Depth (m)	Water content (%)[a]	K (%)[b]	Th (ppm)[b]	U (ppm)[b]	Cosmic dose additions (Gy/ka)[c]	Total dose rate (Gy/ka)	Equivalent dose (Gy)	n[d]	Age (ka)[e]
WP55: sand ramp northeast of Oraibi										
E-1	2.3	1 (22)	1.33 ± 0.01	2.19 ± 0.12	0.64 ± 0.06	0.21 ± 0.01	1.85 ± 0.05	25.2 ± 1.10	17 (30)	13.6 ± 0.69
E-2	4.1	8 (31)	1.97 ± 0.02	6.71 ± 0.23	1.88 ± 0.13	0.18 ± 0.01	2.97 ± 0.07	33.7 ± 1.68	23 (35)	11.4 ± 0.60
E-3	6.1	2 (21)	1.42 ± 0.01	2.46 ± 0.10	0.67 ± 0.04	0.14 ± 0.01	1.88 ± 0.04	32.4 ± 2.10	22 (38)	17.2 ± 1.21
WP169: falling dune in Echo Canyon										
E-23	2.4	2 (27)	1.88 ± 0.04	4.16 ± 0.27	1.15 ± 0.11	0.22 ± 0.22	2.62 ± 0.09	52.7 ± 3.95	20 (20)	20.1 ± 1.65
E-24	3.2	2 (31)	1.98 ± 0.06	3.94 ± 0.21	1.19 ± 0.09	0.20 ± 0.21	2.70 ± 0.07	56.0 ± 3.29	25 (27)	20.8 ± 1.35
E-25	4.5	2 (29)	1.90 ± 0.02	3.60 ± 0.26	1.10 ± 0.09	0.17 ± 0.21	2.54 ± 0.08	59.2 ± 2.60	10 (10)	23.3 ± 1.27
E-26	8.0	5 (30)	1.88 ± 0.05	4.09 ± 0.23	1.21 ± 0.09	0.11 ± 0.21	2.23 ± 0.06	72.2 ± 5.42	28 (30)	32.4 ± 2.59
WP109: falling dune in Wepo Wash Canyon										
E-11	3.2	2 (26)	1.88 ± 0.07	4.14 ± 0.18	1.09 ± 0.07	0.20 ± 0.01	2.60 ± 0.07	24.3 ± 1.62	41 (50)	9.36 ± 0.68
E-12	4.0	3 (44)	2.37 ± 0.06	5.66 ± 0.22	1.40 ± 0.08	0.18 ± 0.01	3.20 ± 0.07	93.8 ± 4.68	13 (20)	29.3 ± 1.73
WP164: Sand sheet west of Wepo Village										
E-22	2.1	2 (29)	1.98 ± 0.02	4.01 ± 0.24	1.16 ± 0.08	0.22 ± 0.22	2.72 ± 0.07	29.2 ± 2.72	16 (20)	10.7 ± 1.04
WP112-114: dune complex near Blue Gap										
E-14	0.9	2 (53)	1.52 ± 0.04	4.51 ± 0.18	1.27 ± 0.08	0.27 ± 0.02	2.34 ± 0.06	5.14 ± 0.51	18 (30)	2.20 ± 0.24
E-15	2.1	1 (34)	1.48 ± 0.01	2.89 ± 0.16	0.87 ± 0.08	0.23 ± 0.02	2.09 ± 0.06	16.5 ± 0.99	21 (28)	7.91 ± 0.53
E-16	1.8	1 (29)	1.38 ± 0.06	2.96 ± 0.57	0.86 ± 0.10	0.24 ± 0.02	2.01 ± 0.18	17.7 ± 1.09	26 (30)	8.80 ± 0.99
E-17	1.3	2 (25)	1.53 ± 0.01	3.06 ± 0.16	0.83 ± 0.07	0.26 ± 0.02	2.19 ± 0.06	20.6 ± 1.61	23 (30)	9.41 ± 0.78

[a] Field moisture, with figures in parentheses indicating the complete sample saturation (%). Ages calculated using 10% of saturation values (except E-26 which was below water table).

[b] Analyses obtained using laboratory Gamma Spectrometry (high resolution Ge detector).

[c] Cosmic doses and attenuation with depth were calculated using the methods of Prescott and Hutton (1994). See text for details.

[d] Number of replicated equivalent dose (De) estimates used to calculate the mean. Figures in parentheses indicate total number of measurements made including failed runs.

[e] Dose rate and age for fine-grained (125-180 μm) quartz sand. Linear + exponential fit used to estimate age, errors to one sigma.

Table 4: Selected soil descriptions and laboratory data.

Horizon[a]	Depth (cm)	Dry color[b]	Moist color[b]	Structure[c]	Dry cons.[d]	Clay films[e]	CaCO3 stage[f]	Lower boundary[g]	Sand (%)	Silt (%)	Clay (%)	CaCO3 (%)
WP169: falling dune in Echo Canyon												
C	0-20	7.5YR4/4	7.5YR4/3	m	lo	0	0, we	a, s	82.80	12.74	4.46	1.28
2Bwb	20-31	7.5YR5/4	7.5YR4/3	sbk, m, 1	so	0	0, me	c, w	77.89	17.39	4.73	2.42
2Bkb	31-62	7.5YR5/3	7.5YR5/2	sbk, m-c, 1	so-sh	0	I-, se	g, s	84.84	11.92	3.24	2.61
2Cb	62-92	7.5YR6/3	7.5YR5/3	m	so	0	0, we	a, w	87.86	9.45	2.69	1.75
3Btkb	92-122	7.5YR5/4	7.5YR5/3	abk-pr, c, 3	h	1, f, cobr-pf	I+, se	g, w	84.26	11.46	4.28	2.23
3Bkb	122-158	7.5YR5/6	7.5YR5/4	m	so-sh	0	I-, we	g, w	92.84	4.93	2.23	1.22
3Cb	158-270	7.5YR6/5	7.5YR5/4	m	so	0	0, we	a, s	96.82	1.85	1.32	0.66
4Btkb	270-290	7.5YR5/4	7.5YR4/3	sbk, c, 1-2	sh	1, f, cobr	I, me	c, s	82.74	12.84	4.42	2.05
4Cb	290-330	7.5YR5/4	7.5YR4/3	sbk, c, 1	so	0	0, we	a, s	94.37	3.44	2.19	1.69
5Bwkb	330-347	7.5YR5/6	7.5YR4/4	sbk, c, 1	so-sh	0	I-, we	c, s	84.88	11.13	3.98	0.75
5Cb	347-472	7.5YR5/6	7.5YR4/4	m	lo-so	0	0, we	ND	97.12	1.52	1.37	1.00
WP109: falling dune in Wepo Wash Canyon												
AC	0-4	7.5YR4/4	7.5YR4/3	pl, m, 2	so	0	0, we	a, s	*77.97*	*10.95*	*11.08*	0.52
Bt	4-16	7.5YR5/4	7.5YR4/3	abk, c, 2	fr	1, f, pf; 2, f, cobr	0, we	c, s	*72.82*	*13.42*	*13.76*	0.93
Btk	16-41	7.5YR5/4	7.5YR4/3	cpr, vc, 3	h	2, f, cobr; 3, d, po	I, me	g, s	*71.49*	*14.98*	*13.52*	0.90
Btk2	41-65	7.5YR6/4	7.5YR5/4	abk, c, 2	h	1, f, cobr	I+, me	c, s	*78.90*	*10.86*	*10.23*	2.25
Btk3	65-102	7.5YR6/4	7.5YR5/4	abk, c, 3	h	1, f, cobr	I+, me	d, s	*85.95*	*10.86*	*10.23*	1.34
Bk1	102-167	10YR6/4	7.5YR6/4	sbk, c, 2	sh-h	0	I-, we	d, s	*91.55*	*3.25*	*5.20*	0.74
Bk2	167-236	10YR6/6	10YR5/4	sbk, c-vc, 1	sh	0	I-, we	d, s	*94.67*	*1.09*	*4.24*	1.40
C	236-350	10YR6/6	10YR5/4	m	lo*	0	0, we	a, w	*95.44*	*0.71*	*3.84*	0.82
2Cb	350-500	10YR5/4	10YR5/4	m	lo*	0	0, we	ND	*89.37*	*2.82*	*7.81*	0.55
WP164: sand sheet west of Wepo Village												
C	0-15	7.5YR5/4	7.5YR4/3	sbk, c, 2	so-sh	0	0, me	a, w	78.31	15.66	6.02	2.17
2Btk1b	15-31	7.5YR5/4	7.5YR4/3	sbk-abk, c-vc, 3	h	1, d, pf; 3, d, cobr	I+, se	a, w	63.99	28.21	7.80	4.02
2Btk2b	31-63	7.5YR6/3	7.5YR4/3	abk, c, 3	h	1, d, pf; 3, d, cobr	I+, se	g, s	59.60	30.78	9.62	7.40
2Ckb	63-128	10YR6/4	10YR4/4	sbk, m-c, 1	so	0	0, we	d, s	96.77	1.38	1.85	1.90
2Cb	128-198	10YR6/4	10YR4/4	sbk, m-c, 1	so	0	0, we	ND	95.28	2.08	2.64	2.93

Table 4 Continued

Horizon[a]	Depth (cm)	Dry color[b]	Moist color[b]	Structure[c]	Dry cons.[d]	Clay films[e]	CaCO3 stage[f]	Lower boundary[g]	Sand (%)	Silt (%)	Clay (%)	CaCO3 (%)
WP112-114: dune complex near Blue Gap												
C	0-30	7.5YR5/3	7.5YR5/3	gr, f, 1	vfr	0	0, me	a, w	*88.90*	*4.67*	*6.42*	1.79
2Cb	30-58	7.5YR5/3	7.5YR4/3	sbk, f, 1	vfr	0	0, me	a, b	*86.62*	*7.39*	*5.99*	1.83
3Bt1b	58-79	7.5YR5/4	7.5YR4/3	sbk, m, 1	vfr	2, f, co	0, we	c, s	*84.62*	*7.63*	*7.76*	0.69
3Bt2b	79-91	7.5YR4/3	7.5YR4/3	sbk, m, 1	vfr	v1-1, f, co	0, we	a, b	*81.80*	*9.73*	*8.47*	0.86
4Btk1b	91-110	7.5YR4/4	7.5YR4/3	sbk, c, 2	vfr	1, f, po; 2, f, cobr	I-, we	c, s	*82.69*	*7.47*	*9.84*	0.93
4Btk2b	110-130	7.5YR4/3	7.5YR4/3	sbk, c, 2	vfr	1, f, co	I-, we	g, b	*86.95*	*3.89*	*9.16*	1.00
4Bk1b	130-159	10YR5/3	7.5YR5/3	sbk, c-vc, 1	vfr	0	I, me	g, s	*91.15*	*2.74*	*6.11*	1.90
4Bk2b	159-206	10YR6/4	10YR5/3	sbk, vc, 1	lo-vfr	0	I, me	g, s	*93.49*	*2.85*	*3.66*	2.75
4Cb	206-241	10YR6/4	10YR5/4	m	lo*	0	0, we	a, w	*94.32*	*2.17*	*3.51*	1.16
5Btbk	0-15	10YR6/3	10YR5/3	abk, c, 3	fi	obscured	II, ve	a, s	81.92	13.00	5.08	9.11
5Cb	15-120	10YR6/4	10YR5/3	m	lo	0	0, me	a, w	85.64	11.63	2.73	1.87
[1]6Btbk	0-47	7.5YR6/3	7.5YR5/3	pr, vc, 3	fr	obscured	I+, me	a, s	71.34	18.79	9.87	5.38
[1]6Cb	47-148	10YR6/4	10YR5/3	m	lo*	0	0, we	ND	*93.11*	*1.97*	*4.91*	2.63
WP73: sand sheet west of Hard Rocks												
C	0-4	7.5YR5/4	7.5YR4/3	sg	lo	0	0, we	a, s				
2Ab	4-14	7.5YR5/4	7.5YR4/3	sbk, f-m, 1	vfr	0	0, we	c, w				
2Ckb	14-22	7.5YR5/4	7.5YR4/3	m	lo*	0	0, me	g, w				
3Btkb	22-65	5YR5/4	5YR4/3	abk-cpr, c, 2	vfr-fr	1, f, cobr	I+, se	g, w				
3Bwkb	65-91	7.5YR5/4	7.5YR4/3	sbk, m-c, 1	vfr	0	I, se	g, s				
3Bkb	91-109	7.5YR6/3	7.5YR5/4	sbk, c-vc, 1	lo-so	0	0, me	g, s				
3Cb	109-150	7.5YR6/4	7.5YR5/3	m	lo	0	0, we	c, i				
3Coxb	150-200	10YR6/4	7.5YR5/4	m	lo*	0	0, we	ND				
WV10: sand sheet near head of One Cottonwood Canyon												
C	0-5	7.5YR5/3	7.5YR4/3	pl, f, sg	lo	0	0, we	a, l				
2Ab	5-11	7.5YR5/4	7.5YR4/3	sbk, m, m	so	0	0, we	c, w				
2Cb	11-24	7.5YR5/4	7.5YR4/3	sbk, m-c, 1	fr	0	0, we	c, s				
3Bwb	24-46	7.5YR5/4	7.5YR4/3	sbk, c-vc, 1	sh	0	I, me	g, s				
3Btk1b	46-68	7.5YR5/4	7.5YR4/3	sbk, c-vc, 2	h	1, f, po-cobr	I+, me	c, s				
3Btk2b	68-88	7.5YR6/3	7.5YR4/3	pr, vc, 3	vh	1, f, po-cobr	II, se	g, s				
3Bkb	88-112	7.5YR5/3	7.5YR4/3	abk, vc, 2	lo	0	I+, se	a, i				
[1]4Ckb	112-167	10YR5/3	10YR4/3	sg	lo	0	0, me	ND				

[a]Field soil descriptions after Birkeland (1991).
[b]Soil colors determined using Munsell soil color chart.

[c]Structure codes. Type: gr - granular; sbk - subangular blocky; abk - angular blocky; pr - prismatic; cpr - columnar; pl - platy. Size: f - fine; m - medium; c - coarse; vs - very coarse.
[d]Dry consistence codes: lo - loose, noncoherent; lo* - loose and moist; so - soft; sh - slightly hard; h - hard; vh - very hard.
[e]Clay film codes. Amount: vf - very few; 1 - few; 2 - common; 3 - many. Distinctness: f - faint; d - distinct. Location: pf - ped faces; po - pores; cobr - colloid coats and bridges. Obscured means that clay films are likely present but obscured by subsequent accumulation of pedogenic carbonate or silt.
[f]Carbonate field stage and effervescence codes: we - weak; me - moderate; se - strong; ve – violent;
[g]Lower boundary codes: Distinctness: a - abrupt; c - clear; g - gradual; d - diffuse. Topography: s - smooth; w - wavy; b - broken. BOP - bottom of pit.
Laboratory analyses in italics were performed at the Quaternary Soil and Sediment Laboratory at the University of New Mexico, all others were performed at the USGS Soils Laboratory in Denver, Colorado.
ND – no field data; laboratory analyses were not performed for sites WP73 and WV10.
[1]Parent material is interpreted to be alluvium, all other parent materials are eolian.

CHAPTER 3

Soils as a resisting force in a semiarid eolian system: late Quaternary eolian landscape evolution of the Moenkopi Plateau, northeastern Arizona

Abstract

Eolian deposits and landforms exhibiting buried and relict soils are common in one of the largest North American dune fields located in the Four Corners region of the southwestern US. An eolian chronology for the Moenkopi Plateau dune field, developed using soil stratigraphic techniques and optical dating, is broadly similar to other eolian chronologies from the region. The oldest unit (Qe1), comprising sand sheets and linear dunes that stabilized from ~ 12-7.5 ka, is regionally extensive and linked to increase in sediment supply from the Little Colorado River and its tributary watersheds during the late Pleistocene. Soil development proceeded rapidly during the early Holocene and the development of argillic horizons has strengthened internal cohesion enough to prevent substantial reactivation of Qe1. Two younger units, Qe2 (~ 4.2-3.5 ka) and Qe3 (< 2.8 ka), are only locally abundant and linked to proximal sediment sources. Indices widely used to predict eolian activity, such as drift potential, the mobility index, or the ratio of precipitation to evapotranspiration, suggest that dune fields on and near the Moenkopi Plateau should be more active than observed and predict reactivation of eolian sand under modeled climate change scenarios. However, strong pedogenic alteration of the most extensive deposits has prevented regional reactivation under climate change of greater magnitude during the middle Holocene. To improve predictions of future dune activity, the degree of soil development in eolian deposits should be considered when evaluating sediment availability in eolian systems.

Introduction

Eolian deposits are ubiquitous on the southern Colorado Plateau (e.g. Hack, 1941; Hack, 1942; Wells et al., 1990) and strongly influence landscape evolution (e.g. Wells et al., 1990; McFadden and McAuliffe, 1997). Buried and relict soils in these eolian deposits potentially record long-term variability in paleoenvironmental conditions (Wells et al., 1990; Ellwein, 1997; Reheis et al., 2005; Ellwein et al., 2011). Global climate change models predict increasing aridity in many dryland settings (e.g. Field et al., 2007) and many researchers speculate that decreasing effective moisture will reactivate dune fields under these model scenarios. Increased aridity, produced either through increased temperature and/or reduced precipitation resulting in decreased effective moisture, is specifically predicted to destabilize vegetative cover on currently stable dunes and cause consequently reactivation of the many North American dune fields, such as the Great Plains dunes (e.g. Muhs and Maat, 1993; Madole, 1994; Muhs and Holliday, 1995; Muhs and Wolfe, 1999; Forman et al., 2008) and even high-latitude dunes on the Canadian prairies (Wolfe et al., 2001; Hugenholtz and Wolfe, 2005). But what will happen to eolian sand dunes that are stabilized, not only by vegetation, but also by moderate to advanced pedogenic alteration?

To answer this question, we conducted an intensive soil-stratigraphic study supported by OSL dating on the Moenkopi Plateau and surrounding areas. The Moenkopi Plateau in northeastern Arizona lies within of one of the largest North American dune fields (fig. 1) and features extensive eolian landforms easily observed from space (Breed et al., 1984). This region is an excellent study area because it: 1) is currently semiarid, but predicted to undergo decreasing effective moisture conditions with future climate change; 2) contains both active dunes and stable dunes and sand sheets (Hack, 1941; 1942) with well-developed surficial and

buried soils (Ellwein et al., 2011), as well as areas of fluvial-eolian sediment recirculation under current conditions (Hack, 1941; Breed and Breed, 1979; Billingsley, 1987; Stokes and Breed, 1993); and 3) has experienced minor human impact primarily through livestock grazing and development of related two-track roads. The goals of this study were to resolve the depositional history, age, and paleoenvironmental setting of eolian deposits and associated soils and buried soils that represent episodes of deposition, erosion, and stability on the Moenkopi Plateau and evaluate their future stability under conditions of decreased effective moisture.

The conventional view of eolian sand dune systems is that their formation or activity indicates arid conditions or decreasing effective moisture, and dune stability indicates either decreased wind power or increased effective moisture and subsequent vegetation and stabilization of eolian landforms (e.g. Hack, 1941; Muhs and Holliday, 1995; Lancaster, 2008). While these relationships often hold true, recent work suggests that eolian system dynamics are more complicated than these simplified scenarios (e.g. Kocurek and Lancaster, 1999; Lancaster, 2008). In fact, increased eolian activity in the southern Colorado Plateau dune fields may be more strongly related to increases in sediment supply than aridity (Karlstrom and Karlstrom, 1986; Wells et al., 1990; McFadden and McAuliffe, 1997; Ellwein et al., 2011). Based on geomorphic and vegetation mapping, soil stratigraphy, and luminescence dating, this study emphasizes the importance of soil-stratigraphy in providing a structural framework in which to evaluate the long-term stability of eolian systems. Additionally, an understanding of the interrelationships between these data sources elucidates the role of soil development as an important geomorphic process that promotes cohesion of sand dunes and therefore resistance to eolian erosion or reactivation. We argue

that significant pedogenic alteration, specifically the development of horizons common in soils of arid to semiarid climates (e.g., argillic horizons with strong soil structure and consistence) should be included in the list of critical factors that can reduce sediment availability in eolian landform morphodynamics.

Study Area and Previous Work

The broad low-relief Moenkopi Plateau ~100 km northeast of Flagstaff, AZ lies at elevations between 1600-1900 m and is mantled with and surrounded by extensive eolian deposits. The ephemeral Little Colorado River and its tributaries, Moenkopi Wash and Dinnebito Wash, drain the surrounding area. The plateau, ~ 400 m above the washes, is relatively undissected and largely removed from extralocal alluvial or colluvial sources of sediment. The regional dip of sedimentary units is approximately 3° to the north-northeast (Billingsley, 1987). The resistant Jurassic Navajo sandstone defines the Adeii Eechii Cliffs escarpment along the southwestern edge of the Moenkopi Plateau. Jurassic Glen Canyon Group and upper Triassic sandstones and shales are exposed to the southwest of the escarpment, and Cretaceous Mesa Verde Group sandstones are exposed on Howell Mesa and areas northeast of the plateau (fig. 2).

Active and stabilized linear dunes, the main dune type on the Moenkopi Plateau (Hack, 1941; Stokes, 1964; Breed et al., 1984; Billingsley, 1987; Stokes and Breed, 1993), trend roughly parallel to the dominant southwestern wind direction (Helm and Breed, 1999). Active linear dune crests, which average ~ 40 m wide near the escarpment edge and extend downwind ~ 3-4 km (Breed and Grow, 1979), constitute a relatively small portion of the field (Breed et al., 1984) and occur along the Adeii Eechii Cliffs (fig. 3; Billingsley, 1987) as well as other northwest-southeast trending escarpments, including Coal Mine Canyon and

Appaloosa Ridge on Coal Mine Mesa (this study). Interdune areas, approximately 100 m wide (Breed and Grow, 1979; Billingsley, 1987), are currently stable throughout the dune field. Dune slopes and crests become increasingly vegetated and stable to the northeast, downwind from the active portion of the field. Breed et al. (1984) used well-log data to show that in places eolian deposits on the Moenkopi Plateau are intercalated with alluvium to a thickness of ~10 m.

Dominant vegetation on the Moenkopi Plateau is a grassland-subshrub community consisting largely of *Ephedra spp*. (mormon tea), *Artemisia filifolia* (sand sage), *Yucca sp*., *Gutierrezia sarothrae* (snakeweed), with *Juniperus sp*. at higher elevations and *Atriplex canescens* (four-winged saltbush) near ephemeral washes. *Bouteloua gracilis* (blue grama), *Muhlenbergia pungens* (sandhill muhly), *Oryzopsis hymenoides* (Indian ricegrass), *Hilaria jamesii* (galleta), and *Hesperostipa comata* (needle and thread grass) are locally abundant. Two invasive species, *Bromus tectorum* (cheat grass) and *Salsola tragus* (Russian thistle), are common in disturbed areas.

Though climbing dunes that extend from the Little Colorado River valley to the elevation of the Moenkopi Plateau are uncommon today, Billingsley (1987) showed petrographic evidence that eolian sediments on the Moenkopi Plateau are in part derived from eolian sandstones that outcrop between the Little Colorado River and the Adeii Eechii Cliffs. Two late Triassic to early Jurassic eolian sandstone units that occur upwind of the Moenkopi Plateau, the Lukachukai member of the Wingate sandstone and sandstones of the overlying Moenave Formation, are composed predominantly of distinctive pale to dark red quartz sand grains. Through extensive sampling and analysis, Billingsley showed that grains from these sandstones are present in most eolian sediments on the Moenkopi Plateau except

for the active linear dune crests along the Adeii Eechi Cliffs, which he shows to be derived from the Navajo sandstone. Eolian and fluvial mixing of sediment derived from both local and regional sources makes the definitive determination of source rocks for the Moenkopi dunes and sandsheets problematic, however, fluvial sediments aggregated from many watersheds are the most likely ultimate source of sediments that compose the extensive eolian deposits on the Moenkopi Plateau.

The climate of the study area is semiarid, cool, and windy with bimodal annual precipitation peaking during the monsoon season and winter months. On the northwestern edge of the Moenkopi Plateau at Tuba City (~1500 m), nearly 37% of the yearly average precipitation falls during the monsoon season (July through early September) and May and June typically have the least precipitation (period of record 1900-2005; WRCC, 2010). Mean annual precipitation (MAP) averages 163 mm (6.43 in.) with a mean average temperature (MAT) of 12.8° C (55.1° F). The USGS Gold Spring Geomet station along the Adeii Eechii Cliffs reports 143 mm MAP and 12.0°C MAT (period of record 1980-1992; Helm and Breed, 1999). Winds of sand moving strength measured at the Gold Spring station are dominantly from the southwest with maximum average wind speeds occurring in April and May (Billingsley, 1987; Helm et al., 1995). Winds at this site are more than sufficient to transport sand (Helm and Breed, 1999; Lancaster and Helm, 2000). In fact, calculated drift potentials for the Gold Spring Station are among the highest reported globally (Fryberg and Dean, 1979). The historical summary from Cameron, AZ along the Little Colorado River (period of record 1962-1992; WRCC, 2010) shows that this lower elevation station (~ 1270 m) experiences lower effective moisture (MAT = 14.2 °C, MAP = 144 mm).

The mobility index (Lancaster, 1988), a widely used index of dune mobility, incorporates sediment transport capacity as well as climate variables that limit sediment supply and availability through soil moisture and vegetative cover:

$$M = \frac{W}{P/PE};$$

where dune mobility (M) is a function of the a ratio of the percentage of time winds are of sand-moving strength (W) to the ratio of precipitation (P) over potential evapotranspiration (PE). The mobility index predicts that eolian landforms in the study area should be entirely active, with M values between 133-164 (Lancaster and Helm, 2000). However, deposits on the Moenkopi Plateau are largely stabilized except for localized areas with semi-active dune crests. The ratio of precipitation to potential evapotranspiration (P/PE) alone has been shown to a better predictor of eolian activity in some semiarid eolian systems (e.g. Muhs and Holliday, 1995), but this approach also predicts that most eolian deposits should be active on Black Mesa (Muhs and Been, 1999). Models used to predict eolian activity (drift potential, the mobility index, and the ratio of P/PE) are not characterizing the actual conditions on the Moenkopi Plateau, as most eolian sand deposits are currently stable and vegetated.

Methods

The distribution of eolian deposits was mapped using orthorectified Landsat images at ~28.5 m resolution and a mosaic of USGS black and white digital orthophoto quadrangles (DOQs) with 1 m resolution. Criteria used to map eolian units included 1) relative brightness on DOQs, 2) spectral variations in Landsat bands, 3) vegetation type and density, and 4) the

shape, distribution, and spatial scale of geomorphic features. Initial units were chosen during field reconnaissance. After extensive field reconnaissance and field checking of map units, eolian deposits were mapped at ~1:50,000 on Landsat scenes using either a 4-2-1 or 2-4-7 band combination in RGB for optimum visualization of eolian units and differentiation from non-eolian materials. Initial mapping was refined at scales between 1:5000 and 1:20,000 using 1-m DOQs and a 10-m digital elevation model (DEM) mosaic. All data were georeferenced and compiled in a GIS for analysis.

Eolian landscape evolution of the Moenkopi Plateau was reconstructed using standard soil stratigraphic techniques in conjunction with optically stimulated luminescence for age control. Field reconnaissance and initial field mapping included examination of surficial materials and small cores taken with a hand auger, mapping field relationships, recording vegetation and soil associations, and checking access to potential sites in this large (~ 3000 km^2) sparsely-populated study area. Eolian stratigraphy and soil development were evaluated in detail at multiple representative sites in soil pits dug by hand from the surface, as well as in pre-existing exposures such as blowouts and road cuts. Field descriptions of soil profiles include depth and thickness of soil horizons, horizon boundaries, soil colors, texture, structure, consistence, and morphology of clay films and pedogenic carbonate (e.g. Birkeland, 1999).

Bulk soil samples were collected from each horizon of each described profile or stratigraphic section, air-dried and split for various analyses. Prior to particle size analysis, carbonate was extracted with a 15% hydrochloric acid solution, and organic matter was extracted with a 30% solution of hydrogen peroxide when necessary. Particle size analysis on the < 2mm fraction was performed using sodium pyrophosphate dispersion, sieve separation,

and pipet extraction following settling time procedures (Day, 1965) for several samples; others were determined as volume percentage by a laser-light scattering method (McCave and Syvitski, 1991) using a Malvern 2000 Laser Particle Size Analyzer. Carbonate content was measured using a manometric technique following procedures described in Machette (1985).

Eolian quartz sand was dated directly using optically stimulated luminescence (OSL), which provides the timing of last exposure of quartz grains to direct sunlight. For a complete outline of OSL methods used in this study, see chapter 2. Our sampling strategy consisted of obtaining OSL samples from fourteen well-defined soil-stratigraphic contexts. Eight of the fourteen were sampled for a total of eleven OSL samples. Highly variable field moisture values reflect that samples were collected throughout the year. Dose rates were calculated assuming a 10% average soil moisture value, as a reasonable average of potential field in this arid to semiarid setting. OSL ages from this study and dated deposits from other regional eolian chronostratigraphies (e.g. Wells et al., 1990; Stokes and Breed 1993; Reheis, et al., 2005; Ellwein et al., 2011) were used to develop correlated ages for soil profiles not dated in the study.

We also conducted a small pilot project to test whether the active linear dunes along the Adeii Eechii Cliffs are derived from sediments from the adjacent Navajo sandstone as suggested by Billingsley (1987). To test whether geomorphic evidence supports Billingsley's petrographic evidence, we described sediments along three transects, from crest to interdune, along the length of a typical linear dune. Natural exposures in linear dunes along the Adeii Eechii Cliffs are rare, so samples were described from hand-augered cores taken vertically to bedrock or a maximum depth of 400 cm (total depth of auger). Field descriptions include dry

color, sediment composition, grain size, sorting, rounding, soil texture, approximate depth of boundaries of units, effervescence and approximate carbonate stage as well as dominant vegetation and vegetation density at each site. We measured the bulk magnetic susceptibility of dune sediments and compared them to values from the Navajo sandstone, which in this region is a white (5Y8/2) weakly-cemented sandstone composed of clear quartz grains (Billingsley, 1987). We did not evaluate the mineralogy or grain size of soil magnetic carriers, here we use magnetic susceptibility only as an independent measure of comparability. Bulk magnetic susceptibility was measured using an AGICO MFK1 kappabridge available at the UNM Paleomagnetism Laboratory. Bulk samples were prepared from the Navajo sandstone, and from individual units described along three transects that spanned the crest and interdune of a semi-active linear dune positioned just downwind of an actively eroding exposure of the Navajo sandstone. Individual samples were packed into plastic cubes of known mass, the mass of the sample was determined, and then measured three times under a 300 A/m field to determine an average bulk magnetic susceptibility for each specimen. The resulting measured bulk susceptibility values were normalized to sample mass and reported in SI units.

Results

Geomorphic Mapping

Linear dunes are the predominant dune forms in the study area. Linear dunes and sand sheets cover most of the surface of the Moenkopi Plateau (fig. 4), especially on slopes < 5-10°. Approximately 70% of eolian deposits are stabilized in the study area; however, southwest facing escarpments (e.g. Adeii Eechii Cliffs and escarpments within the Coal Mine Canyon area) and the northwestern edge of the Moenkopi Plateau commonly host linear

dunes with active crests. Linear dunes with active, lightly vegetated crests are easily identified on DOQs and Landsat imagery as bright northeast-trending streaks. In contrast, stabilized vegetated linear dunes and interdunes with strong soil development (described below) appear much darker than crests. Image analysis shows that active linear dune crests along the Adeii Eechii Cliffs have similar spectral response to outcrops of the Jurassic Navajo sandstone positioned immediately upwind of active dune crests (fig. 5). Active linear dune crests are also observed downwind from alluvial channels that drain bedrock slopes of Appaloosa Ridge towards the southwest. These ephemeral channels end near the tails of active dune crests that head at the Adeii Eechii Cliffs (fig. 5). Active linear dune crests are commonly 4-6 m above interdune areas, whereas, in the stabilized parts of the field area dune crests are typically only ~ 1-2 m high.

Upwind of the Moenkopi Plateau, on the lower, more arid landscapes of the Painted Desert and Ward Terrace, linear dunes are uncommon and two major, dominantly active, eolian map units were identified based on spectral response. The first unit, floodplain-adjacent dunes, consists of thin sand sheets adjacent to local channels (depicted as red polygons in fig. 4). These sand sheets locally contain a wide variety of active eolian landforms, such as barchan and parabolic dunes, small climbing and falling dunes, and complex dune forms that exhibit characteristics of more than one eolian landform (Billingsley, 1987). Landsat imagery is particularly useful for mapping these floodplain-adjacent eolian landforms that have high spectral contrast with bedrock (fig. 4). Because patches are thin, mapped areas may encompass small areas of exposed bedrock. This unit was not fully field-checked as this region is not widely accessible. Where examined, most floodplain-adjacent deposits are thinly vegetated (visually estimated at <20% cover) and

pedogenic modification was either very weak or not observed. The other mapped eolian unit in this landscape position (bedrock-adjacent dunes) exhibits very little spectral contrast between bedrock and eolian landforms; however, eolian landforms are clearly identifiable in the 1m DOQ mosaic. This unit is found exclusively within the section of the Jurassic Glen Canyon Group that contains the Moenave Formation and the Wingate member of the Lukachukai Formation. Both bedrock units are red, fine-grained eolian sandstones with grain size and composition similar to the active dunes (Billingsley, 1987).

Eolian Stratigraphy, Generalized Soil Characteristics, and Unit Ages

Extensive field reconnaissance led to identification of fourteen sites on the Moenkopi Plateau (fig. 4) with characteristics representative of eolian soil stratigraphy observed throughout the study area. Soil profiles were exposed and described at each site and dominant vegetation was recorded (table 1). Vegetation characteristics were useful in predicting the degree of soil development in underlying eolian deposits before excavating soil pits. For example, vegetation density is highest on stabilized dunes with Qe1 near or at the surface and vegetation density is lowest, but the number of plant species observed is highest, on Qe3 active linear dune crests. Soil profiles were grouped into three major units on the basis of patterns of soil and sediment characteristics, image analysis, vegetation type and density, and OSL dates. The related development of soil structure, consistence, and oriented clay films were particularly good indicators of the relative ages of eolian deposits. Three eolian units were defined using these criteria before OSL ages were determined; relative ages of the three units endured that test.

The most spatially and volumetrically extensive eolian deposits in the study area exhibit the strongest soil development and oldest OSL ages. The unit associated with these

deposits, Qe1, occurs as sand sheets with low relief linear dune crests mantling bedrock to an average thickness of 2-3 meters. Six of fourteen representative soil profiles (WP40, 81, 87, 145, 149, 154) show that this unit is generally characterized by a stage II calcic horizons (e.g. Birkeland, 1999) and weak to moderate argillic horizons based on soil morphology and particle size distribution (table 2; Soil Survey Staff, 1994). Where parent material was not completely pedogenically modified to the underlying contact with bedrock, the unmodified sediment colors range from yellowish red to brown (5YR to 7.5YR). Any original stratigraphy within deposits of unit Qe1, such as cross bedding, has been completely obliterated by pedogenesis and bioturbation. These stable eolian landforms currently sustain a relatively dense *Ephedra spp.-Yucca spp.- H. jamesii -M. pungens* community (~50-80% cover; table 1), except where overlain by younger soil-stratigraphic units. OSL ages for the Qe1 soil stratigraphic unit range from ~12 to 7.5 ka (E-7, E-19, E-20, E-21; table 3).

Unlike other eolian units in this study, Qe2 is not identified on the basis of its associated biotic community, vegetation density, distinctive eolian landforms or patterns in imagery; Qe2 is solely identified instead on the basis of soil attributes observed in exposures and excavations. Qe2 is the least extensive unit in the study area, less pedogenically altered than Qe1, and observed and described only in trenches that expose the interior of active linear dune crests or in uncommon blowouts. Seven soil pits expose Qe2 deposits (WP63, 65, 66, 69, 86, 144, 149; table 2) and are characterized by calcic horizons with stages that range from I- to I+ (Bk horizons) and B-horizon rubification (Bwk horizons); coarse texture precludes classification of these B horizons as cambic horizons. Qe2 is almost always capped with weakly to pedogenically unmodified sand (Qe3, discussed below) along linear dune crests; therefore, Qe2 is associated with the high-relief landforms and vegetation patterns

characteristic of active linear dune crests of Qe3 age. Qe2 deposits yield OSL ages of ~4.2 to 3.5 ka (E-6, E-9, E-18; table 3).

The unit designated Qe3, includes the most recently deposited eolian sand or eolian materials associated with currently active eolian landforms. Qe3 deposits occur in all landscape positions and are associated with the widest variety of eolian landforms observed in the study area. In fact, most surfaces on the Moenkopi Plateau are covered with at least a thin (10-20cm) layer of pedogenically-unmodified sand. Eleven of the fourteen described soil profiles (excluding WP40, 145, 154) either consist entirely of or are capped with Qe3 deposits. Qe3 exhibits the widest range in parent material colors from yellowish red, to brown, to yellowish brown (5YR, 7.5YR, 10YR) and either very weak color or soil carbonate stage development (incipient B horizon) or show no discernable soil horizonation. As a result, sedimentary structures, such as trough and low-angle cross bedding, are only observed and/or preserved in Qe3 deposits. Qe3 is usually expressed on the Moenkopi Plateau as active linear dune crests ~1-2 m thick over previously stabilized (Qe1 and/or Qe2) linear dune crests. Active linear dune crests are up to 6 m higher than the interdune elevation, thinly vegetated (< 30%) landforms that support a variety of grasses (e.g. *Muhlenbergia pungens, Hilaria jamesii, Oryzopsis hymenoides*), sand-adapted perennials (e.g. *Tripterocalyx cyclopterus, Penstemon ambiguous, Poliomintha incana*), and a wide variety of annual herbaceous plants, though only dominant plants were recorded. Coppice dunes supporting a nearly monotypic Ephedra spp. community are common on linear dune flanks where crests are active. Though not described, field reconnaissance observations suggest that most eolian landforms and deposits upwind from the Moenkopi Plateau, in the lower elevation position between the Little Colorado River and the Adeii Eechii Cliffs, cluster

within unit Qe3. Three OSL ages (E-4, E-5 and E-10; table 3) show that sampled sediments with Qe3 characteristics are younger than 2.8 ka. This large range suggests that periodic late Holocene destabilization of Qe3 has precluded the development of weak soils (e.g. Bw horizons).

Eolian transportation winnows and sorts sediments, and as such we might expect that the texture of original parent material comprising sand dunes would be well-sorted sand. The typical trajectory of Aridisol development includes the accumulation of increasing amounts of silt and clay, as well as soil carbonate, with time. In keeping with the expected results, those samples with the most fines (silt and clay) and most soil carbonate are from Qe1soils, but overlap between all units renders them virtually indistinguishable using these criteria (fig. 5). Therefore, soil texture and mass percent carbonate were not primary characteristics used to define units in this study.

Soil Properties Associated with Sediment Cohesion

In this study, all Qe1 profiles are characterized by argillic horizons (Bt) defined by the presence of oriented clay films that form as clay particles are mechanically translocated into the B horizon (Birkeland, 1999). Oriented clay films were observed as bridges between or colloidal coatings on sand grains. Soil structure is relatively advanced and is typical of argillic horizons in Aridisols. Soil structural units (peds) are moderately to strongly developed with structural type ranging from angular blocky to prismatic (table 4).

Dry consistence of Qe1 argillic horizons, evaluated in the field, ranges from slightly hard to very hard, with 75% ranked hard to very hard; every Qe1 soil profile (except WP87) has at least one argillic horizon with hard consistence (see Birkeland, 1999 for definitions of morphological properties). Dry consistence is a measure of the "cohesion of soil particles to

one another and the resistance of the soil mass to deformation" (Birkeland, 1999). The upper 0.5 m of the WP87 profile was notably moist at the time this profile was described in the field. Atmospheric humidity can strongly influence the erodibility of sediments (e.g. Ravi et al., 2006) and may account for the weak cohesion in WP87 despite relatively strong soil structure.

In contrast, 13 of 18 Qe3 soil horizons are classified as C horizons with very weak to weak aggregation (structural grade) and noncoherent to weakly coherent consistence (table 2). Qe3 soil horizons range widely in the amount of fines (72-95% sand) and soil carbonate (1-4%).

Qe2 soil profiles bridge soil characteristics of Qe1 and Qe3, but are generally more similar to Qe3 sediments and soils. The most well-developed Qe2 soil horizons, rubified and/or carbonate-rich B horizons (Bwk and Bk, respectively), are usually characterized by weak to moderate aggregation (structural grade) and range from weakly coherent (soft) to slightly hard consistence. WP144 is the only Qe2 soil profile exhibiting horizons with hard dry consistence and elevated soil carbonate (see horizon 3Bkb in table 2); this thin hillslope deposit consists of intercalated eolian and colluvial sediments. Besides this particular Qe2 profile, soil carbonate typically ranges from ~1-4% and sand from 75-96% in Qe2 soils and sediments (table 2).

Boundaries between eolian stratigraphic units are more sharply defined than boundaries between soil horizons within units (table 5). Abrupt contacts within units usually occur where a unit consists of more than one deposit. For example, the Qe3 unit identified at WP69 is composed of two distinct deposits (parent materials) separated by an abrupt boundary. In contrast, Qe1 deposits commonly have abrupt upper boundaries in well-

developed B horizons (Btk). The sharp upper contact of Qe1 and lack of buried A horizons suggests that the uppermost horizons of Qe1 have been eroded, presumably because such eluvial horizons would have been less cohesive than the most clay enriched part of the argillic horizons or carbonate-cemented Btk horizons. However, the bulk of the most structurally cohesive argillic horizons have remained intact.

Evaluating bedrock contributions to escarpment-adjacent linear dunes

Landsat image analysis shows that active linear dune crests along the Adeii Eechii Cliffs escarpment are spectrally similar to outcrops of the Navajo sandstone along the escarpment. Billingsley (1987) proposed on the basis of petrographic analyses that these crests are probably composed of sand derived from the Navajo sandstone. The Navajo sandstone is composed of 94-97% well to very well rounded, clear frosted quartz and 3-6% clear to light red quartz (Billingsley, 1987) in this particular study area. In contrast, eolian sandstones upwind of the Navajo sandstone, the Lukachukai member of the Wingate sandstone and the Moenave Formation, are dominantly composed of pale red to dark red or yellow quartz grains (Billingsley, 1987). Given that the parent material of the active linear dunes is clear frosted quartz sand, the local Navajo sandstone outcrops do not contain magnetic minerals, and that eolian sediments on the Colorado Plateau commonly gain silt-sized magnetic phases during soil formation (e.g. Reynolds et al., 2001; Reynolds et al., 2003; Reheis et al., 2005), a single dune was evaluated to determine changes in magnetic susceptibility as a function of position. This was done to evaluate the importance of a bedrock contribution to the linear dunes found upwind of the Adeii Eechii Cliffs. The stratigraphy within an active linear dune of average length (~2.5 km) at Gold Springs was examined to test how much sand is derived from local bedrock exposures. Because of lack

of natural exposures at this location, samples were described from hand-augered cores taken vertically to bedrock or 400cm (total depth of auger) obtained along three transects perpendicular to linear dune orientation (fig. 7, table 6). At the head of the dune, roughly 200 m from the steepest edge of the escarpment, total sand thickness is estimated to be ~10 m.

Our studies show that sand on the crest of the linear dune is very similar in grain size, sorting, and rounding to sedimentologic features observed in the Navajo sandstone (Billingsley, 1987). It also has the lowest magnetic susceptibility values and is most similar to Navajo sandstone (inset charts in figure 7) and does not contain the clear red quartz grains common in the other cored units (table 6). From the first transect to the third, surface crest samples become redder and magnetic susceptibility values and vegetation density (table 7) increase with distance downwind from the Adeii Eechii Cliffs. Red quartz grains become more common both downwind and with depth in cores. In general, soil and sediment colors get redder with depth in all cores except the crest core at the head of the dune. Field textural classifications show that active crest samples are classified as sand, but units below have increasing amounts of silt and clay. Effervescence and estimated carbonate stage increase with depth, as do magnetic susceptibility values, suggesting increasing concentrations of magnetic phases (e.g., hematite) presumably as dust is incorporated into soils. The rate of change of described characteristics along the dune crest is much less than the rate of change from dune crest to interdune or the rate of change with increasing depth at any core site except 1A. In all cases, those units correlated to Qe2 and Qe1 based on soil characteristics, contain fine, rounded, frosted, clear red quartz grains that based on petrographic analysis (Billingsley, 1987) are likely derived from either the late Triassic- early Jurassic Wingate Formation or Moenave Formation sandstones and not from the Navajo Formation sandstone.

Well log analyses suggest that the combined alluvial and eolian cover on the Moenkopi Plateau can be up to 10 m thick in places (Breed and others, 1984); however, this pilot study indicates that eolian sand along the Adeii Eechii escarpment is less than 4 m thick in the interdune position and thickest (6-10 m) along the linear dune crests. Alluvium was not observed at this site.

Outside of the Gold Spring linear dune coring site, all described soil profiles contain the very-fine to fine, rounded and frosted, clear red quartz grains shown to be derived from eolian sandstones located in areas upwind of those soils (Billingsley, 1987). The only exceptions are the uppermost ~90 cm at WP38, the top ~240 cm at WP63, and the entire section at WP149. WP38 is located downwind of an active channel eroding Jurassic sandstones and WP63 is located immediately upwind of heavily fluted exposures of the Navajo sandstone. WP149 is located along an escarpment of Coal Mine Canyon that exposes strongly fluted upper Jurassic sandstones and active but small climbing dunes. The latter dunes are observed upwind of linear dunes with active crests. Proximity suggests a very local source for sand at these particular locations.

Climbing dunes or sand ramps are not observed along the majority of the Adeii Eechii Cliffs, except as small, eroded remnants (e.g. WP144). One exception is a climbing dune that occurs near the northwestern end of the escarpment (fig. 4). Active sand (Qe3) immediately downwind of the ramp is spectrally similar to both the ramp and Moenave outcrops, suggesting a mainly local (immediately upwind) source for the sand composing the climbing dunes and the sand along the northwestern edge of the Moenkopi Plateau.

Discussion

Based on soil stratigraphic relationships, geomorphic mapping, and OSL ages, three major periods of eolian sand stabilization or activity have been identified in the Moenkopi Plateau study area. We define units Qe1, Qe2, and Qe3 on the basis of their soil profiles, buried soils and stratigraphic relationships. A topographic profile through the study area illustrates that Qe1 is the most widespread unit and active linear dune crests are located primarily along major escarpments (fig. 8). More than 70% of the surface of the Moenkopi Plateau is mapped as Qe1 and this unit has been shown to underlie Qe2 and Qe3 in most landscape positions.

Two important interpretations from the soil descriptions and laboratory data are that 1) Qe2 and Qe3 are, in places, derived from older Qe1 deposits and 2) cohesion imparted by the formation of strong soil structure and consistence in argillic horizons promoted widespread stability of Qe1. The overlap in soil texture and soil carbonate values shown in figure 5 suggests that the parent materials for Qe2 and Qe3 were not always restricted to well-sorted quartz sand devoid of carbonate; the "missing" uppermost horizons of Qe1 are a likely local source of sand for some of these deposits. Supporting evidence includes weak soil profile development (weak structure, consistence and carbonate morphology) in Qe2 and Qe3 soil profiles despite the fact that they may contain as much silt, clay, and carbonate as some Qe1 soils. This inference is supported by the sharp upper boundaries of Qe1 in strongly developed argillic horizons (table 5), which suggest that eolian deflation removed the less resistant, uppermost soil horizons of the Qe1 soil throughout the study area

Timing and Paleoenvironmental Interpretation of the Moenkopi Plateau Eolian Deposits

In the following discussion, we first compare the timing of eolian events on the

Moenkopi Plateau with other eolian records from the Colorado Plateau. To provide paleoenvironmental context for the eolian records, we then compare them with alluvial, lacustrine, and other paleoenvironmental proxies from the southern Colorado Plateau and northern New Mexico (fig. 9). Within this context we then infer dominant eolian geomorphic processes in the study area from the late Pleistocene through the Holocene.

The late Pleistocene and early Holocene

The presence of widespread sand sheets with similar well-developed soil profiles (stage II carbonate morphology and argillans in B horizons), deposited on bedrock, with OSL ages clustered between 7.5-12 ka (Qe1), strongly suggest that the oldest eolian sediments on the Moenkopi Plateau stabilized during the Pleistocene-Holocene climatic transition. Published regional eolian records (from Canyonlands National Park, the Chaco River drainage basin, Black Mesa, as well as the Moenkopi Plateau) show some overlap in dune deposition or stabilization around the time of this major climatic transition. The oldest eolian deposits identified in the Chaco dune field have similar soil characteristics (Btk horizons) and morphology as Qe1 in this study and are estimated to have stabilized between 12-16 ka based on field relationships and a single radiocarbon age (~ 15 cal ka; Wells et al., 1990). Eolian deposits of late Pleistocene age (18-12 ka) in the Canyonlands (Reheis et al., 2005) overlap with the oldest eolian deposits in Chaco, but not with Qe1 from this study. The Black Mesa record (Ellwein et al., 2011) shows stabilization of sand sheets in mesa top landscape positions at roughly the same interval (8-12 ka), with accumulation of eolian sediment in topographically controlled eolian deposits (sand ramps and falling dunes) throughout the late Pleistocene (35 – 10 ka; chapter 2).

The accumulation and stabilization of Qe1 eolian sediments reflects climatic and environmental conditions established by numerous studies. For example, pollen studies from lake sediments of MIS 2 age along the Mogollon Rim yield regional estimates for mean annual temperature (MAT) ~5°C cooler than today (e.g. Weng and Jackson, 1999; Anderson et al., 2000). Packrat midden analyses corroborate these findings with estimated 3-5°C cooler MAT and summer temperatures up to ~6°C (Betancourt, 1990) cooler than present with resulting 600-900 m depression of ecotones recorded at many sites around the Colorado Plateau (e.g. Betancourt, 1990; Anderson, 2000). Atmospheric circulation patterns were strongly affected by the position of the North American ice sheet, driving the jet stream and storm tracks to the south, increasing winter storms and winter precipitation in the southwestern US, and generating strong winds (COHMAP, 1988; Kutzbach et al., 1993; Thompson et al., 1993). Extreme millennial-scale climate variability characterizes the Greenland isotope record during MIS 2 (e.g. Overpeck and Cole, 2006) and lacustrine and speleothem records from the southwestern US reflect both the magnitude and timing of this variability (e.g. Benson et al., 2003; Wagner et al., 2005).

In the early Holocene, temperatures rose with increasing summer insolation, strengthening the summer monsoon circulation between 11-8ka (e.g. Weng and Jackson, 1999) but the rapidly melting ice sheet still influenced air circulation patterns (COHMAP, 1988; Thompson et al., 1993) maintaining the southerly storm track leading to greater precipitation in the southwest relative to today. At this time, "subalpine and montane conifers continued to dominate the modern woodland zone across much of the Colorado Plateau" (Betancourt, 1990) and pollen assemblages suggest increased summer precipitation (Davis and Shafer, 1992). The early Holocene was wetter in some locations than others. The Plains

of San Augustine of central New Mexico (located ~ 350 km to the southeast of the Moenkopi Plateau) received more moisture during the period 10-8.5 ka than before or after (Markgraf et al., 1984) and the pollen record at Montezuma Well on the Mogollon Rim suggests greater precipitation before 8.4 ka than today (Davis and Shafer, 1992), but groundwater levels in southeastern Arizona fall to Holocene levels after 10.6 ka (Pigati et al., 2009). Reheis et al. (2005) report greater atmospheric dustiness and dust fall on the Colorado Plateau during the early Holocene as pluvial lakes in the Mojave began to dessicate with warming and drying climate conditions.

Common falling dunes on Black Mesa, only ~ 40-50 km east of the Moenkopi Plateau study area, indicate that eolian sediment supply was high during MIS 2 and 3 (Ellwein et al., 2011; chapter 2). Sediment supply was apparently high throughout the Colorado River watershed, with more sediment delivered to channels than could be transported as shown by extensive terraces in the eastern Grand Canyon (Anders et al., 2005; fig. 9). This is also consistent with the backfilling of the lower Colorado River during glacial conditions, despite lowered sea-level (Bull, 1991, p. 50). The large volume of sand represented in Qe1 also suggests a regional source such as the Little Colorado River and associated local watersheds; yet, intact climbing dunes or sand ramps that reach the elevation of the Moenkopi Plateau are uncommon. Climbing dunes and sand ramps that delivered these sediments must have largely eroded from the Adeii Eechii Cliffs since sand was delivered to this local highland (Ellwein et al., 2011). Distinctive clear red quartz grains identified by Billingsley (1987) as having their source in the Jurassic Glen Canyon sandstones upwind of the Moenkopi Plateau are commonly found in Qe1 deposits except for those downwind of Coal Mine Canyon. We therefore suggest that eolian sediments, including the distinctive

bright red sand derived from Jurassic Glen Canyon sandstones, were transported to the Moenkopi Plateau via climbing dunes built from sediments from local watersheds as well as the Little Colorado River during the extreme windiness and climate variability of the late Pleistocene (MIS 2 and 3).

OSL ages show that linear dunes and sand sheets in the study area stabilized during the relatively cool and moist late Pleistocene-early Holocene climatic transition. Falling dunes and sand ramps of late Pleistocene age (MIS 2 and 3) are common to the east on Black Mesa (chapter 2). The lack of eolian sediments of this age suggests that the largely undissected Moenkopi Plateau acted predominantly as a transport surface. High effective moisture and decreased climatic variability at the Pleistocene-Holocene transition would have encouraged initial vegetative stabilization of the eolian sand in transport. Increased atmospheric dustiness (~12-8.5 ka) led to rapid soil formation in eolian sand deposits across the Colorado Plateau (Wells et al., 1990; Reheis et al., 2005). Accumulated clay, silt, and soil carbonate act as cementing agents in initially noncohesive sand, increasing resistance to deflation as described above. The addition of fines also increases the water holding capacity of the sediments, likely enabling at least some drought resistant shrubs and grasses to persist through the mid Holocene "climatic optimum" (see below).

The early middle Holocene "climatic optimum" (~ 8-6 ka)

Eolian deposits dating to this period are lacking in the study area except for the WP65 site (7.2 ± 0.7 ka), which is exposed in a blowout in a Qe1 sand sheet on Coal Mine Mesa. The soil profile was not excavated to bedrock at this location, but bedrock was observed within the deepest part of the blowout and was not capped with eolian deposits with typical Qe1 soil characteristics. In fact, none of the published eolian records from the Colorado

Plateau capture significant dune deposition during this most arid part of the Holocene. Wells et al. (1990) infer that the Qe2 unit they described in the Chaco River drainage basin was deposited under conditions of increased effective moisture during the neoglacial (~ 5.6-2.8 ka) with mid-Holocene aridity contributing "the least to eolian depositional volume". Reheis et al. (2005) also report only minor eolian deposition during the middle Holocene.

Many regional studies show that the early middle Holocene (~ 8-6 ka) is generally characterized by very low effective moisture and the highest post-glacial temperatures across the southwestern US (e.g. Overpeck and Cole, 2006; Anderson et al., 2008). Lake levels fell on the Kaibab Plateau (Weng and Jackson, 1999), the Mogollon Rim (Hasbargen, 1994), and in the San Juan Mountains (Toney and Anderson, 2006), with dessication of Chihuahueños Bog in the Jemez Mountains, NM (Anderson et al., 2008). Reheis et al. (2005) report dominant "desertlike" vegetation from ~8.5-6 ka from pollen assemblages in the Canyonlands. The warmest conditions occurred slightly later in southeastern Arizona (Waters and Haynes, 2001) and at ~ 5.6 ka in the Sangre de Cristo Mountains (Jimenez-Moreno et al., 2008).

The late middle Holocene and the late Holocene (6-0 ka)

Eolian records from the Colorado Plateau dune fields at show considerable overlap during the mid to late Holocene (fig. 9). In the Chaco dune field, Wells et al. (1990) report deposition of their Qe2 unit from ~ 2.8- 5.6 ka, with most basal radiocarbon dates occurring ~ 4.0-3.7 ka. Similar to our findings, Holocene eolian deposits thinly and/or incompletely mantle Pleistocene sand sheets at Chaco with Qe2 being the volumetrically smallest deposit. Uncommon, small volume eolian and fluvial deposits are observed in the Canyonlands National Park area from ~ 6-3 ka (Reheis et al., 2005) and Stokes and Breed (1993)

suggested episodic eolian activity after 5 ka on the Moenkopi Plateau and Ward Terrace (4.7, 3-2, and 0.4 ka). The Black Mesa chronostratigraphy (chapter 2) does not capture Qe2 deposition, but linear dunes are uncommon in that study area. Episodic eolian deposition in all four of these study areas resumed by ~ 2 ka and continues to the present day.

During the late middle Holocene (~ 6-4 ka), lacustrine pollen records and midden assemblages show near modern vegetation assemblages (e.g. Hasbargen, 1994; Betancourt, 1990; Jimenez-Moreno et al., 2008; Anderson et al., 2008). Ely (1997) reports a "widespread and synchronous" cluster of floods from 5-3.6 ka across the southwestern US and roughly concurrent alluviation is reported in the Canyonlands (Reheis et al., 2005) and on Black Mesa (Qa1 of McFadden and McAuliffe, 1997). Evidence for the poorly-constrained mid Holocene northern hemispheric cool phase, the neoglacial, is expressed in Arizona and New Mexico as cool periods centered at 5.1 and 4.3 ka from pollen records at Montezuma Well (Davis and Shafer, 1992), two periglacial events in the Sangre de Cristos centered at 5.6 and 2.9 ka and a cirque glacier advance at 4 ka (Armour et al., 2002), and advance or formation of cirque glaciers in the Rocky Mountains (Burke and Birkeland, 1983; Wesling, 1988).

As insolation continued to decrease, effective moisture increased and climate became somewhat cooler and moister during the late Holocene (e.g. Weng and Jackson, 1999; Waters and Haynes, 2001; Anderson et al., 2008; Jimenez-Moreno et al., 2008), though still variable, encompassing both the Little Ice Age and Medieval Warm Period. During the last half of the late Holocene, Ely (1997) shows increasing frequency of floods at 2.2-1.2 ka followed by numerous large magnitude flood events from 1.2-1 ka. Hereford (2002) documents 3 major intervals of alluviation in the Paria River watershed in southern Utah during the past two millennia, which he attributes to changes in flood frequency related to ENSO fluctuations. A

periglacial event at ~ 120 14C yr B.P. in the Sangre de Cristos (Armour et al., 2002) is consistent with Little Ice Age conditions (e.g. cooler and wetter conditions with glacial advances and higher lake levels) experienced throughout the Northern Hemisphere. Using the tree ring record, several studies show that during the last millenium, the western US suffered several, abrupt, multidecadal "megadroughts" of much greater severity than historical droughts (e.g. Stahle et al., 2000; Cook et al., 2004; Meko et al., 2007; Scuderi et al., 2008), including the megadrought coincident with the abandonment of Chaco Canyon (summarized in Cook et al., 2007, p. 109) and roughly concurrent with the Medieval Warm Period.

Valley alluviation and backfilling on Black Mesa (Karlstrom, 1988; Karlstrom, 2005) appears related to wetter phases, as do the eolian deposits on the southern Colorado Plateau. In fact, both Qe2 and Qe3 from this study, the last two periods of eolian activity at Chaco (Wells et al., 1990), and the latest eolian depositional event at Canyonlands (Reheis et al., 2005) occurred during Holocene climates with increased effective moisture (fig. 9). Greater variability in summer precipitation, and in resulting discharge, leads to wider, less vegetated floodplains (Muhs and Holliday, 1995; Hereford, 2002), increasing both sediment supply and availability for the eolian system (Muhs and Holliday, 1995; Kocurek and Lancaster, 1999). Etheredge et al. (2004) argue that the hillslopes of small basins (< 20 km2) produce most sediment/runoff as a result of convective summer storms. The Qe2 climbing dune core (4ka) dates to the tail end of a long phase (5.8 to 4.2 ka) of increased floods (Ely, 1997) and about the same time as lake levels began to rise on the Kaibab Plateau (Weng and Jackson, 1999) signaling increased effective moisture. Hypothesized hillslope stripping during Holocene monsoon storms (as in Etheredge et al., 2004), combined with wide sand-dominated floodplains, increased sediment available to build climbing dunes during Qe2 time. The

relatively small volume of Qe2 deposits is consistent with either 1) more extensive Qe2 deposits that have since been eroded or 2) more localized, small volume event(s), whether eolian sediments were transported to the Moenkopi Plateau via sand ramps or were derived locally from the uppermost horizons of Qe1. In the absence of evidence to the contrary, we prefer the second interpretation.

The volumetrically small and spatially constrained Qe3 unit in the study area represents either 1) local increases in sediment supply from local bedrock outcrops, 2) relatively small volumes of sand supplied to the Moenkopi Plateau by climbing dunes or local washes or 3) local erosion of the uppermost horizons of Qe1 deposits. Active linear dunes along the Adeii Eechii Cliffs are built in part from local increases in sediment supply from local Navajo sandstone outcrops, as evidenced in field relationships (soil and sediment properties) and bulk magnetic susceptibility measurements along the Gold Spring linear dune transects. Increases in soil carbonate, clay and silt, and rubification with depth are all consistent with increasing age and soil development, as are increasing bulk magnetic susceptibility values with depth, which are related to changes in sediment texture resulting from increased abundance of illuvial magnetic phase bearing dust (silt and clay). In contrast, the striking absence of Jurassic Glen Canyon derived clear red quartz grains in the active Qe3 crest sediments, but common presence in underlying Qe2 and Qe1 deposits suggests a change in sand source. The observed relationships are best explained by both more advanced soil development in progressively underlying units as well as a change in sand source from Qe2 to Qe3. The latter interpretation is supported by the presence of prominent fluting features over large expanses of Navajo sandstone outcrops along the Adeii Eechii Cliffs escarpment. The timing of flute formation has not been established, yet the flutes are consistent with a

bedrock source for some Qe3 sand. Linear dunes with active crests are also locally associated with floodplains of internally drained washes on the Moenkopi Plateau (e.g. WP38, 86, 149; fig. 6) with small washes draining the bedrock-dominated hillslopes in the center of the Moenkopi Plateau. Because of the slight northern tilt of bedrock units and the high infiltration rate of dunes, this part of the study area is internally drained and supports seasonal standing water under modern conditions (round dark patches in figure 6). Sediments delivered to these unincised channels are readily available for eolian transport, as shown by active linear dune crests downwind from this source on Appaloosa Ridge. Because Qe3 is spatially and volumetrically restricted, we suggest that this soil stratigraphic unit reflects a period of relatively limited eolian activity.

Implications for the future of the Moenkopi Plateau dune field

Based on the output of 19 IPCC climate models, Seager et al. (2007) predict "the most severe future droughts… will be worse than any since the Medieval period." How might this scenario affect the long-term stability of the Moenkopi dunes? Severe late Holocene megadroughts (e.g. Cook et al., 2004; Cook et al., 2007; Meko et al., 2007) and the mid Holocene climatic optimum, the warmest and driest period experienced since Qe1 deposition, probably caused the observed erosion of the uppermost soil horizons of the extensive Qe1 deposits but did not significantly reactivate this unit. Therefore, we suggest that warming and drying trends predicting by global climate change models may not appreciably reactivate the extensive stabilized southern Colorado Plateau sand sheets and linear dune fields of Qe1 age or older, even if vegetation is strongly affected by drought. However, land use practices that decrease vegetative cover (e.g. overgrazing) or increase

runoff (e.g. from dirt roads and off-road vehicle use) will decrease the resistance of these soil-enhanced eolian deposits to either eolian or fluvial erosion.

Conclusions

The ubiquitous eolian deposits on the Moenkopi Plateau have a relatively simple depositional history elucidated by detailed soil stratigraphic investigations and geomorphic mapping that has allowed recognition of three correlative soil-stratigraphic units and associated landforms. Abundant eolian sediments were supplied to the Black Mesa region during the late Pleistocence (MIS 2 and 3), which enabled the development of climbing dunes and transport of sand over the Adeii Eechii Cliffs (see chapter 2). These sediments stabilized on the elevated Moenkopi Plateau during the Pleistocene-Holocene climatic transition (~12-7.5 ka) with cessation of active eolian transport as sediment supply declined (chapter 2) coupled with high dust flux and associated rapid soil formation (Reheis et al., 2005). Because of pedogenic alteration of the existing Qe1 mantle, widespread eolian reactivation of the entire Moenkopi Plateau has not occurred throughout the Holocene despite the occurrence of conditions under which widespread, extensive dune reactivation would be expected. Small volume and spatially restricted eolian deposits that date to the mid to late Holocene (Qe2 ~ 4.2-3.5 ka; Qe3 < 2.8 ka) are attributed to reworking of the uppermost soil horizons of Qe1 or, in the case of linear dunes near prominent escarpments, increases in sediment supply from local sources.

Active portions of the Moenkopi dune field are spectacular in orbital imagery and air photos, but the majority of the field is inactive. Inactive eolian deposits on the Moenkopi Plateau have remained so throughout the Holocene despite 1) predictions based on current climatic conditions that suggest the dunes should be active, 2) intensive grazing or the

increasing presence of invasive species such as cheat grass and Russian thistle, and 3) periods of elevated aridity, such as the mid Holocene climatic optimum. Stratigraphic and geomorphic relationships delineated in this study, in conjunction with OSL ages, clarify the roles of climate change in driving eolian geomorphic and pedologic processes. We argue that the Moenkopi Plateau dunes are dominantly inactive not because of recently increased effective moisture (Muhs and Been, 1999) or any diminishment of driving forces in the eolian system (e.g. insufficient winds), but because of increased cohesion due to advanced soil development enhancing resistance to erosion within this eolian system.

Although recognized by Hack (1942) as a stabilizing influence in eolian deposits, soil profile development is not explicitly considered in climate-based models used to predict eolian activity (e.g. the mobility index Lancaster, 1988) or more robust recent models that evaluate the factors controlling the eolian system sediment state (Kocurek and Lancaster, 1999). Such models could be improved by explicitly evaluating the stabilizing influence of the geomorphic process of soil formation thus improving the predictive power of the models.

References

Anders, M.D., Pederson, J.L., Rittenour, T.M., Sharp, W.D., Gosse, J.C., Karlstrom, K.E., Crossey, L.J., Goble, R.J., Stockli, L., and Yang, G., 2005, Pleistocene geomorphology and geochronology of eastern Grand Canyon: linkages of landscape components during climate changes, Quaternary Science Reviews, v. 24, p. 2428-2448.

Anderson, R.S., Betancourt, J.L., Mead, J.I., Hevly, R.H., and Adam, D.P., 2000, Middle- and late-Wisconsin paleobotanic and paleoclimate records from the southern Colorado Plateau, USA, Palaeogeography, Palaeoclimatology, Palaeoecology, v. 155, p. 31-57.

Anderson, R.S., Jass, R.B., Toney, J.L., Allen, C.D., Cisneros-Dozal, L.M., Hess, M., Heikoop, J., and Fessenden, J., 2008, Development of the mixed conifer forest in northern New Mexico and its relationship to Holocene environmental change, Quaternary Research, v. 69, p. 263-275.

Armour, J., Fawcett, P.J., Geissman, J.W., 2002, 15 kyr paleoclimatic and glacial record from northern New Mexico, Geology, v. 30, p. 723-726.

Benson, L., Lund, S., Negrini, R., Linsley, B., and Zic, M., 2003, Response of North American Great Basin lakes to Dansgaard-Oeschger oscillations, Quaternary Science Reviews, v. 22, p. 2239-2251.

Betancourt, J.L., 1990, Late Quaternary biogeography of the Colorado Plateau, in Betancourt, J.L., Van Devender, T.R., and Martin, P.S. (eds.), Packrat middens: the last 40,000 years of biotic change, University of Arizona Press, Tucson, p. 259-292.

Billingsley G.H., 1987, Geology and geomorphology of the southwestern Moenkopi Plateau and southern Ward Terrace, Arizona, U.S. Geological Survey Bulletin 1672, 18 p.

Birkeland, P.W., 1999, Soils and Geomorphology, 3rd Ed., Oxford University Press, 430 p.

Breed, C.S. and Breed, W.J., 1979, Dunes and other windforms of Central Australia, and a comparison with linear dunes on the Moenkopi Plateau, Arizona, *in* El-Baz, F. and Warner, D.M., eds, Apollo-Souyez Test Project Summary Science Report, v. 2, Earth Observations and Photography: National Aeronautics and Space Administration Special Publication 412, p. 319-358.

Breed, C.S. and Grow, T., 1979, Morphology and distribution of dunes in sand seas observed by remote sensing, *in* McKee, E.D., ed., A Study of Global Sand Seas, US Geological Survey Professional Paper 1052, p. 253-302.

Breed, C.S., McCauley, J.F., Breed, W.J., McCauley, C.K., and Cotera, A.S., Jr., 1984, Eolian (wind-formed) landscapes, *in* Smiley, T.L., Nations, J.D., Péwé, T.L., and Schafer, J.P. eds., Landscapes of Arizona - the Geological Story: University Press of America, Inc., p. 359-413.

Burke, R.M. and Birkeland, P.W., 1983, Holocene glaciation in the mountain ranges of the western United States, *in* Wright, Jr., H.E., ed., Late-Quaternary Environments of the United States, v. 2, The Holocene, University of Minnesota Press, Minneapolis, MN, p. 3-11.

Bull, W. B., 1991, Geomorphic Responses to Climate Change, Oxford University Press, New York, 575 p.

COHMAP members, 1988, Climatic changes of the last 18,000 years: Observations and model simulations, Science, v. 241, p. 1043-1052.

Cook E.R., Woodhouse, C.A., Eakin, C.M., Meko, D.M., and Stahle, D.W., 2004, Long-term aridity changes in the western United States, Science, v. 306, p. 1015-1018.

Cook, E.R., Seager, R., Cane, M.A., and Stahle, D.W., 2007, North American drought: reconstructions, causes, and consequences, Earth Science Reviews, v. 81, p. 93-134.

Davis, O.K. and Shafer, D.S., 1992, A Holocene climatic record for the Sonoran Desert from pollen analysis of Montezuma Well, Arizona, USA, Palaeogeography, Palaeoclimatology, Palaeoecology, v. 92, p. 107-119.

Day, P.R., 1965, Particle fractionation and particle-size analysis, in Black, C.A., and Evans, D.D., White, J.L., Ensminger, L.E., and Clark, F.E., eds., Methods of Soil Analysis, Part I, n. 9, p. 545-567.

Ellwein, A.L., 1997, Quaternary evolution of eolian landforms, soils, and landscapes of the Petrified Forest National Park, Arizona, New Mexico Geology, v. 19, no. 2.

Ellwein, A.L., Mahan, S.A., and McFadden, L.D., in press, New optically stimulated luminescence ages provide evidence of MIS3 and MIS2 eolian activity on Black Mesa, northeastern Arizona, USA, Quaternary Research.

Ellwein, A.L., chapter 2, this dissertation.

Ely, L.E., 1997, Response of extreme floods in the southwestern United States to climatic variations in the late Holocene, Geomorphology, v. 19, p. 175–201.

Etheredge, D., Gutzler, D.S., and Pazzaglia, F.J., 2004, Geomorphic response to seasonal variations in rainfall in the southwest United States: Geological Society of America Bulletin, v. 116, p. 606–618.

Forman, S.L., Marin, L., Gomez, J., and Pierson, J, 2008, Late Quaternary eolian sand depositional record for southwestern Kansas: landscape sensitivity to droughts, Paleogeography, Paleoclimatology, Paleoecology, v. 265, p. 107-120.

Fryberger S.G. and Dean, G., 1979, Dune Forms and Wind Regimes, in McKee, E.D., ed., A Study of Global Sand Seas, US Geological Survey Professional Paper 1052, p. 137-169.

Hack, J.T., 1941, Dunes of the western Navajo Country: Geographical Review, v. 31, p.240-263.

Hack, J.T., 1942, The Changing Physical Environment of the Hopi Indians of Arizona, Papers of the Peabody Museum, v. 35, no. 1, Harvard University, Cambridge.

Hasbargen, J., 1994, A Holocene paleoclimatic and environmental record from Stoneman Lake, Arizona, Quaternary Research, v. 42, p. 188-196.

Helm, P.J., and Breed, C.S., 1999, Instrumented field studies of sediment transport by wind, in Breed, C.S., and Reheis, M.C., eds., Desert winds: Monitoring wind-related surface processes in Arizona, New Mexico, and California: U.S. Geological Survey Professional Paper 1598, p. 31–54.

Helm, Paula J., Breed, Carol S. , Tigges, Richard, and Garcia, Patricia A. , 1995, Geometeorological data collected by the USGS Desert Winds Project at Gold Spring, Great Basin Desert, northeastern Arizona, 1979 - 1992: U.S. Geological Survey Open-File Report 95-78, U.S. Geological Survey, Flagstaff, Arizona.

Hereford, R., 2002, Valley-fill alluviation during the Little Ice Age (ca. A.D. 1400-1880), Paria River basin and southern Colorado Plateau, United States, Geological Society of America Bulletin, v. 114, p. 1550-1563.

Hugenholtz, C.H. and Wolfe, S.A, 2005, Recent stabilization of active sand dunes on the Canadian prairies and relation to recent climate variations, Geomorphology, v. 68, p. 131-147.

Field, C.B., Mortsch, L.D., Brklacich, M., Forbes, D.L., Kovacs, P., Patz, J.A., Running, S.W., and Scott, M.J., 2007, North America. Climate Change 2007: Impacts, Adaptation and Vulnerability, *in* M.L. Parry, O.F. Canziani, J.P. Palutikof, P.J. van der Linden and C.E. Hanson, eds., Contribution of Working Group II to the Fourth Assessment Report of the Intergovernmental Panel on Climate Change, Cambridge University Press, Cambridge, UK, p. 617-652.

Jiménez-Moreno, G., Fawcett, P.J., and Anderson, R.S., 2008, Millennial- and centennial-scale vegetation and climate changes during the late Pleistocene and Holocene from northern New Mexico (USA), Quaternary Science Reviews, v. 27, p. 1442-1452.

Karlstrom, E.T., 2005, Late Quaternary landscape history and geoarchaeology of two drainages on Black Mesa, northeastern Arizona, USA, Geoarchaeology, v. 20, no. 1, p. 1-28.

Karlstrom, E.T. and Karlstrom, T.N.V., 1986, Late Quaternary alluvial stratigraphy and soils of the Black Mesa – Little Colorado River Areas, northern Arizona, in Nations, J.D., Conway, C.M., and Swann, G.A., eds., Geology of Central and Northern Arizona, Geological Society of America, Rocky Mountain Section Guidebook, p. 71-92.

Karlstrom, T.N.V., 1988, Alluvial chronology and hydro- logic change of Black Mesa and nearby regions, *in* Gumerman, G.J., ed., The Anasazi in a Changing Environment, Cambridge, Cambridge University Press, p. 45–91.

Kocurek, G. and Lancaster, N., 1999, Aeolian system sediment state: theory and Mojave Desert Kelso dune field example, Sedimentology, v. 46, p. 505-515.

Kutzbach, J.E., Guetter, P.J., Behling, P.J, and Selin, R., 1993, Simulated climatic changes: results of the COHMAP climate-model experiments, *in* Wright, Jr., H.E., Kutzbach, J.E., Webb, III T., Ruddiman, W.F., Street-Perrott, F.A., and Bartlein, P.J., eds., Global Climates since the Last Glacial Maximum, University of Minnesota Press, Minneapolis, MN, p. 24-93.

Lancaster, N., 1988, Development of linear dunes in the southwestern Kalahari, southern Africa: Journal of Arid Environments, v. 14, p. 233–244.

Lancaster, N., 2008, Desert dune dynamics and development: insights from luminescence dating, Boreas, v. 37, p. 559-573.

Lancaster, N. and Helm, P., 2000, A test of a climatic index of dune mobility using measurements from the southwestern United States, Earth Surface Processes and Landforms, v. 25, p. 197-207.

Machette, M.N., 1985, Calcic soils of the southwestern United States, *in* Weide, D.L. ed., Soils and Quaternary Geology of the Southwestern United States, Geological Society of America Special Paper 203, p. 1-21.

Madole R.F., 1994, Stratigraphic evidence of desertification in the west-central Great Plains within the past 1000 yr, Geology, v. 22, p. 483-486.

Markgraf, V., Bradbury, J.P., Forester, R.M., Singh, G., Sternberg, R.S., 1984, San Agustin Plains, New Mexico: age and paleoenvironmental potential reassessed, Quaternary Research, v. 22, p. 336–343.

McCave, I.N. and Syvitski, J.P.M., 1991, Principles and methods of geological particle size analysis, *in* Syvitski, J.P.M., ed., Principles, methods and applications of particle size analysis: New York, Cambridge University Press, p. 3–21.

McFadden, L.D., McAuliffe, J.R., Pazzaglia, F.J., 1994, Late Quaternary eolian landscapes and soils of the south central Colorado Plateau, American Geophysical Union 1994 Fall Meeting, EOS Supplement 75, n. 44.

McFadden, L.D., and McAuliffe, J.R., 1997, Lithologically influenced geomorphic responses to Holocene climatic changes in the southern Colorado Plateau, Arizona: A soil-geomorphic and ecologic perspective, Geomorphology, v. 19, p. 303-332.

Meko D.M., Woodhouse, C.A., Baisan, C.A., Knight, T., Lukas, J.J., Hughes, M.K., and Salzer, M.W., 2007, Medieval drought in the upper Colorado River Basin, Geophysical Research Letters, v. 34,

Muhs, D.R. and Been, J.M., 1999, Reactivation of stabilized sand dunes on the Colorado Plateau: U.S. Geological Survey, http://geochange.er.usgs.gov/sw/impacts/geology/sand (last accessed 7/24/2010).

Muhs, D.R. and Holliday, V.T., 1995, Evidence of active dune sand on the Great Plains in the 19th century from accounts of early explorers, Quaternary Research, v. 43, p. 198-208.

Muhs, D.R. and Maat, P.B., 1993, The potential response of eolian sands to greenhouse warming and precipitation reduction on the Great Plains of the United States, Journal of Arid Environments, v. 25, p. 351-361.

Muhs, D.R., and Wolfe, S.A. 1999, Sand dunes of the northern Great Plains of Canada and the United States, *in* Lemmen D.S., Vance R.W. eds., Holocene climatic and

environmental change in the Palliser Triangle: A geoscientific context for evaluating the impacts of climate change on the southern Canadian prairies: Geological Survey of Canada Bulletin 534, p. 183– 197.

Overpeck, J.T. and Cole, J.E., 2006, Abrupt change in Earth's climate system, Annual Review of Environment and Resources, v. 31, p. 1-32.

Pigati, J.S., Bright, J.E., Shanahan, T.M., and Mahan, S.A., 2009, Late Pleistocene paleohydrology near the boundary of the Sonoran and Chihuahuan Deserts, southeastern Arizona, USA, Quaternary Science Reviews, v. 28, p. 286-300.

Ravi, S., Zobeck, T.M., Over, T.M., Okin, G.S., and d'Odorico, P., 2006, On the effect of moisture bonding forces in air-dry soils on threshold friction velocity of wind erosion, Sedimentology, v. 53, p. 597-609.

Reheis, M.C., Reynolds, R.L., Goldstein, H., Roberts, H.M., Yount, J.C., Axford, Y., Cummings, L.S., and Shearin, N., 2005, Late Quaternary eolian and alluvial response to paleoclimate, Canyonlands, southeastern Utah, GSA Bulletin, v. 117, n. 7/8, p. 1051-1069.

Reynolds, R., Belnap, J., Reheis, M., Lamothe, P., and Luiszer, F., 2001, Aeolian dust in Colorado Plateau soils: Nutrient inputs and recent change in source: Proceedings of the National Academy of Sciences of the United States of America, v. 98, no. 13, p. 7123–7127.

Reynolds, R.L., Neff, J., Reheis, M., Goldstein, H., and Lamothe, P., 2003, Distribution of aeolian dust determined from magnetic and chemical properties in surficial substrates of grassland and shrubland, central Colorado Plateau (Utah): Eos (Transactions, American Geophysical Union), v. 84, Fall Meeting Supplement, abstract B11F-06.

Scuderi, L.A., McFadden, L.D., and McAuliffe, J.R., 2008. Dendrogeomorphically derived slope response to decadal and centennial scale climate variability: Black Mesa, Arizona, USA. Natural Hazards and Earth System Science v. 8, p. 869–880.

Seager, R., Ting, M., Held, I., Kushnir, Y., Lu, J., Vecchi, G., Huang, H., Harnik, N., Leetmaa, A., Lau, N., Li, C., Velez, J., and Naik, N., 2007, Model projections of an imminent transition to a more arid climate in southwestern North America, Science, v. 316, p. 1181-1184.

Soil Survey Staff, 1994, Keys to Soil Taxonomy, 6th Edition, Soil Conservation Service, US Department of Agriculture, Pocahontas Press, Inc., Blacksburg, VA, USA, 524 p.

Stahle, D.W., Cook, E.R., Cleaveland, M.K., Therrell, M.D., Meko, D.M., Grissino-Mayer, H.D., Watson, E., and Luckman, B.H., 2000, Tree-ring data document 16th century megadrought over North America, Eos Transactions, AGU, 81(12), p. 121-125.

Stokes, W.L., 1964, Incised, wind-aligned stream patterns of the Colorado Plateau, American Journal of Science, v. 262, p. 808-816.

Stokes, S. and Breed, C.S., 1993, A chronostratigraphic re-evaluation of the Tusayan Dunes, Moenkopi Plateau and southern Ward Terrace, northeastern Arizona, in Pye, K., ed., The dynamics and environmental context of aeolian sedimentary systems, Geological Society Special Publication No. 72, p. 75-90.

Thompson, R.S., Whitlock, C., Bartlein, P.J., Harrison, S.P., and Spaulding, W.G., 1993, Climatic changes in the western United States since 18,000 yr B.P., *in* Wright, H.E., Jr., Kutzbach, J.E., Webb, T. III, Ruddiman, W.F., Street-Perrott, F.A., and Bartlein, P.J., eds., Global Climates since the Last Glacial Maximum, University of Minnesota Press, Minneapolis, MN, 569 p.

Toney, J.L. and Anderson, R.S., 2006, A postglacial palaeoecological record from the San Juan Mountains of Colorado USA: fire, climate, and vegetation history, The Holocene, v. 16, p. 505-517.

Wagner, J.D., Cole, J.E., Beck, J.W., Patchett, P.J., and Henderson, G.M., 2005, Abrupt millennial climate change in the Arizona desert inferred from a speleothem isotopic record, EOS 86 (abstract), PP31A, p. 1499.

Waters, M.R. and Haynes, C.V., 2001, Late Quaternary arroyo formation and climate change in the American Southwest, Geology, v. 29, p. 399-402.

Wells, S.G., McFadden, L.D., and Schultz, J.D., 1990, Eolian landscape evolution and soil formation in the Chaco dune field, southern Colorado Plateau, New Mexico, Geomorphology, v. 3, p. 517-546.

Weng, C. and Jackson, S.T., 1999, Late glacial and Holocene vegetation history and paleoclimate of the Kaibab Plateau, Arizona, Palaeogeography, Palaeoclimatology, Palaeoecology, v. 153, p. 179-201.

Wesling, J.R., 1988, Glacial chronology and soil development in Windsor Creek drainage basin, southernmost Sangre de Cristo Mountains, New Mexico, M.S. thesis, University of New Mexico, Albuquerque.

Western Regional Climate Center (WRCC), Western U.S. Historical Summaries for individual stations, accessed December 1, 2010. Available on-line at [http://www.wrcc.dri.edu/CLIMATEDATA.html] from the Desert Research Institute, Reno Nevada, USA.

Wolfe, S.A., Huntley, D.J., David, P.P., Ollerhead, J., Sauchyn, D.J., and MacDonald, G.M., 2001, Late 18th century drought-induced sand dune activity, Great Sand Hills, Saskatchewan, Canadian Journal of Earth Science, v. 38, p. 105-117.

Figures

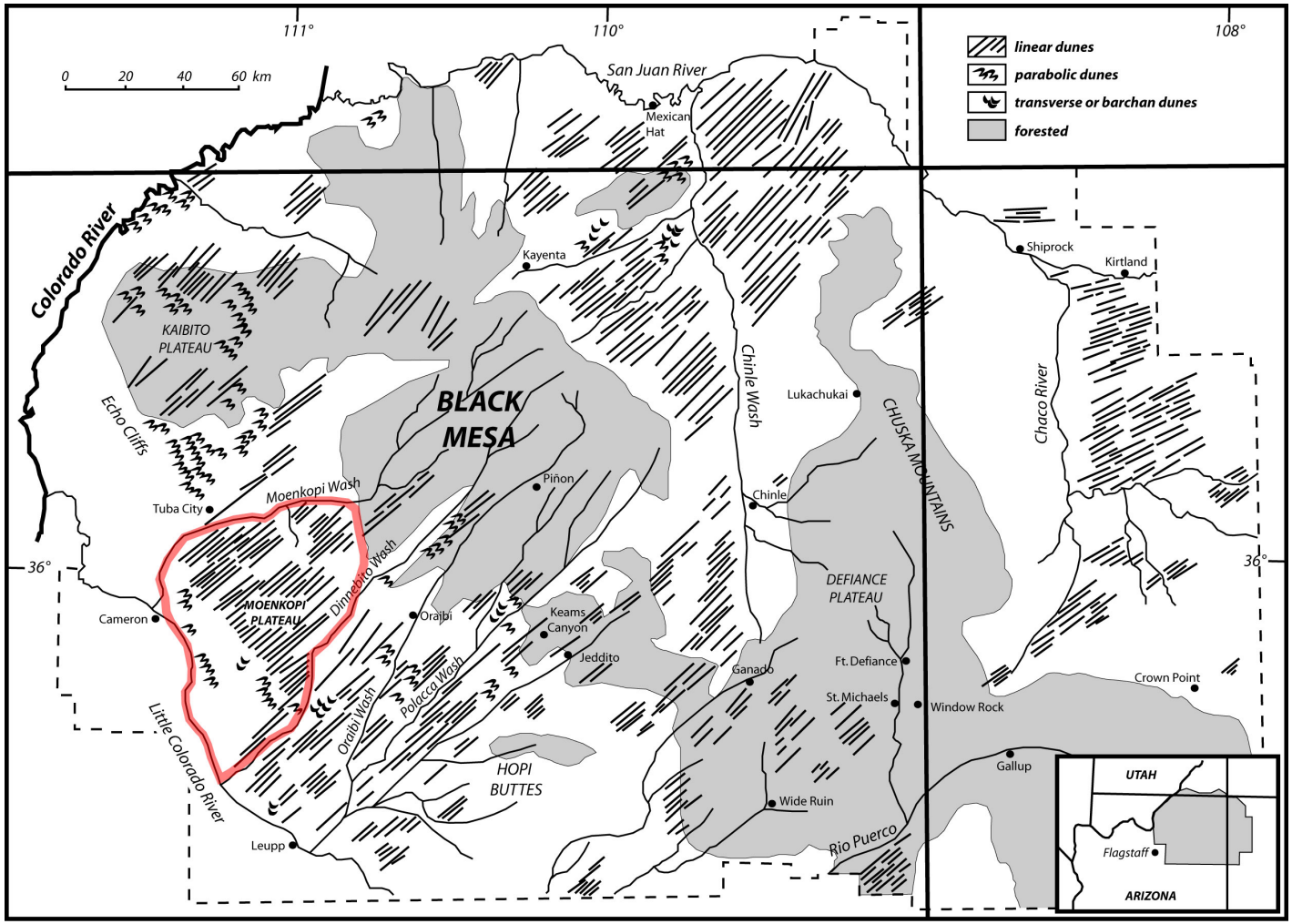

Figure 1: Distribution of eolian landforms and forested areas of the Navajo Nation and Hopi Lands as mapped by J.T. Hack (1941).

The study area is outlined in red.

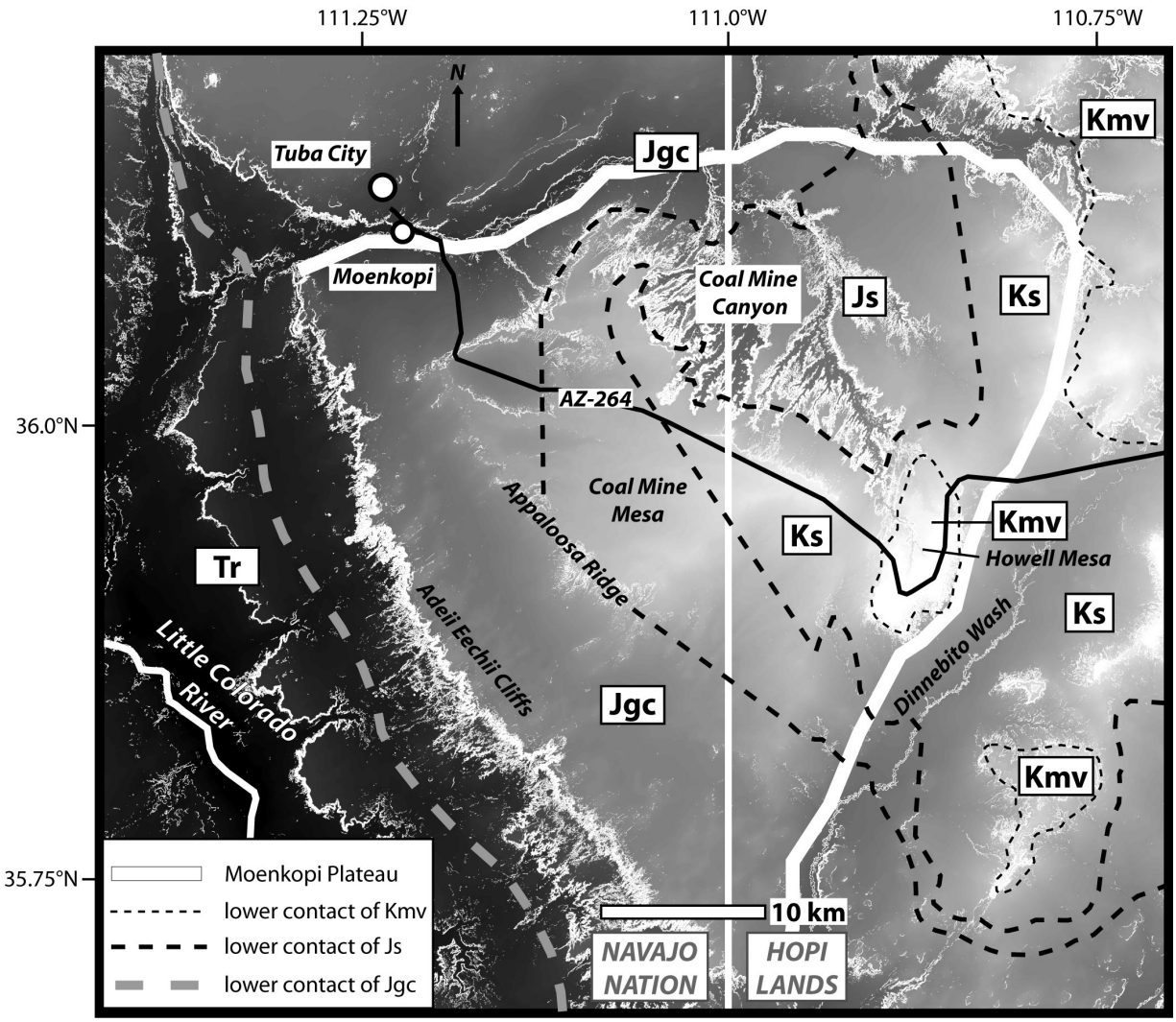

Figure 2: Digital elevation model (DEM) with geographic locations mentioned in the text. All slopes > 10° are depicted by white pixels. Geologic contacts shown using dashed lines. Tr – undifferentiated Triassic rocks; Jgc – Jurassic Glen Canyon Group; Js – Jurassic San Rafael Group; Ks – Cretaceous Mancos shale; Kmv – Cretaceous Mesa Verde Group. Lowest elevations (~1200m) in this figure occur along the Little Colorado River, highest elevations (~2000m) occur on Howell Mesa, the Kmv mesa north of the Dinnebito Wash label. The extent of the Moenkopi Plateau is bounded by a thick white line, the Adeii Eechii Clifffs comprise the southwestern border.

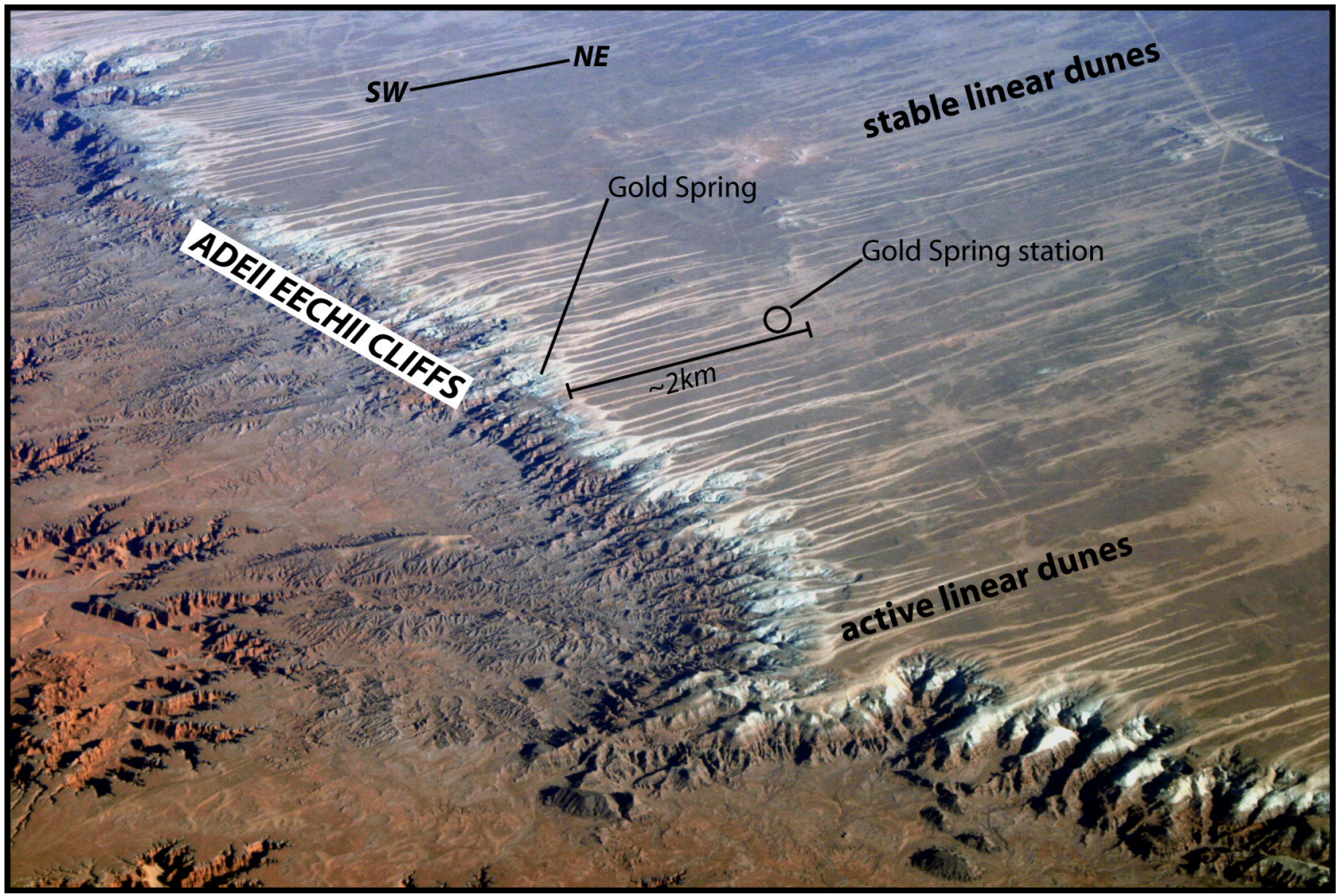

Figure 3: Aerial photo of the Adeii Eechii Cliffs escarpment, active and stable linear dune crests, and the USGS Gold Spring station. Photo taken March 22, 2008, courtesy of Grant Meyer.

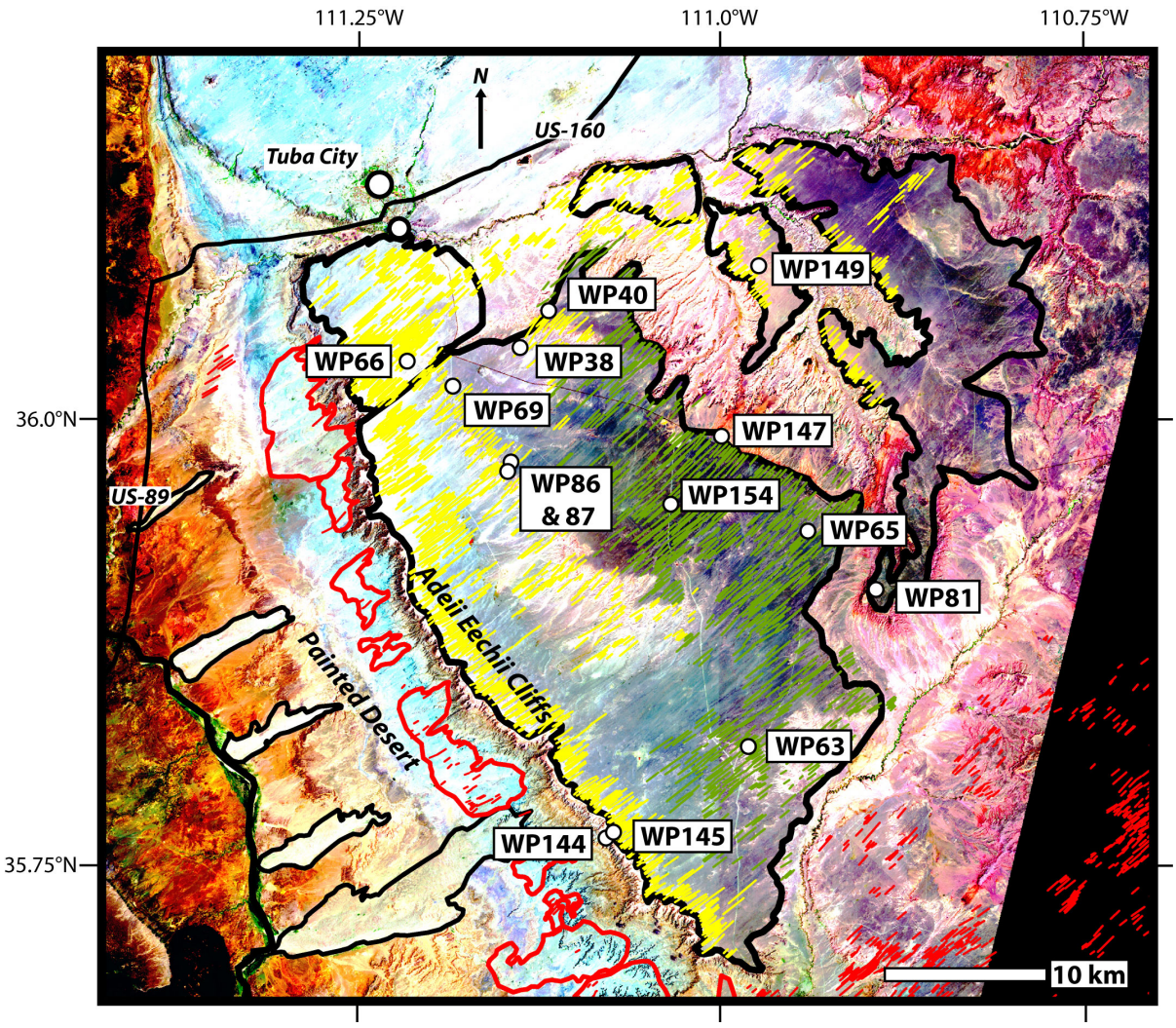

Figure 4: Landsat scene from June, 2000 in 2-4-7 band combination (RGB). Stable linear dunes depicted as green lines, active linear dune crests with stable plinths in yellow, completely active linear dunes in red. Sand sheets of the Moenkopi Plateau are outlined in the thick black lines. Painted Desert floodplain-adjacent dunes outlined in the thin black lines, bedrock-adjacent dunes outlined in red.

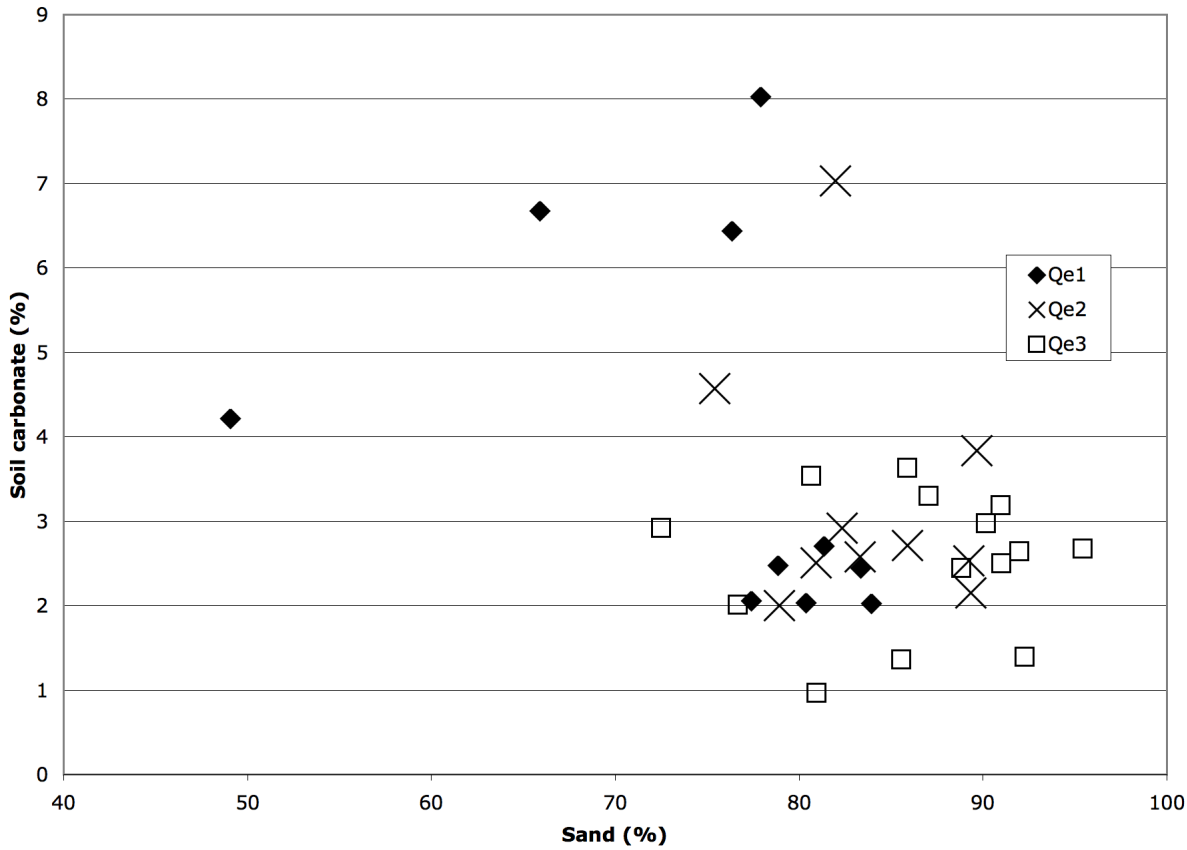

Figure 5: Sand and carbonate percentages for the most competent soil horizons in Qe1 (Btk horizons) and Qe2 (Bk or Bwk horizons). All Qe3 horizons listed in table 2 are plotted in this figure. Eolian units are indistinguishable based solely on texture and mass of soil carbonate.

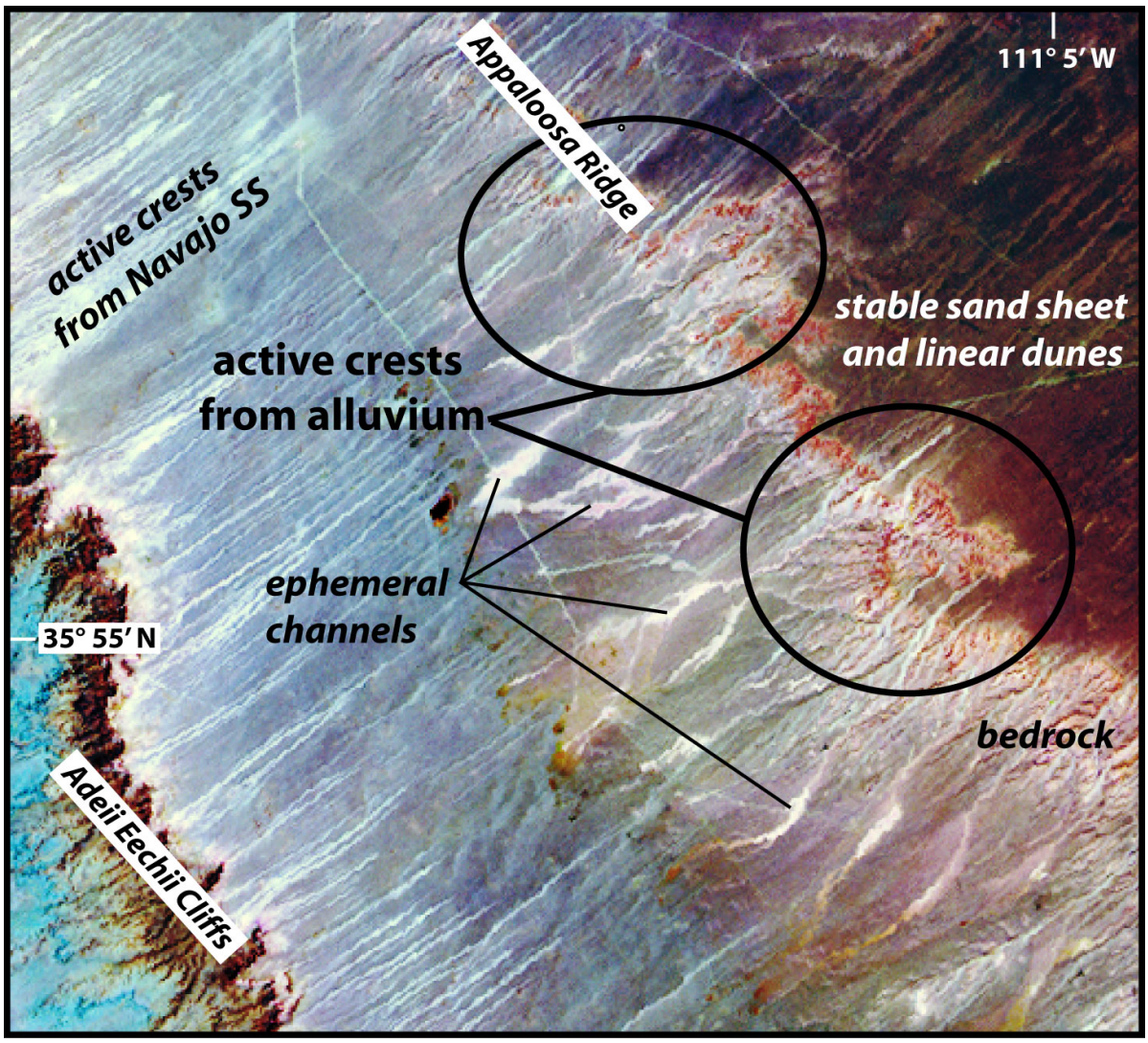

Figure 6: Active linear dune crests on the Moenkopi Plateau are bright in landsat imagery. Some active crests head at the Adeii Eechii Cliffs, others form downwind from alluvial channels and climb onto Appaloosa Ridge. Base imagery is a Landsat scene from June, 2000 in 2-4-7 band combination (RGB).

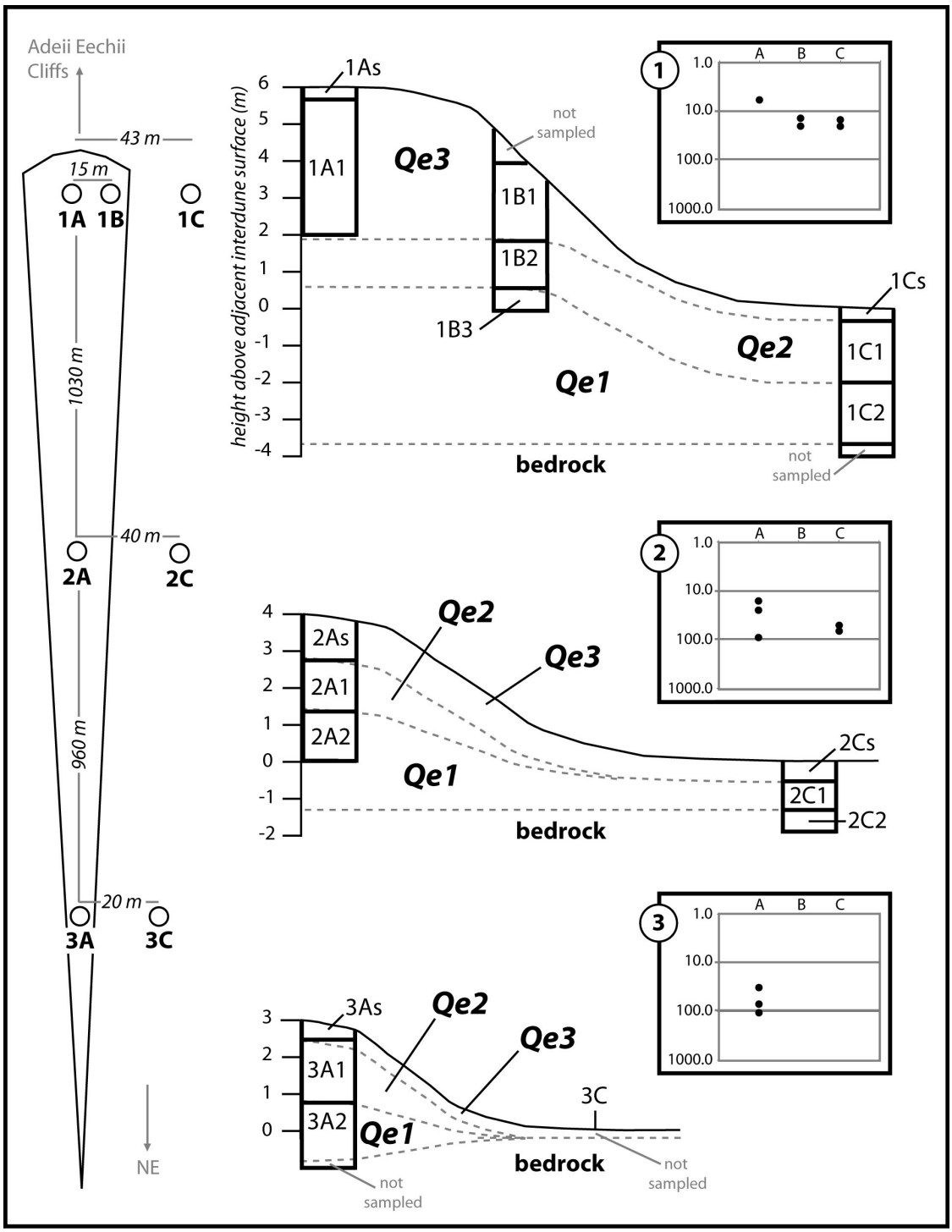

Figure 7: On the left is a schematic diagram showing the position of coring locations. Transects are numbered and core locations are lettered. Linear dune crest (A) and adjacent interdune (C) positions were sampled at all three transects; the side slope position (B) was

only sampled along the first transect. Cross sections show the location of cores, position of described units (numbered), and inferred correlations and correlated ages; see table 4 for field descriptions. The graphs to the upper right of each cross section plot the ratio of magnetic susceptibility values (see table 4) relative to the value of unweathered Navajo sandstone for each core.

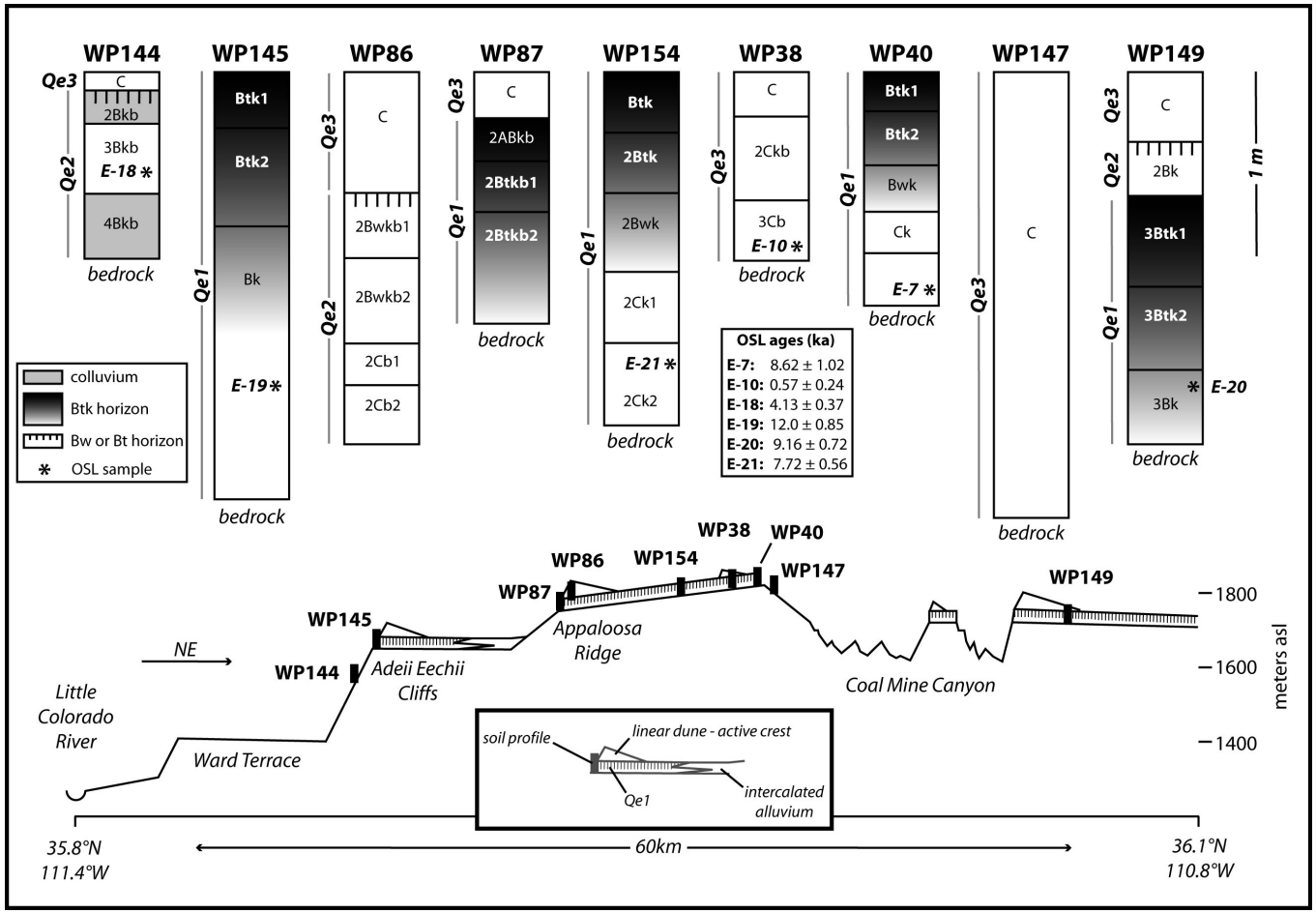

Figure 8: Simplified topographic profile from the Little Colorado River to the northern extent of the Moenkopi Plateau with schematic representation of Qe1 and linear dunes with active crests. Representative soil profiles are shown along the transect with details of soil horizontation, OSL ages, and correlated ages above. WP144 is a climbing dune remnant, WP147 is a falling dune, all other profiles are described in linear dunes or sand sheets. Transect has 100x vertical exaggeration.

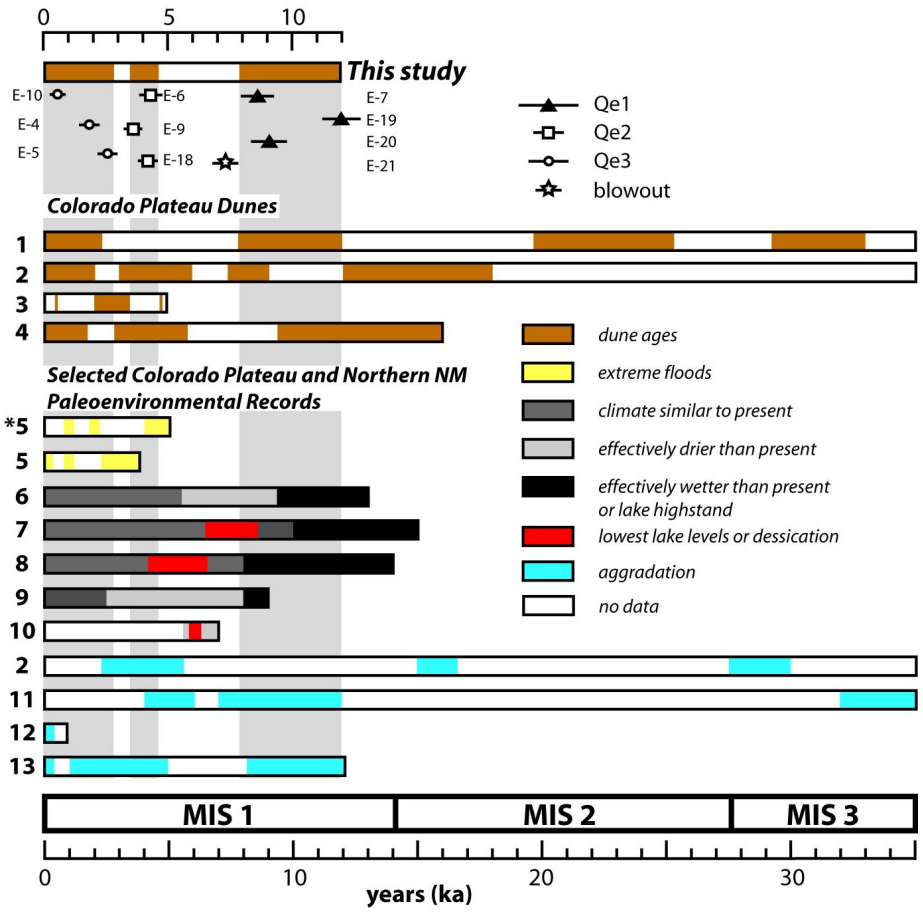

Figure 9: Correlation of OSL age estimates from eolian deposits on the Moenkopi Plateau (this study) with other Colorado Plateau dunes and paleoenvironmental records from the Colorado Plateau and northern New Mexico. *Regional eolian records:* 1) Ellwein et al., 2011 Black Mesa, AZ; 2) Reheis et al., 2005 Canyonlands, UT; 3) Stokes and Breed, 1993 Moenkopi Plateau and Ward Terrace, AZ; 4) Wells et al., 1990 Chaco Dunes, NM. *Colorado Plateau and northern NM paleoenvironmental records:* 5) Ely, 1997 (*5 is the record from the Little Colorado River only); 6) Jiménez-Moreno, et al., 2008; 7) Anderson et al., 2008; 8) Weng and Jackson, 1999; 9) Hasbargen, 1994, 10) Toney and Anderson, 2006, 11) Anders et al., 2005; 12) Hereford, 2002; 13) Hack, 1942, modified by Karlstrom and Karlstrom, 1986, Karlstrom, 1988, and Karlstrom, 2005.

Tables

Table 1: Site location, associated landform, and dominant vegetation. Latitude, longitude, and elevation acquired at field sites using a Garmin GPSmap 60 handheld unit. Datum: WGS 1984.

Site Name	Lat. (°N)	Long. (°W)	Elev. (m)	Landform	Dominant vegetation
WP38	36.04	111.14	1675	Linear dune	*Ephedra spp., Salsola tragus, Oryzopsis hymenoides, Bromus tectorum, Bouteloua gracilis*
WP40	36.06	111.12	1732	Linear dune	*Ephedra spp., Yucca spp., B. gracilis, B. tectorum, Muhlenbergia pungens*
WP63	35.82	110.98	1719	Linear dune	*Ephedra spp., Yucca spp., Artemesia filifolia, Gutierrezia sarothrae, M. pungens, O. hymenoides, B. tectorum*
WP65	35.94	110.94	1812	Sand sheet	*Yucca spp., G. sarothrae, M. pungens, O. hymenoides, Hilaria jamesii B. tectorum*
WP66	36.03	111.22	1599	Linear dune	*Yucca spp., G. sarothrae, M. pungens, Hesperostipa comata*
WP69	36.02	111.19	1693	Sand sheet	*Ephedra spp., Yucca spp., G. sarothrae, M. pungens, O. hymenoides, H. comata*
WP81	35.91	110.89	1942	Sand sheet	*Juniperus monosperma, Ephedra spp., Yucca spp., G. sarothrae, B. gracilis, H. jamesii, H. comata, O. hymenoides*
WP86	35.97	111.15	1734	Linear dune	*Ephedra spp., G. sarothrae, M. pungens, O. hymenoides, H. comata*
WP87	35.97	111.15	1724	Interdune	*Ephedra spp., Yucca spp., B. gracilis, H. jamesii, O. hymenoides, Plantago spp.*
WP144	35.77	111.08	1609	Climbing dune	*G. sarothrae, A. filifolia, S. tragus, M. pungens, O. hymenoides, H. jamesii*
WP145	35.77	111.07	1648	Sand sheet	*Ephedra spp., Yucca spp., G. sarothrae, S. tragus, M. pungens, O. hymenoides, H. jamesii*
WP147	35.99	111.00	1827	Falling dune	*Atriplex canescens, Ephedra spp., Yucca spp., G. sarothrae, M. pungens, O. hymenoides, H. jamesii, H. comata, B. tectorum*
WP149	36.09	110.97	1639	Sand sheet	*Ephedra spp., Yucca spp., G. sarothrae, O. hymenoides, M. pungens, H. jamesii*
WP154	35.95	111.03	1807	Sand sheet	*Ephedra spp., Yucca spp., G. sarothrae, Opuntia spp., M. pungens, H. jamesii, B. tectorum*

Table 2: Selected soil descriptions and laboratory data.

Horizon[a]	Depth (cm)	Dry color[b]	Moist color[b]	Structure[c]	Dry cons.[d]	Clay films[e]	$CaCO_3$ stage[f]	Lower Bound.[g]	Sand size[h]	Sand (%)	Silt (%)	Clay (%)	$CaCO_3$ (%)	Correlated Age
WP38: linear dune near the Hollow Place														
C	0-23	7.5YR6/4	7.5YR5/4	m	lo*	0	0, we	c, s	cL-vfU	***90.97***	***2.52***	***6.52***	3.19	Qe3
2Ckb	23-89	7.5YR6/4	7.5YR5/3	m	lo	0	0, we	g, s	cL-fU	***95.42***	***1.45***	***3.13***	2.67	Qe3
3Cb	89-121	7.5YR6/4	7.5YR5/4	m	lo	0	0, we	ND	mU-vfL	***90.18***	***3.23***	***6.59***	2.98	Qe3
WP40: linear dune northeast of WP38														
Btk1	0-21	5YR5/4	5YR4/3	sbk-abk, m-c, 2	sh	2, f, cobr	I+, me	c, s	ND	***76.34***	***8.55***	***15.11***	6.44	Qe1
Btk2	21-50	5YR5/4	5YR4/3	abk, c-vc, 2	h	2, f, cobr	II, se	g, s	mU-fL	***77.92***	***7.52***	***14.56***	8.03	Qe1
Bwk	50-74	5YR6/3	5YR5/4	sbk, m, 1	so	0	II, se	d, s	mL-fU	***90.80***	***2.99***	***6.21***	6.63	Qe1
Ck	74-98	7.5YR6/4	7.5YR5/4	sbk, c, 1	so	0	0, we	g, s	mL-fU	***89.30***	***6.57***	***4.13***	3.58	Qe1
C	98-153	7.5YR6/4	7.5YR5/4	sbk, m, 1	lo*	0	0, we	ND	mL-fU	***94.62***	***1.23***	***4.15***	1.75	Qe1
R	153													
WP63: linear dune on Tribal Road 5 southwest of Howell Mesa														
C	0-75	10YR6/4	ND	m	lo	0	0, we	d, s	mL-vfU	80.95	16.87	2.18	0.97	Qe3
2Cb	75-241	7.5YR6/4	ND	m	so	0	0, we	g, b	mU-vfL	76.67	20.68	2.66	2.01	Qe3
3Bwkb	241-303	5YR5/4	ND	sbk, c, 1	so	0	I-, we	ND	cL-vfL	80.92	15.54	3.54	2.51	Qe2
R	303	10YR7/3												
WP65: sand sheet north of WP63														
C	0-64	ND	5YR5/4	m	lo	0	0, me	c, s	mL-vfL	85.90	10.64	3.46	3.63	Qe3
2Bwkb	64-94	7.5YR5/4	7.5YR4/4	sbk, c, 1	so	0	I-, me	g, s	mU-fL	89.65	7.86	2.49	3.84	Qe2
2Ckb	94-139	7.5YR6/4	ND	sbk, c, 1	so	0	I-, we	g, s	mU-fU	95.85	2.68	1.48	2.11	Qe2
2Cb	139-200	ND	7.5YR6/4	m	lo*	0	0, we	ND	mL-fL	94.07	3.87	2.06	1.40	Qe2
WP66: linear dune downwind from Adeii Eechii Cliffs due south of Tuba City														
C	0-112	5YR5/4	5YR5/4	sbk, c, 1	so	0	0, we	g, s	mU-vfL	Field texture - sand				Qe3
2Bwk1b	112-167	5YR5/4	5YR4/3	sbk, m, 1	vfr	0	I, me	g, s	mL-vfL	Field texture - loamy sand				Qe2
2Bwk2b	167-225	5YR6/4	5YR5/4	sbk, m-c, 1	vfr	0	I-, me	g, w	cL-vfL	Field texture - loamy sand				Qe2
2Ckb	225-294	7.5YR6/4	7.5YR5/4	sbk, m-c, 1	vfr	0	0, we	a, b	ND	Field texture - sand				Qe2
R	294-300	10YR7/3												
WP69: sand sheet along Tribal Road 6710 just south of AZ Hwy 264														
C	0-22	5YR6/4	5YR5/4	gr, m, 1	vfr	0	0, me	a, w	mU-vfL	***90.99***	***5.97***	***3.04***	2.50	Qe3
2Bwkb	22-35	5YR5/4	5YR4/4	sbk, m-c, 1	sh	0	I-, me	c, w	mL-fU	***88.82***	***5.96***	***5.22***	2.44	Qe3
2Bk1b	35-57	5YR6/5	5YR5/4	sbk, m-c, 1	so	0	I, me	c, s	mU-vfL	***92.00***	***4.39***	***3.61***	2.64	Qe3
2Bk2b	57-76	5YR6/5	5YR5/4	abk, c-vc, 1	so-sh	0	I, me	a, s	mU-vfL	***87.06***	***6.73***	***6.21***	3.30	Qe3
3Bwkb	76-92	5YR6/4	5YR5/4	abk, c, 2	sh	0	I+, se	c, s	mL-vfL	85.88	11.10	3.02	2.71	Qe2
3Bkb	92-120	5YR5/4	5YR4/4	sbk, m, 1	so	0	I, me	ND	mU-vfL	82.34	14.32	3.31	2.92	Qe2
R	120													

Table 2 Continued

Horizon[a]	Depth (cm)	Dry color[b]	Moist color[b]	Structure[c]	Dry cons.[d]	Clay films[e]	$CaCO_3$ stage[f]	Lower Bound.[g]	Sand size[h]	Sand (%)	Silt (%)	Clay (%)	$CaCO_3$ (%)	Correlated Age
WP81: sand sheet on top of Howell Mesa														
ABk	0-17	7.5YR5/4	7.5YR4/3	sbk, m-c, 2	sh	ND	0, me	c, w	ND	Field texture - loam				Qe3
Bwk	17-33	7.5YR5/5	7.5YR4/4	sbk, m-c, 2	fr	ND	I+, me	c, w	ND	Field texture - loam				Qe3
2Btkb	33-60	7.5YR5/4	7.5YR4/3	abk-cpr, vc, 3	h	ND	II, se	g, s	ND	Field texture - sandy clay loam				Qe1
3Btkb	60-118	7.5YR5/4	7.5YR4/3	abk, vc, 3	h	ND	II, se	ND	ND	Field texture - sandy clay loam				Qe1
R	118													
WP86: Linear dune downwind from Appaloosa Ridge														
C	0-64	7.5YR6/4	7.5YR5/4	m	*lo	0	0, ne	a,w	mU-vfL	92.27	5.48	2.24	1.39	Qe3
2Bwkb1	64-99	5YR6/4	5YR5/4	sbk, c, 1	*vfr	0	I-, we	c, s	mU-mL	89.35	7.98	2.66	2.15	Qe2
2Bwkb2	99-143	5YR6/4	5YR5/3	sbk-abk, c, 1	so	0	I-, we	g, s	mU-mL	89.24	8.40	2.36	2.53	Qe2
2Cb1	143-168	5YR6/4	5YR5/4	sbk, c-vc, 1	so	0	0, we	c, s	cL-vfL	96.01	3.55	0.43	2.15	Qe2
2Cb2	168-205	5YR6/4	5YR5/3	sbk, c-vc, 1	so	0	0, we	ND	cL-vfL	95.90	3.41	0.69	2.02	Qe2
WP87: Interdune west of WP86 on Appaloosa Ridge														
C	0-24	5YR5/4	5YR5/3	sbk, f-m, 1	*lo	0	0, me	a, w	mU-vfL	85.55	11.27	3.18	1.36	Qe3
2ABkb	24-48	5YR6/4	5YR5/3	sbk, m-c, 1	*vfr	0	I, me	c, s	cL-vfL	83.73	13.43	2.83	2.48	Qe1
2Btkb1	48-76	5YR5/4	5YR4/3	abk, m-c, 2	sh	1, f, cobr	I, se	d, s	cL-vfL	83.92	13.07	3.01	2.03	Qe1
2Btkb2	76-135	5YR5/4	5YR4/4	abk, c-vc, 2	sh	1, f, cobr	I+, se	ND	cL-vfL	83.34	13.78	2.88	2.44	Qe1
R	135													
WP144: Climbing dune remnant, near Gold Spring, Adeii Eechii Cliffs														
C	0-10	7.5YR6/3	5YR5/3	sbk, m, 1-2	so	0	0, we	a, w	fU-fL	72.49	22.03	5.48	2.92	Qe3
[1]2Bkb	10-26	5YR6/4	5YR5/3	sbk, c, 2	sh	0	I-, me	a, s	mU-fU	78.92	16.75	4.33	2.00	Qe2
3Bkb	26-64	5YR6/4	5YR5/4	abk, vc, 3	h	0	I+, se	c, s	fU-fL	81.98	13.01	5.01	7.03	Qe2
[1]4Bkb	64-95	5YR6/4	5YR5/3	abk, vc, 3	h	0	I+, se	a, i	fU-fL	83.32	12.09	4.59	2.58	Qe2
R	95-120													
WP145: Sand sheet, Gold Spring, Adeii Eechii escarpment														
Btk1	0-31	5YR5/4	5YR4/4	pr, c, 3	h	2, f, cobr	II, se	c, s	fU-fL	65.90	28.16	5.95	6.68	Qe1
Btk2	31-82	5YR6/4	5YR4/4	sbk-abk, vc, 2	h	1, f, cobr	II, se	g, s	fU-fL	49.07	41.31	9.62	4.21	Qe1
Bk	82-230	5YR6/4	5YR5/4	sbk, c-vc, 2	so	0	I, me	a, i	fL-vfL	74.25	20.82	4.94	2.89	Qe1
R	230													
WP147: Falling dune northeast of Coal Mine Canyon Chapter House														
C	0-197	5YR5/4	5YR4/4	m	lo	0	ne	ND	ND	Field texture - sand				Qe3
WP149: Sand sheet north of Coal Mine Canyon														
C	0-38	7.5YR6/3	7.5YR5/3	m	so	0	0, me	a, w	fU-vfU	80.68	14.26	5.06	3.54	Qe3
2Bkb	38-66	7.5YR6/4	7.5YR5/4	sbk-abk, c, 2	sh	0	II, se	a, s	fU-fL	75.41	18.99	5.60	4.57	Qe2
3Btkb1	66-114	7.5YR6/4	7.5YR4/3	pr, c, 3	vh	2, d, pf, cobr	II, se	d, s	fL-vfL	77.41	17.62	4.97	2.06	Qe1
3Btkb2	114-160	7.5YR6/4	7.5YR5/4	pr, c-vc, 3	h	1, f, pf, cobr	II, se	c, s	fL-vfL	78.84	16.41	4.75	2.48	Qe1
3Bkb	160-200	7.5YR6/4	7.5YR5/4	sbk-abk, c-vc, 2	sh	0	I+, me	a, i	cL-vfL	87.73	9.13	3.14	2.94	Qe1
R	200													

Table 2 Continued

Horizon[a]	Depth (cm)	Dry color[b]	Moist color[b]	Structure[c]	Dry cons.[d]	Clay films[e]	$CaCO_3$ stage[f]	Lower Bound.[g]	Sand size[h]	Sand (%)	Silt (%)	Clay (%)	$CaCO_3$ (%)	Correlated Age
WP154: Sand sheet along Tribal Road 6720														
Btk	0-32	7.5YR5/4	7.5YR4/3	abk, vc, 2	h	2, f, cobr	I+, se	c, i	cU-fU	80.37	15.34	4.29	2.03	Qe1
2Btk	32-64	5YR5/4	5YR4/3	abk-pr, vc, 3	h	3, d, cobr	II, se	d, s	cL-vfU	81.37	14.10	4.53	2.71	Qe1
2Bwk	64-108	7.5YR5/4	7.5YR4/3	sbk, c, 1	so	0	I-, me	d, s	cL-vfL	94.54	3.77	1.69	1.34	Qe1
2C	108-166	7.5YR6/4	7.5YR5/4	sbk, m, 1	so	0	0	a, i	mu-vfU	95.97	2.41	1.62	1.59	Qe1
R	166													

[a]Field soil descriptions after Birkeland (1999).
[b]Soil colors determined using Munsell soil color chart.
[c]Structure codes: Type: m – massive; gr - granular; sbk - subangular blocky; abk - angular blocky; pr - prismatic; cpr - columnar. Size: f - fine; m - medium; c - coarse; vc - very coarse.
[d]Dry consistence codes: lo - loose, noncoherent; so - soft; sh - slightly hard; h - hard; vh - very hard; *lo - loose (moist); *vfr – very friable (moist).
[e]Clay film codes: Amount: vf - very few; 1 - few; 2 - common; 3 - many. Distinctness: f - faint; d - distinct. Location: pf - ped faces; po - pores; cobr - colloid coats and bridges.
[f]Carbonate field effervescence codes: we - weak; me - moderate; se - strong; ve – violent;
[g]Lower boundary codes: Distinctness: a - abrupt; c - clear; g - gradual; d - diffuse. Topography: s - smooth; w - wavy; b – broken; i - irregular.
[h]Grain size described in the field, codes use the Modified Wentworth scale: vc – very coarse; c – coarse; m – medium, f – fine; vf – very fine. U – upper; L – lower.
Laboratory analyses in bold italics were performed at the Quaternary Soil and Sediment Laboratory at the University of New Mexico, all others were performed at the USGS Soils Laboratory in Denver, Colorado.
ND – no field data; laboratory analyses were not performed for sites WP66, WP81 and WP147.
[1]Parent material contains up to 10% matrix supported angular to subangular gravel and is interpreted to be colluvium, all other parent materials are eolian.

Table 3: Optical ages for eolian sand sedimentary deposits from sites on the Moenkopi Plateau, northeastern Arizona. Equivalent dose and OSL age determined using single aliquot regeneration (SAR) protocols under blue light excitation (514 nm; Murray and Wintle, 2003).

Sample number	Depth (m)	Water content (%)[a]	K (%)[b]	Th (ppm)[b]	U (ppm)[b]	Cosmic dose additions (Gy/ka)[c]	Total dose rate (Gy/ka)	Equivalent dose (Gy)	n[d]	Age (ka)[e] and correlated age[f]
WP38: linear dune near the Hollow Place										
E-10	1.1	2 (28)	1.37 ± 0.01	3.06 ± 0.13	0.62 ± 0.05	0.25 ± 0.01	1.96 ± 0.04	1.11 ± 0.48	22 (30)	0.57 ± 0.24 (Qe3)
WP40: linear dune northeast of WP38										
E-7	1.4	2 (20)	0.61 ± 0.01	1.56 ± 0.06	0.58 ± 0.06	0.25 ± 0.02	1.10 ± 0.03	9.50 ± 1.04	34 (40)	8.62 ±1.02 (Qe1)
WP63: linear dune on Tribal Road 5 southwest of Howell Mesa										
E-4	0.7	2 (24)	1.13 ± 0.01	1.45 ± 0.15	0.56 ± 0.07	0.26 ± 0.02	1.62 ± 0.06	3.16 ± 0.56	23 (37)	1.95 ± 0.37 (Qe3)
E-5	2.2	3 (28)	1.34 ± 0.02	2.70 ± 0.20	1.05 ± 0.09	0.22 ± 0.01	1.97 ± 0.06	5.55 ± 0.59	20 (30)	2.82 ± 0.31 (Qe3)
E-6	2.7	3 (28)	1.28 ± 0.01	2.67 ± 0.13	0.91 ± 0.05	0.21 ± 0.01	1.86 ± 0.04	7.83 ± 0.86	20 (30)	4.21 ± 0.50 (Qe2)
WP65: sand sheet north of WP63										
E-9	0.5	6 (30)	1.40 ± 0.01	3.26 ± 0.19	0.89 ± 0.05	0.28 ± 0.01	2.09 ± 0.05	7.25 ± 0.67	19 (24)	3.47 ± 0.34 (Qe2)
E-8	2.0	2 (23)	1.24 ± 0.01	2.22 ± 0.12	0.57 ± 0.05	0.23 ± 0.01	1.75 ± 0.04	12.6 ± 1.13	20 (30)	7.21 ± 0.67 (-----)
WP144: climbing dune remnant near Gold Spring, Adeii Eechii Cliffs										
E-18	0.6	2 (37)	1.44 ± 0.04	1.31 ± 0.07	2.40 ± 0.16	0.26 ± 0.22	2.13 ± 0.06	8.80 ± 0.76	18 (20)	4.13 ± 0.37 (Qe2)
WP145: sand sheet at Gold Spring, Adeii Eechii Cliffs escarpment										
E-19	1.7	3 (37)	1.61 ± 0.11	1.43 ± 0.23	3.21 ± 0.22	0.23 ± 0.22	2.35 ± 0.11	28.1 ± 1.54	21 (30)	12.0 ± 0.85 (Qe1)
WP149: sand sheet north of Coal Mine Canyon										
E-20	1.7	3 (30)	1.51 ± 0.08	1.22 ± 0.09	3.57 ± 0.18	0.23 ± 0.22	2.25 ± 0.07	20.6 ± 1.48	26 (30)	9.16 ± 0.72 (Qe1)
WP154: sand sheet along Tribal Road 6720										
E-21	1.5	2 (27)	1.39 ± 0.06	0.91 ± 0.09	2.42 ± 0.22	0.25 ± 0.22	1.99 ± 0.08	15.4 ± 0.95	26 (30)	7.72 ± 0.56 (Qe1)

[a] Field moisture, with figures in parentheses indicating the complete sample saturation (%). Ages calculated using 10% of saturation values.
[b] Analyses obtained using laboratory Gamma Spectrometry (high resolution Ge detector).
[c] Cosmic doses and attenuation with depth were calculated using the methods of Prescott and Hutton (1994). See text for details.
[d] Number of replicated equivalent dose (De) estimates used to calculate the mean. Figures in parentheses indicate total number of measurements made including failed runs.
[e] Dose rate and age for fine-grained (125-180 μm) quartz sand. Linear + exponential fit used to estimate age, errors to one sigma.
[f] Correlated age determined from soil stratigraphy and geomorphic field relationships.

Table 4: Comparison of argillic horizons from Qe1 soil profiles in the study area.

Horizon[a]	Structure[b]	Dry cons.[c]	Clay Films[d]	$CaCO_3$ Stage[e]	Upper Bound.[f]	Sand (%)	$CaCO_3$ (%)
WP40: linear dune northeast of WP38							
Btk1	sbk-abk, m-c, 2	sh	2, f, cobr	I+, me	at surface	76.34	6.44
Btk2	abk, c-vc, 2	h	2, f, cobr	II, se	2-5 cm	77.92	8.03
WP81: sand sheet on top of Howell Mesa							
2Btkb	abk-cpr, vc, 3	h	ND	II, se	2-5 cm	50-75[g]	
3Btkb	abk, vc, 3	h	ND	II, se	5-15 cm	50-75[g]	
WP87: Interdune west of WP86 on Appaloosa Ridge							
2Btkb1	abk, m-c, 2	sh	1, f, cobr	I, se	2-5 cm	83.92	2.03
2Btkb2	abk, c-vc, 2	sh	1, f, cobr	I+, se	>15cm	83.34	2.44
WP145: Sand sheet, Gold Spring, Adeii Eechii escarpment							
Btk1	pr, c, 3	h	2, f, cobr	II, se	< 2cm	65.90	6.68
Btk2	sbk-abk, vc, 2	h	1, f, cobr	II, se	2-5 cm	49.07	4.21
WP149: Sand sheet north of Coal Mine Canyon							
3Btkb1	pr, c, 3	vh	2, d, pf, cobr	II, se	< 2 cm	77.41	2.06
3Btkb2	pr, c-vc, 3	h	1, f, pf, cobr	II, se	> 15 cm	78.84	2.48
WP154: Sand sheet along Tribal Road 6720							
Btk	abk, vc, 2	h	2, f, cobr	I+, se	<2 cm	80.37	2.03
2Btk	abk-pr, vc, 3	h	3, d, cobr	II, se	2-5 cm	81.37	2.71

[a]Field soil descriptions after Birkeland (1999).
[b]Structure codes: Type: m – massive; gr - granular; sbk - subangular blocky; abk - angular blocky; pr - prismatic; cpr - columnar. Size: f - fine; m - medium; c - coarse; vc - very coarse.
[c]Dry consistence codes: lo - loose, noncoherent; so - soft; sh - slightly hard; h - hard; vh - very hard; *lo - loose (moist); *vfr – very friable (moist).
[d]Clay film codes: Amount: vf - very few; 1 - few; 2 - common; 3 - many. Distinctness: f - faint; d - distinct. Location: pf - ped faces; po - pores; cobr - colloid coats and bridges.
[e]Carbonate field effervescence codes: we - weak; me - moderate; se - strong; ve – violent;
[f]Upper boundary codes: Distinctness: < 2 cm - abrupt; 2-5 cm - clear; 5-15 cm - gradual; >15 cm - diffuse.
[g]Soil texture described in the field only.
ND – no field data

Table 5: Unit boundaries from soil profile descriptions in table 2. Boundary descriptions after Birkeland (1999).

	Between Units			Within Unit		
Boundaries	**Qe1 to Qe2**	**Qe1 to Qe3**	**Qe2 to Qe3**	**Qe1**	**Qe2**	**Qe3**
Abrupt (< 2 cm)	1	1	4	0	1	1
Clear (2-5 cm)	0	1	1	5	4	4
Gradual (5-15 cm)	0	0	2	4	5	1
Diffuse (> 15 cm)	0	0	0	5	0	1

Table 6: Dune coring and magnetic susceptibility experiment. Within the < 2-mm fraction, samples were greater than 95% quartz and all quartz grains were frosted. Magnetic susceptibility analyses were performed using an AGICO MFK1 kappabridge at the Paleomagnetism Laboratory at the University of New Mexico.

Site	Sample	Depth (cm)	Dry color[a]	Texture[b]	Sand size[c]	Sorting and Rounding[d]	Presence of red qtz grains?	$CaCO_3$ Stage[e]	Average Magnetic Susceptibility (unitless)	Average Standard Deviation	Correlated Age
Transect 1: 35.7676°N, 111.0718°W, elevation 1657 ± 3.4 m											
1A	1As	0-20	7.5YR6/4	S	mL-fL	ws; r-wr	no	0, ne	1.48 E-05	3.33 E-06	Qe3
	1A1	20-400	7.5YR6/4	S	fU-fL	ws; r-wr	no	0, we	1.49 E-05	4.65 E-06	Qe3
1B	1B1	0-214	7.5YR6/4	S	fU-fL	ws; r-wr	no	0, we	3.47 E-05	7.75 E-06	Qe3
	1B2	214-360	5YR6/4	S	fU-vfL	ms; r-wr	yes	I, me	5.11 E-05	1.20 E-06	Qe2
	1B3	360-400	5YR6/4	LS	fU-vfL	ms; r-wr	yes	II, se	3.54 E-05	2.24 E-07	Qe1
1C	1Cs	0-20	7.5YR6/4	S	fU-fL	ws; r-wr	yes	0, we	-	-	Qe3
	1C1	20-200	5YR6/4	S	mU-fL	ms; r-wr	yes	I, me	3.76 E-05	8.83 E-07	Qe2
	1C2	200-360	5YR6/4	SL	fU-vfL	ms; sa-r	yes	II, se	5.06 E-05	1.12 E-06	Qe1
Transect 2: 35.7729°N, 111.0625°W, elevation 1650 ± 1.9 m											
2A	2As	0-135	7.5YR6/4	S	fU-vfL	ms; sa-r	yes	0, ne	4.05 E-05	1.09 E-06	Qe3
	2A1	135-277	5YR5/4	LS	fU-vfL	ms; r-wr	yes	I, me	6.15 E-05	7.16 E-07	Qe2
	2A2	277-400	5YR5/4	SL	mL-vfL	ms; r-wr	yes	II, se	2.23 E-04	1.04 E-06	Qe1
2C	2Cs	0-55	5YR5/4	S	mU-vfL	ps; r-wr	yes	0, me	1.31 E-04	7.14 E-07	Qe3
	2C1	55-130	5YR5/4	LS	mL-vfL	ms; wr	yes	II, se	1.59 E-04	9.55 E-07	Qe1
Weathered Navajo sandstone	2C2	130-150	10YR7/3	S	mL-vfU	ws; wr	no	0, ne	-1.31 E-07	3.75 E-07	-
Transect 3: 35.7779°N, 111.0539°W, elevation 1659 ± 1.8 m											
3A	3As	0-25	7.5YR6/4	S	fU-vfU	ms; ND	yes	0, ne	7.82 E-05	2.46 E-06	Qe3
	3A1	25-235	5YR5/4	S	cL-vfL	ps; wr	yes	I, me	1.71 E-04	1.47 E-06	Qe2
	3A2	235-277	5YR5/4	LS	mU-vfL	ms; wr	yes	II, se	2.54 E-04	4.17 E-07	Qe1
3C		0-30	5YR5/4	S	-	-	-	-			Qe3
Fresh Navajo sandstone	**-**	**-**	**5Y8/2 to 7.5YR8/2**	**S**	**mL-vfU**	**ws, wr**	**no**	**-**	**-2.50 E-06**	**2.22 E-07**	**-**

[a]Soil colors determined using Munsell soil color chart.

[b]Field textural analyses performed on < 2-mm fraction (Birkeland, 1999)
[c]Grain size codes (Modified Wentworth scale): vc – very coarse; c – coarse; m – medium, f – fine; vf – very fine. U – upper; L – lower.
[d]Sorting: ws – well sorted; ms – moderately sorted; ps – poorly sorted. Rounding: wr: well-rounded; r – rounded; sa – subangular.
[e]Carbonate field effervescence codes: we - weak; me - moderate; se – strong (Birkeland, 1999).

Table 7: Dominant vegetation and approximate cover for coring locations shown in figure 7 and table 6.

Site Name	Position	Estimated % cover	Dominant vegetation
Transect 1			
A	Linear dune crest	< 10%	*Penstemon ambiguus var. laevissimus, Poliomintha incana, Muhlenbergia pungens, Oryzopsis hymenoides*
B	Side slope	30%	*Ephedra spp., Hilaria jamesii, M. pungens, O. hymenoides,*
C	Interdune	50%	*Ephedra spp., Artemesia filifolia, H. jamesii, M. pungens, O. hymenoides, Plantago spp.*
Transect 2			
A	Linear dune crest	30%	*Yucca spp., P. ambiguus var. laevissimus, P. incana, S. tragus, M. pungens, O. hymenoides*
C	Interdune	50%	*Ephedra spp., Yucca spp., A. filifolia, G. sarothrae, S. tragus, Bouteloua gracilis, M. pungens, O. hymenoides, Plantago spp.*
Transect 3			
A	Linear dune crest	50%	*Ephedra spp., Yucca spp., G. sarothrae, Hesperostipa comata, M. pungens, H. jamesii, O. hymenoides,*
C	Interdune	60%	*Ephedra spp., Yucca spp., H. comata, B. gracilis, H. jamesii, O. hymenoides, M. pungens, Plantago spp.*

Note: all cored sediments were moist below 20-40 cm except interdune cores. Sampling was conducted on June 15, 2008.

APPENDIX A:

Additional Optically Stimulated Luminescence (OSL) tests performed on the samples

I. Dose Rate Response Tests:

Dose recovery is a very important and reliable test required for determining the paleodose when using single aliquot regeneration (SAR) procedures. The dose recovery tests were carried out on five aliquots of selected samples: WP63 (E-5), WP38 (E-10), WP109 (E-11), WP149 (E-20) and WP154 (E-21). The aliquots were bleached for 500 seconds using natural sunlight to remove the natural OSL. A dose of 20 Gy was given to observe the variation in the precision of recovered dose. SAR was applied on bleached aliquots after irradiating with 20 Gy. The regeneration doses were 10 Gy, 20 Gy, 40 Gy, 0 Gy, and 10 Gy again for the recycling point to check the correctness of sensitivity change monitoring. The data shows a good recovery of the laboratory dose and the average lies within 10-15% of the given dose; however all of the aliquots show a considerable amount of deviation, although most average 20 Gy.

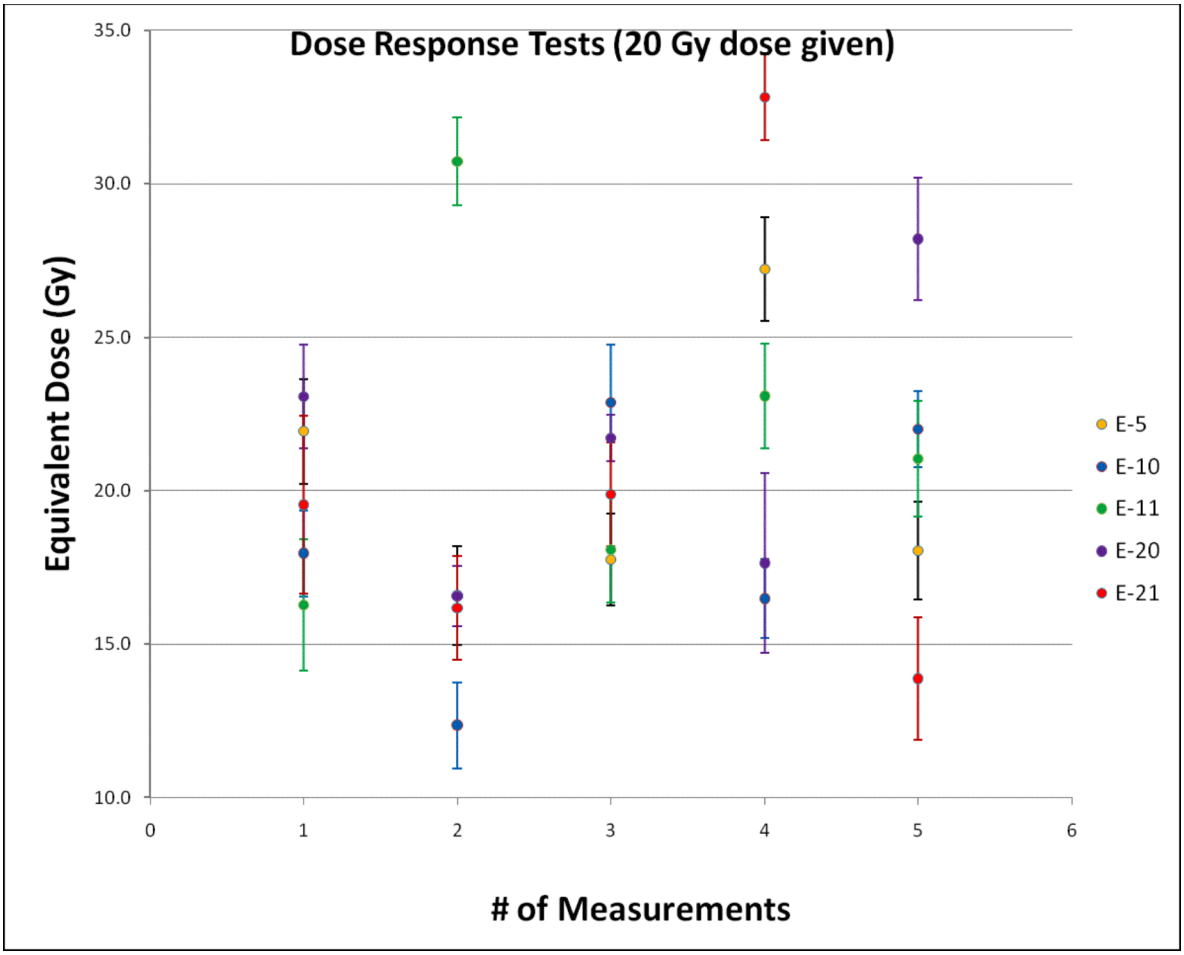

II. Preheat Plateau Tests:

Preheating prior to measurements of the OSL signal allows detection of any thermally unstable component of the OSL signal induced by laboratory irradiation (e.g. Murray and Wintle, 2000). Preheat plots show equivalent dose values obtained for various preheat temperatures for two test samples WP109 (E-11) and WP154 (E-21). The values are shown with the given dose as a horizontal line. Three aliquots (shown in each box as diamonds) were run for each preheat temperature shown. The average of the three aliquots is delineated with a horizontal bar within the box. The biggest equivalent dose variation occurs with increasing temperature. The estimated equivalent dose should remain constant with increasing preheat temperatures indicating that unstable components have been removed from the laboratory induced signals. Although there is scatter in the De values, these do not vary as a function of preheat temperature, indicating that a stable component of the OSL signal was measured. However, because the dose recovery varies with higher temperature, all samples were run at either 200 °C or 220 °C.

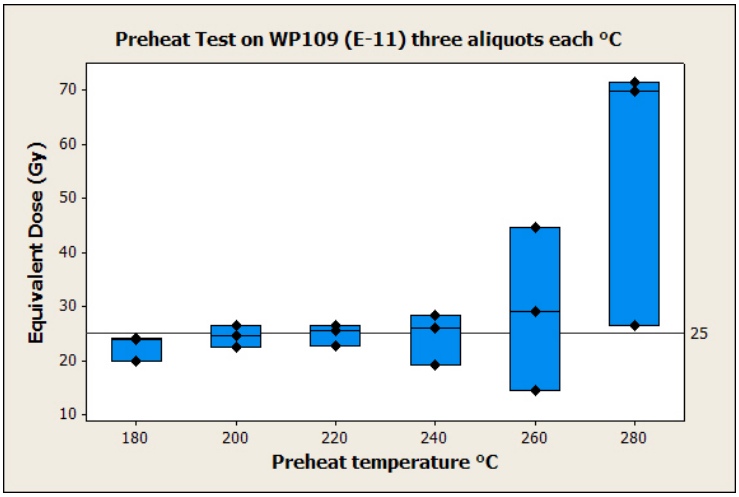

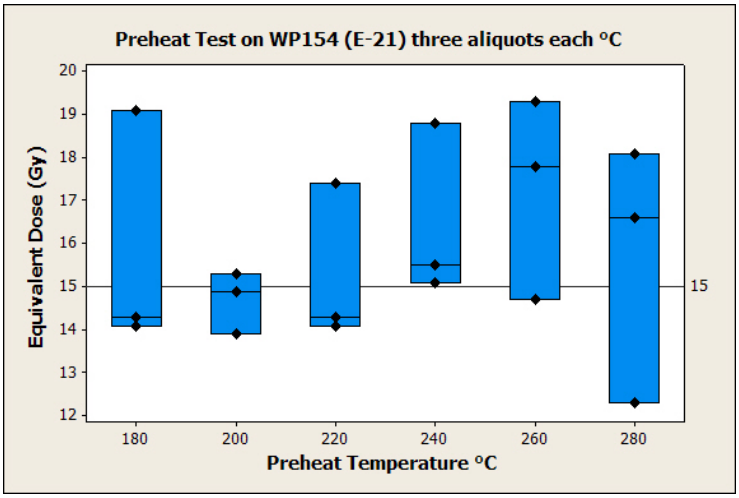

III. Radial Plots:

Radial plots for each OSL sample are provided; plots extend from this page to the end of this appendix. This type of graphical presentation allows visualization of dose distributions, where focus is drawn to the best-known results (Wallinga, 2002). Radial plots allow each data point to be plotted with its associated precision, which is linked to individual aliquot sensitivities (aliquots may contain hundreds to several hundreds of grains). Any radius passing through the origin represents a line of constant dose and the precision of the measurement increases from left to right. Unless otherwise noted, all samples are plotted using data generated from an exponential + linear best fit function. N equals the numbered of measured aliquots, specifying actual accepted values as N = accepted aliquots (all aliquots measured).

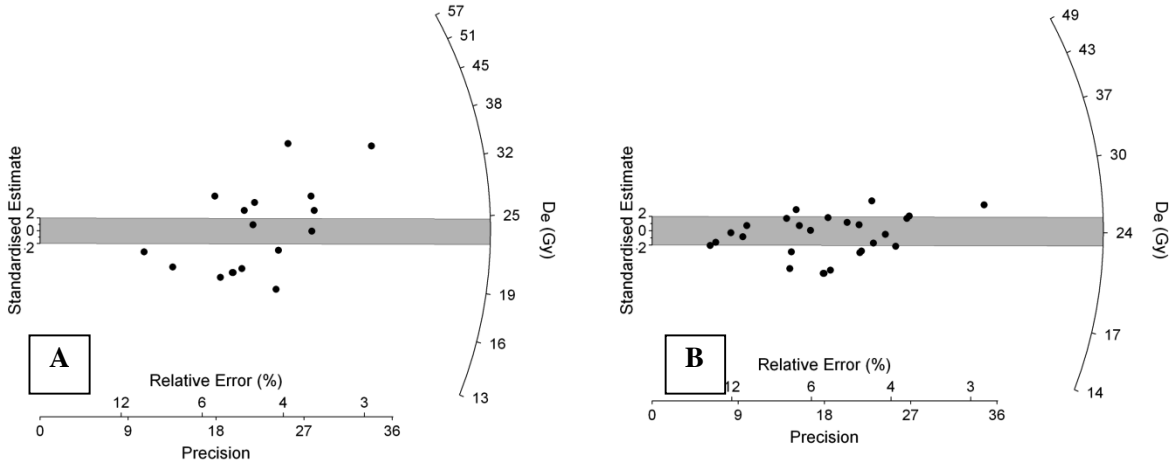

Sample E-1 (Sand ramp site WP55, 2.3 m depth): A) Results above are shown for sample E-1 (N = 17 of 30). There are only two data points centered within the two-sigma radius, largely because of large over-dispersion (> 40 percent). This dispersion does not arise from the measured equivalent doses, rather it reflects the poor fitting of the exponential + linear function to this sample. Many equivalent doses were rejected by the program as it was unable to force a fit to the exponential + linear program. **B)** Results are shown for sample E-1 (N = 27 of 30) using a linear fit to the data.

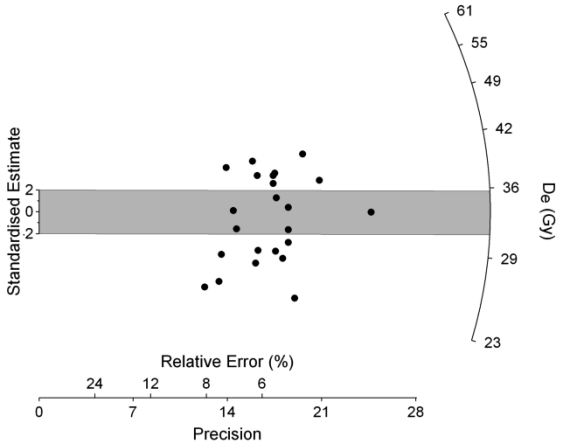

Sample E-2 (Sand ramp site WP55, 4.1 m depth): Results above are shown for sample E-2 (N = 23 of 35). There are two concentrations; one centered at 45 Grays, the other around 25 Grays. Because there is also an intermediate composition centered around 35 Grays it was deemed more reliable to draw one radial plot centered at the intermediate composition.

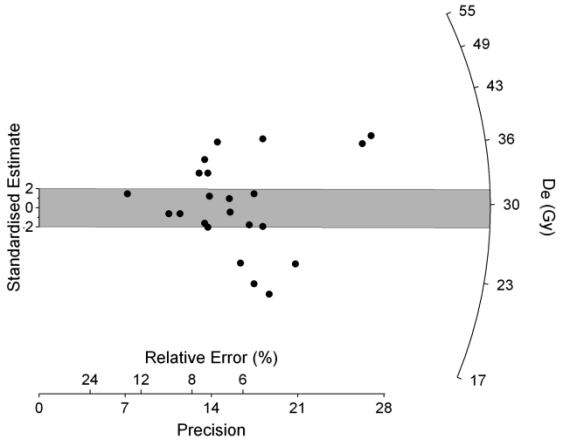

Sample E-3 (Sand ramp site WP55, 6.1 m depth): Results above are shown for sample E-3 (N = 22 of 38).

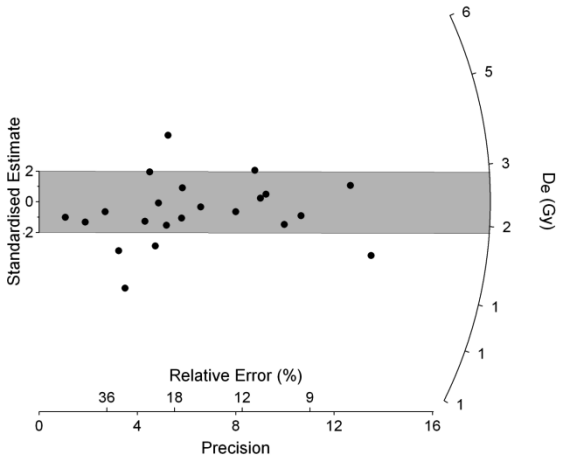

Sample E-4 (Linear dune site WP63, 0.7 m depth): Results above are shown for sample E-4 (N = 23 of 37).

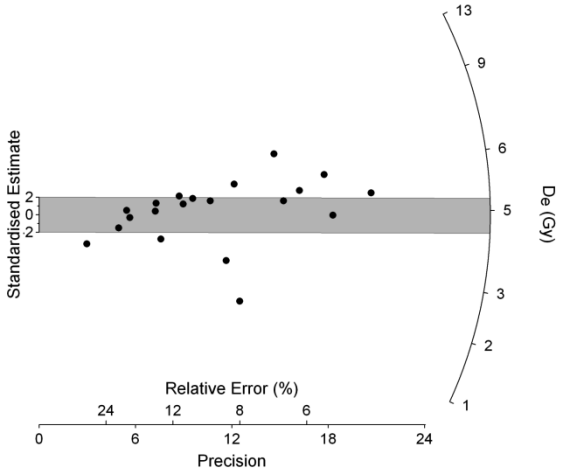

Sample E-5 (Linear dune site WP63, 2.2 m depth): Results above are shown for sample E-5 (N = 20 of 30).

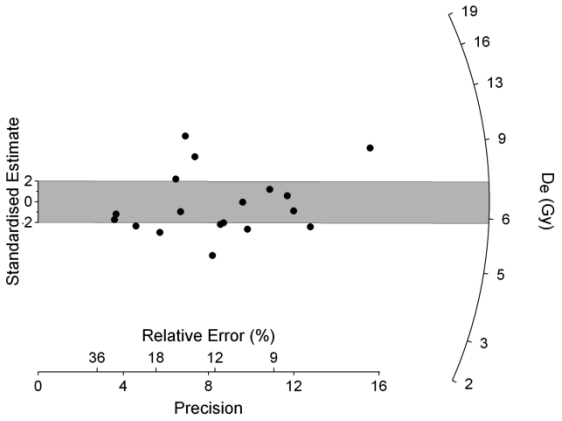

Sample E-6 (Linear dune site WP63, 2.7 m depth): Results above are shown for sample E-6 (N = 20 of 30).

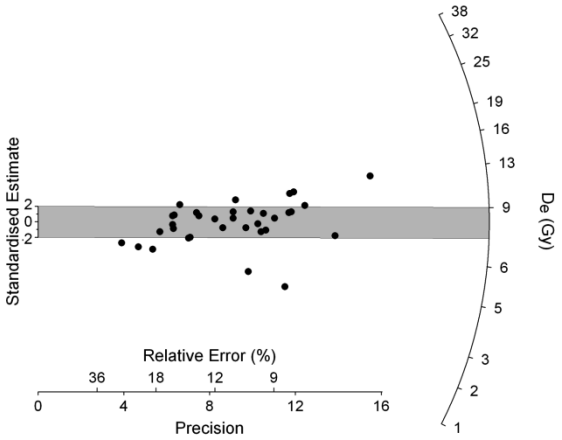

Sample E-7 (Linear dune site WP40, 1.4 m depth): Results above are shown for sample E-7 (N = 34 of 40).

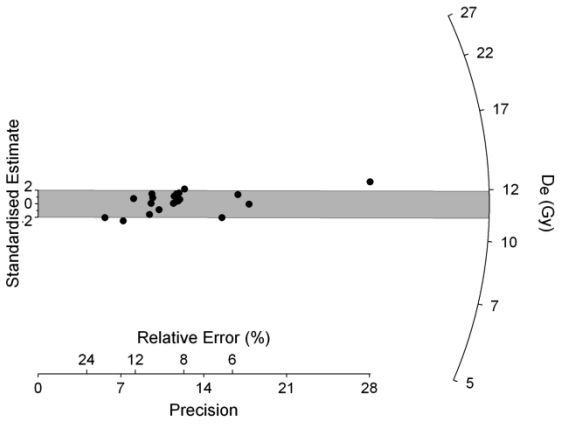

Sample E-8 (Linear dune site WP65, 2.0 m depth): Results above are shown for sample E-8 (N = 20 of 30).

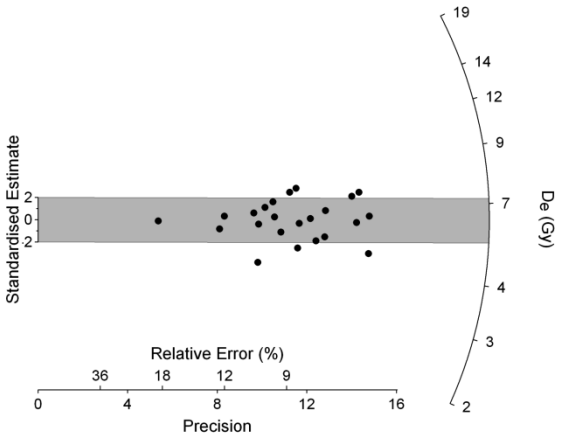

Sample E-9 (Linear dune site WP65, 0.5 m depth): Results above are shown for sample E-9 (N = 24 of 30).

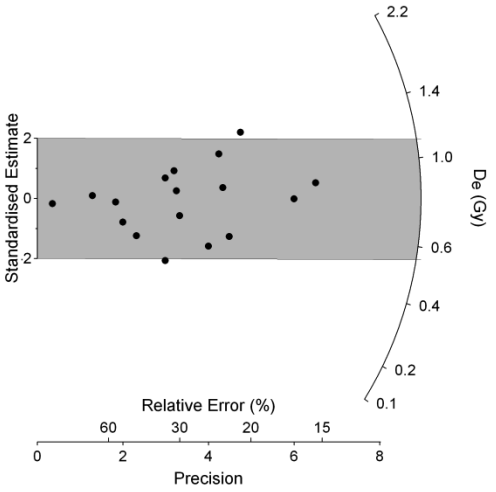

Sample E-10 (Linear dune site WP38, 1.1 m depth): Results above are shown for sample E-10 (N = 22 of 30). This sample has the lowest precision of the entire set (20 to 60 % relative error).

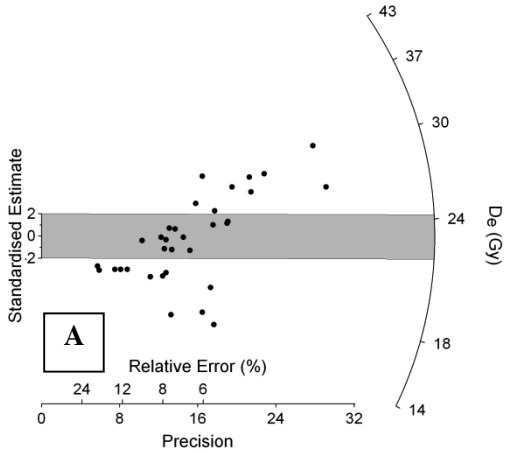

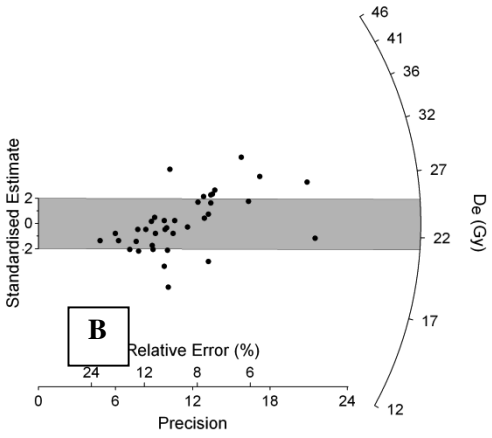

Sample E-11 (Falling dune site WP109, 3.2 m depth): A) Results are shown for sample E-11 (N = 40 of 50). There are only two data points centered within the two-sigma radius, primarily because of large over-dispersion (>40 percent). This dispersion does not arise from the measured equivalent doses, rather it reflects the poor fitting of the exponential + linear function to this sample. Many equivalent doses were rejected by the program as it was unable to force a fit to the exponential + linear program. The linear fit is shown below. **B)** Results are shown for sample E-11 (N = 43 of 50). This is the linear fit to the data.

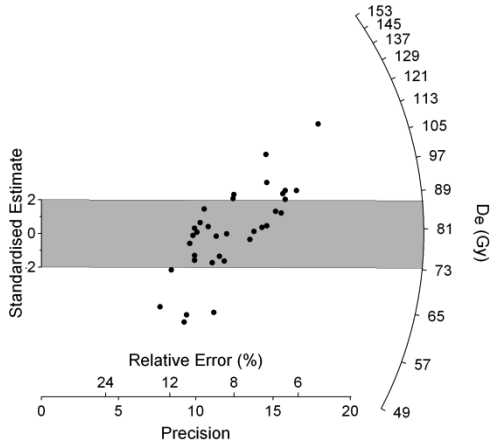

Sample E-12 (Falling dune site WP109, 4.0 m depth): Results above are shown for sample E-12 (N = 50 of 55). Two points plot on top of each other (118 ± 6.6 Gy).

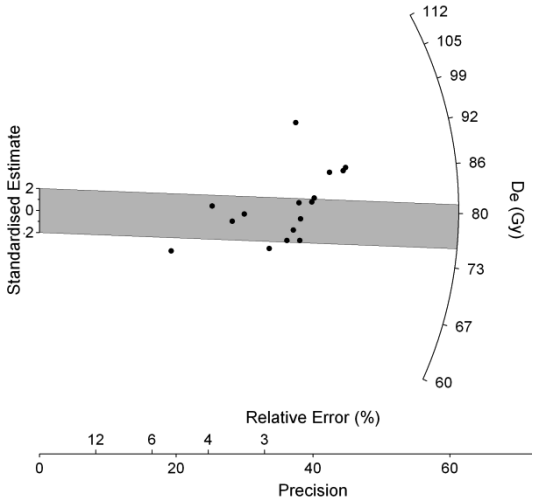

Sample E-13 (Falling dune site WP109 – toe of dune, 4.0 m depth): Results above are shown for sample E-13 (N = 16 of 18). The errors associated with the values are extraordinarily low (most are less than 3%, i.e. 101.3 ± 2.7 or 88.9 ± 2.0) causing the relative error to plot strongly in the right quadrant and off the page.

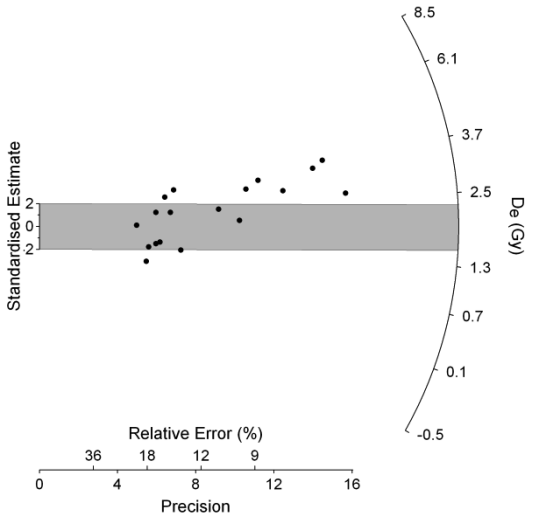

Sample E-14 (Dune complex site WP112-114, 0.9 m depth): Results above are shown for sample E-14 (N = 18 of 30).

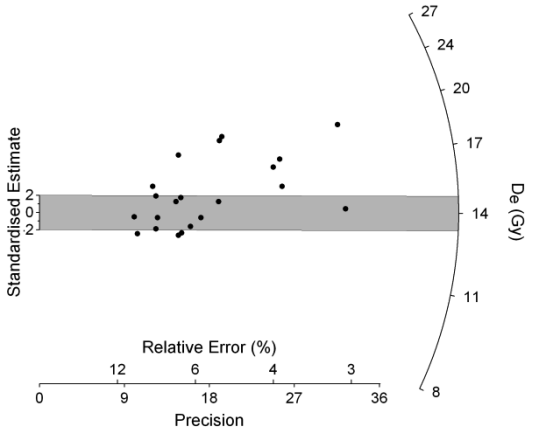

Sample E-15 (Dune complex site WP112-114, 2.1 m depth): Results above are shown for sample E-15 (N = 21 of 28).

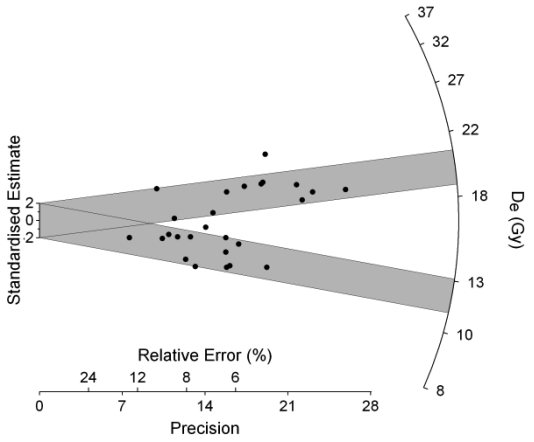

Sample E-16 (Dune complex site WP112-114, 1.8 m depth): Results above are shown for sample E-16 (N = 26 of 30). There are two populations: one centered at 20 Grays, the other around 12 Grays. The average of the population is around 16 to 17 Grays. Because it was impossible to distinguish the more "correct" population due to geologic sources the two populations were combined for one final equivalent dose.

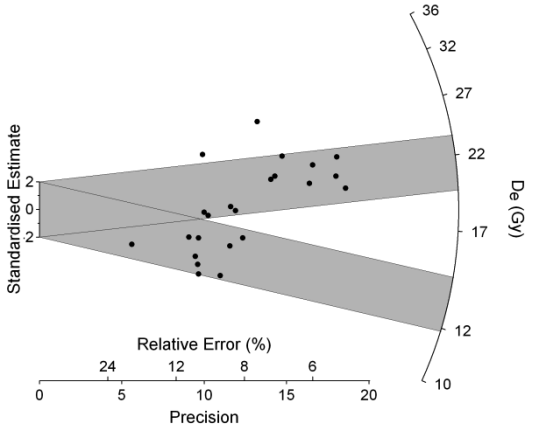

Sample E-17 (Dune complex site WP112-114, 1.3 m depth): Results above are shown for sample E-17 (N = 23 of 30). There are two populations: one centered at 23.5 Grays, the other around 15.5 Grays. The average of the population is around 19 to 20 Grays. Because it was impossible to distinguish the more "correct" population due to geologic sources the two populations were combined for one final equivalent dose.

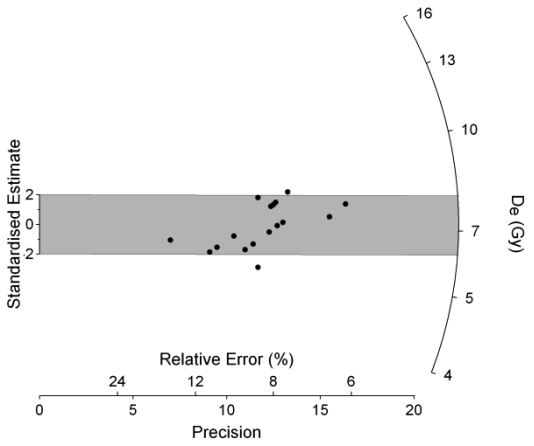

Sample E-18 (climbing dune site WP144, 0.6 m depth): Results above are shown for sample E-18 (N = 18 of 20).

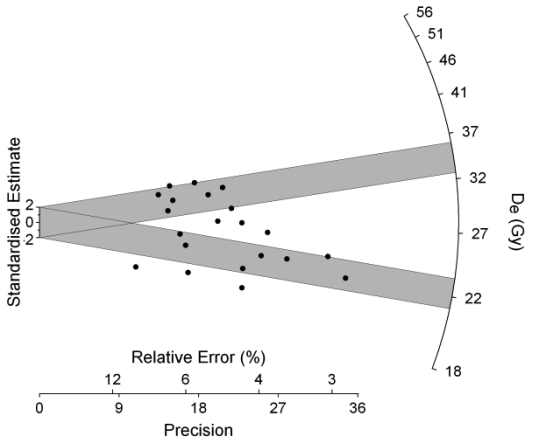

Sample E-19 (Sand sheet site WP145, 1.7 m depth): Results above are shown for sample E-19 (N = 21 of 30). There are two populations with a fair amount of outliers; one centered at 36 Grays, the other around 24.5 Grays. The average of the population is roughly 30 Grays. Because it was impossible to distinguish the more "correct" population due to geologic sources the two populations were combined for one final equivalent dose.

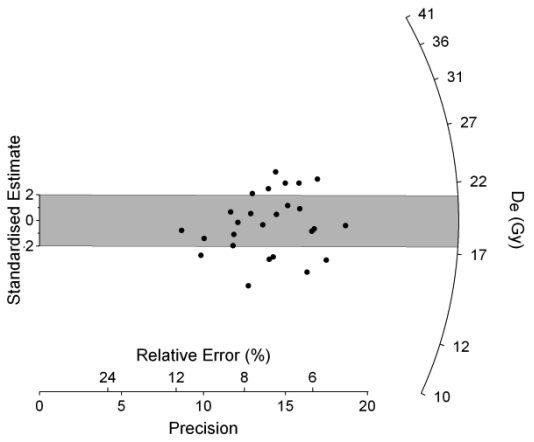

Sample E-20 (Sand sheet site WP149, 1.7 m depth): Results above are shown for sample E-20 (N = 26 of 30).

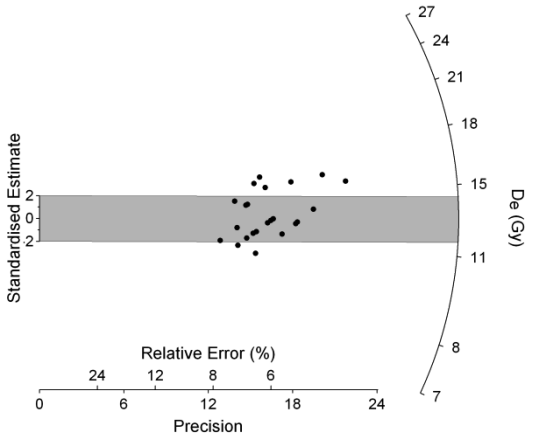

Sample E-21 (Sand sheet site WP154, 1.5 m depth): Results above are shown for sample E-21 (N = 26 of 30).

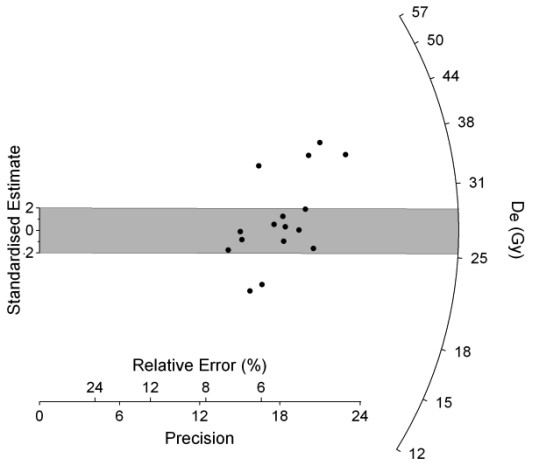

Sample E-22 (Sand sheet site WP164, 2.1 m depth): Results above are shown for sample E-22 (N = 16 of 18).

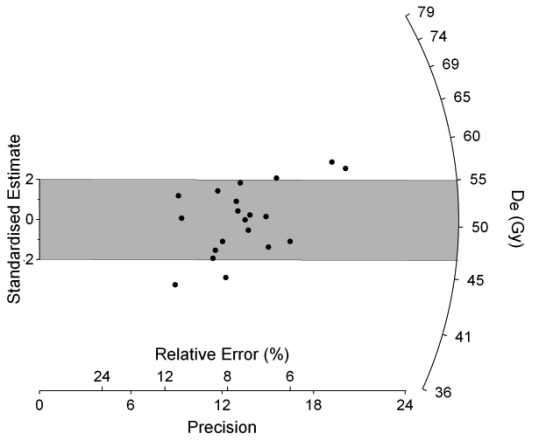

Sample E-23 (Falling dune site WP169, 2.4 m depth): Results above are shown for sample E-23 (N = 20 of 20).

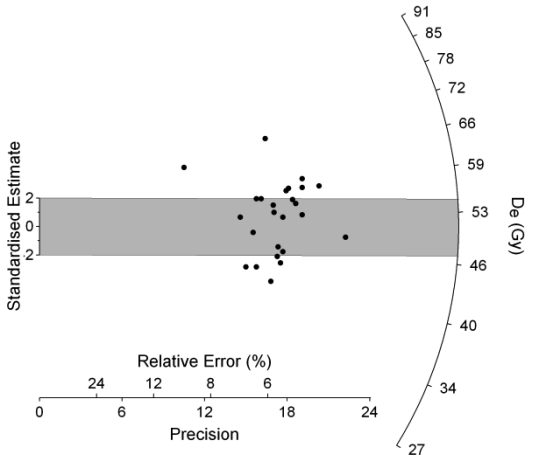

Sample E-24 (Falling dune site WP169, 3.2 m depth): Results are shown for sample E-24 (N = 25 of 27).

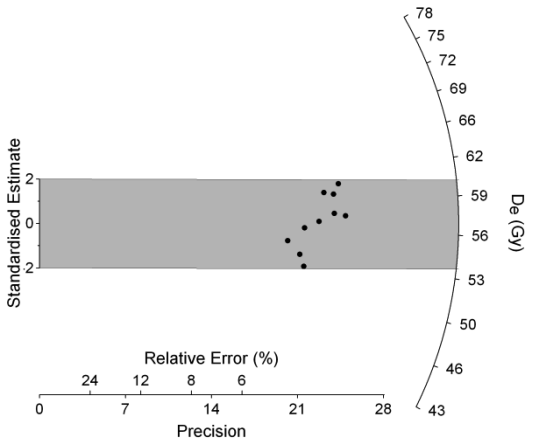

Sample E-25 (Falling dune site WP169, 4.5 m depth): Results above are shown for sample E-25 (N = 10 of 10). There was no more sample available to run because it was spilled.

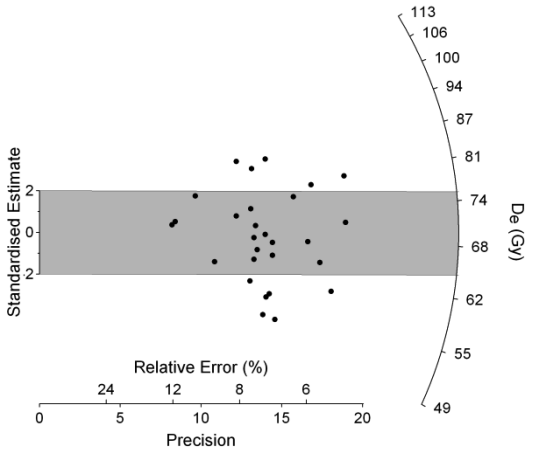

Sample E-26 (Falling dune site WP169, 8.0 m depth): Results above are shown for sample E-26 (N = 28 of 30).